Critical Behavior of Jamming Transition in One-Dimensional Nonequilibrium Models

A Thesis

Submitted for the Degree of

DOCTOR OF PHILOSOPHY

IN THE FACULTY OF SCIENCE

by

PRIYANKA

THEORETICAL SCIENCES UNIT
JAWAHARLAL NEHRU CENTRE FOR ADVANCED SCIENTIFIC RESEARCH
(A Deemed University)
Bangalore – 560 064

August 2016

To My Mother and Kavita

DECLARATION

I hereby declare that the matter embodied in the thesis entitled "**Critical Behavior of Jamming Transition in One-Dimensional Nonequilibrium Models**" is the result of investigations carried out by me at the Theoretical Sciences Unit, Jawaharlal Nehru Centre for Advanced Scientific Research, Bangalore, India under the supervision of **Prof. Kavita Jain**, and that it has not been submitted elsewhere for the award of any degree or diploma.

In keeping with the general practice in reporting scientific observations, due acknowledgement has been made whenever the work described is based on the findings of other investigators.

Priyanka

CERTIFICATE

I hereby certify that the matter embodied in this thesis entitled "**Critical Behavior of Jamming Transition in One-Dimensional Nonequilibrium Models**" has been carried out by **Ms. Priyanka** at the Theoretical Sciences Unit, Jawaharlal Nehru Centre for Advanced Scientific Research, Bangalore, India under my supervision and that it has not been submitted elsewhere for the award of any degree or diploma.

Prof. Kavita Jain
(Research Supervisor)

Acknowledgements

First and foremost, I am very thankful to my mother for her unconditional love, support and encouragement. She is always there, by all means, to make my life easier. Her love and care is a source of my strength and happiness. Without her, this moment would be impossible.

I would like to express my sincere gratitude to my advisor Prof. Kavita Jain for helping me to fulfill my dream with her constant support, encouragement and guidance. I thank her for the constant push to learn and make the things perfect. I feel great respect for her brilliance, hardwork and honesty. Her uncompromising approach toward problems is always a incentive for me. Her ideas and efforts have contributed a lot to this thesis. I hope, I have learnt some of her ways of doing problems.

It gives me great pleasure in acknowledging the fruitful collaboration with Dr. Arvind Ayyer. Many discussions with him lead to better understanding of my work.

I acknowledge University Grant Commission (UGC) for support through a research fellowship. Also to JNCASR for financial support and excellent research facilities. I thank Milind (EMU) for letting me use his computer for some of the simulations

Further, I would like to thank all faculty members of TSU for their support in various ways. I would also like to express my gratitute to Prof. Chandan Dasgupta, Prof. Shobana Narasimhan, Prof. N. S. Vidhyadhiraja, Prof. Subir K. Das, and Prof. Swapan K. Pati for the wonderful courses they provided.

The journey of such a long time is impossible without pleasant and supportive lab environment. I thank all my past and present labmates – Sarada, Sona, Ananthu, Jyoti, and Archana for their support. I am blessed to have wonderful labmates and friends: Sarada

and Sona with their love, care and strength to bear all my drama and also thanks to my pseudo labmate Meha for everything.

*"***Friendship***, "said Christopher Robin, "***is a very comforting thing to have***."* – A.A. Milne.

I am very lucky to have lots and lots of wonderful friends and I would thank all of them for being there for me at any moment. The list is long but, I would like to mention few of them. I am grateful to Dherendra and Abhishek for encouraging me to pursue higher studies and show me the way to JNU. It gives me great pleasure to thank some of my dearest friends Deb, Nishi, Deepak, Meha, Sankalp, Kanwar, Sumit, Sruthi, PP, Milind, Ponnu, Suman, Sutapa, Vinay, Nitin and Malay for support, help and encouragement during my PhD. I thank Divya di, Shaista di, I am grateful to have such caring seniors. I learn lot of academic and non-academic things from all of them. I would also like to give special thanks to Vicky, Arun, Croor, Ronak, Sankalp, Meha, Sandhaya and Sruthi for helping me in thesis correction. I am also thankful to Rajesh for the nice thesis template.

I am very thankful to Deepak and Milind for introducing me to music and a special thanks to Vicky for all his encouragement, support, love and critics which help me to improve myself at every stage.

I owe my deepest gratitude to my flute teacher, Prasanth sir and yoga teacher, Rajshree mam for keeping the mind and body calm and healthy. It is always difficult to complete a day without Saranapa's coffee and hence, would like to thank the best coffee maker: Saranapa.

And now, last but not least, I appreciate the help I have received from administrative staff, complab staff, library staff, and academic staff at various stages in duration for my PhD. I also thank hostel staff and Dhanvantri staff for making my life comfortable in JNC.

Abstract

Statistical mechanics is an essential tool to describe the behavior of complex systems ranging from bacterial growth to universe expansion. For a system in equilibrium, this approach is well established and the stationary state distribution is given by the Boltzmann weight. Nonequilibrium systems are much more common than the equilibrium ones but a complete formalism analogous to equilibrium statistical mechanics has not been developed for nonequilibrium processes. We therefore study some simple nonequilibrium models in detail to gain an insight in these systems. In this thesis, we focus on one-dimensional nonequilibrium interacting particle systems which are driven by an external force. Such systems can show a non-trivial phase transition even in one-dimension and we are interested in understanding the critical behavior of these systems. The models studied in this thesis are motivated by the common phenomenon of jamming that occurs in traffic flow of vehicles, molecular motors, fluid flow through narrow pipe, etc.

In this thesis, we study two generic classes of one-dimensional stochastic models: (a) lattice gas models of hard core particles in which a particle hops to an empty site according to the hop rule assigned to it and (b) mass transport models in which each site can contain many particles and a particle hops to another site according to the prescribed rule. Below we list four lattice gas models that we have worked on in this thesis and their correspondence to the mass transport models:

i. A particle hops to a nearest neighbor provided it is empty depending on the number of vacancies in front of it; this model can be mapped exactly to a zero range process.

ii. A particle hops to a nearest neighbor if it is empty depending on the number of vacancies in front and back of it; this model can be mapped exactly to a misanthrope process.

iii. A particle hops to a nearest neighbor with a hop rate that is chosen from a distribution; this model can be related to a zero range process with the sitewise disorder.

iv. A particle can have both short range as well as long range hops; this model can be mapped to an aggregation-fragmentation model.

In stationary state, these lattice gas models show a phase transition between fluid phase and jammed phase as the total density of the system is varied [1]. In fluid phase, the particles are uniformly distributed while in the jammed phase, a hole cluster of macroscopic length is formed in front of a particle. Some of the questions regarding stationary state and dynamical properties of these models have been addressed in previous studies and are reviewed briefly in Chapter 2.

In Chapter 3, we calculate the equal time density-density correlation function in the stationary state in the fluid phase and at the critical point for the models listed above. Our main result is that at the critical point, the correlation function shows a power law decay with an exponent that varies continuously with the parameters in the models (i)-(iii). However, in the model (iv), the exponent associated with the correlation function decay is a constant. We also find that the correlation length diverges in thermodynamic limit with an exponent which varies continuously in one parameter regime of hop rates in models (i)-(iii), otherwise it is a constant [2, 3].

The stationary state dynamics of these models are addressed in Chapter 4. We studied the decay of density-density autocorrelation function with time both analytically and numerically. Our main result is that the autocorrelation function decays as a power law in time with an exponent 2/3 [4] when equal time correlation function decays faster than inverse distance otherwise the decay is slower and the exponent is continuously varying [3].

Besides the stationary state properties of the models of interest, we also studied the quench dynamics for hop rule (i) in Chapter 5. For this model, infinitely rapid quench dy-

namics (coarsening) have been studied [5]. However the dynamics of this model under slow annealing have not been investigated, and we study the decay of the domain wall density with the inverse quench rate using numerical simulations and analytical arguments. We find that the standard Kibble-Zurek scaling [6, 7] explains our results in the critical region but close to the critical point and for quenches deep in the jammed phase, the excess domain wall density decay with quench time can be understood using the corresponding results for rapid quench dynamics [8].

We conclude the thesis in Chapter 6 by presenting our preliminary results on the slow quench dynamics of a zero range process in mean field geometry [9] and also discuss some open questions.

List of publications

- *Two-point correlation function of an exclusion process with hole-dependent rates,* Priyanka, Arvind Ayyer and Kavita Jain, ***Phys. Rev. E.*** 90, 062104 (2014).
- *Critical dynamics of the jamming transitions in one dimensional nonequilibrium models,* Priyanka and Kavita Jain, ***Phys. Rev. E.*** 93, 042104 (2016).
- *Critical dynamics of classical systems under slow quench,* Priyanka and Kavita Jain, arXiv:1607.00617.
- *Slow quench dynamics of zero range process in mean field geometry,* Priyanka, in preparation.

Table of contents

List of figures

Chapter 1

Introduction

Statistical mechanics is a branch of physics that applies probability theory to study the behavior of systems composed of a large number of particles. It provides an essential tool to connect the microscopic properties of individual particles to the macroscopic bulk properties of materials that can be observed in everyday life. For example, in the kinetic theory of gases, by treating every atom or molecule of the gas as a particle undergoing classical Newtonian mechanics and focusing only on the average behaviour of a large number of particles of the same kind, one can find the expression for the average macroscopic physical observable like pressure or temperature. Thus, statistical mechanics uses minimum details from the microscopic constituents to produce macroscopic observable quantities correctly. It was originally introduced in the late nineteenth century as a theoretical description of thermodynamics.

1.1 Equilibrium versus nonequilibrium

A system in thermal equilibrium obeys the laws of thermodynamics that are well established in equilibrium statistical mechanics. The connection between the macroscopic description and the microscopic scale is obtained through Boltzmann's formula, $S = k \log \Omega$, where S is the entropy, k is the Boltzmann constant and Ω is the number of different configurations of the system. In canonical ensemble, once the microscopic Hamiltonian $\mathscr{H}$ of

the system at temperature T is specified, the stationary state distribution over configuration space is known to be given by the Boltzmann factor $e^{-\beta\mathcal{H}}$, where $\beta = (kT)^{-1}$.

Nonequilibrium systems are much more common than the equilibrium ones, but a complete formalism analogous to equilibrium statistical mechanics has not been developed for nonequilibrium processes. In contrast to equilibrium systems, nonequilibrium systems can reach a stationary state but their statistical properties are not described by the equilibrium Boltzmann distribution. One important feature that distinguishes a nonequilibrium system from an equilibrium system is the breakdown of detailed balance due to the presence of currents in nonequilibrium systems that drive the macroscopic transport of matter, charge, energy etc. within a system, or between the system and its environment. To see this, consider a classical system following Markov dynamics in which the system evolves from a configuration $\mathscr{C}$ to a configuration $\mathscr{C}'$ between time t and $t+dt$ at a rate $\mathscr{W}(\mathscr{C}',\mathscr{C})$. The evolution of probability, $\mathscr{P}(\mathscr{C},t)$ of being in microstate $\mathscr{C}$ at time t is governed by the master equation [10],

$$\frac{d\mathscr{P}(\mathscr{C},t)}{dt} = \sum_{\mathscr{C}'\neq\mathscr{C}} \mathscr{W}(\mathscr{C},\mathscr{C}')\mathscr{P}(\mathscr{C}',t) - \sum_{\mathscr{C}'\neq\mathscr{C}} \mathscr{W}(\mathscr{C}',\mathscr{C})\mathscr{P}(\mathscr{C},t). \tag{1.1}$$

When the stationary state is reached, the left-hand side of the above equation must vanish. Moreover, at equilibrium, as the microscopic dynamics of the system is time reversible, the local currents must vanish and thus the detailed balance equation is obtained as [10]

$$\mathscr{W}(\mathscr{C},\mathscr{C}')\mathscr{P}^{eq}(\mathscr{C}') = \mathscr{W}(\mathscr{C}',\mathscr{C})\mathscr{P}^{eq}(\mathscr{C}). \tag{1.2}$$

A state for which the right hand side of (1.1) is zero but the detailed balance of (1.2) is not satisfied is a nonequilibrium stationary state [11–13].

Modeling of complex phenomena involves creating simple representations while retaining a close relationship with actual physical systems [12]. For example, Lenz introduced the Ising model [14] in order to understand the nature of the ferromagnetic phase transition [12]. Due to the lack of a general framework for nonequilibrium systems, one usually investigates simple models for such systems and several models have been introduced [15–

18]. Asymmetric simple exclusion process (ASEP) is one of the most commonly studied models for nonequilibrium phenomena. This particle-hole model is defined on a lattice and the particles have excluded volume interactions. The non-vanishing currents are produced in the system by coupling the system to external reservoirs that drive current (transport of particles, energy, heat) through the system, or by introducing some bias in the dynamics that favors motion in a preferred direction. Due to its simplicity, the ASEP has been used in various contexts. It was first proposed as a model to describe the dynamics of ribosomes along RNA [15]. In the mathematical literature, the name exclusion process was first used by Spitzer [16] in context of a Markovian process of particles with hardcore interaction. A very popular application of exclusion process is in understanding the dynamics of molecular motors that transport cargos inside the cells [19] and several variants have been used to model traffic flow [20]. The ASEP has also been used to describe transport phenomena in low-dimensional systems such as macromolecules passing through capillary vessels [21], anisotropic conductors or quantum dots where electrons hop to a vacant site and repel each other due to Coulomb interactions [22].

1.2 Jamming transition in one dimension

An important characteristic of nonequilibrium systems with short range interactions is that unlike equilibrium systems, they can exhibit phase transitions even in one dimension. Variants of ASEP called driven lattice gas models are examples of nonequilibrium systems whose stationary state can show a nontrivial phase transition textcolorredin one dimension. Here we will study the properties of such a nonequilibrium phase transition in one dimension. The physical phenomenon of interest in this thesis is jamming which is commonly observed and disrupts the flow of vehicles on a city road [20], molecular motors in a biological cell [19], fluids in narrow pipes, and food grains through a hopper [23]. Usually one expects a jam to form at high densities and dissolve at lower densities; however, jamming can happen at low particle densities also [24]. For example, consider a bus route along which overtaking is not allowed and, one of the buses gets delayed. The number of

passengers waiting for the bus at the stop increases and so does the time interval to get the passengers on board. As a result, the bus gets delayed even more leading to a cluster of buses behind it even when only few buses are serving on the affected bus route [24]. Of course, a traffic jam can also form behind a slow car on a single-lane highway where overtaking is prohibited even when there are few vehicles [25–27]. Large headways in front of a jam have been observed in experiments on ant trails [28], and camphor boats [29] where the agents (ants and boats) form a platoon at low densities due to the presence of an external field, namely, pheromone and camphor concentration respectively.

1.3 Overview of the thesis

In this thesis, we mainly focus on the critical behavior of the density-density correlation function in several lattice gas models whose stationary state is not in equilibrium. Our studies are based on extensive Monte Carlo simulations, scaling analysis, physical arguments, and analytic solutions. In Chapter 2, we give details of the models that are used in the thesis and review the relevant results from existing literature. In Chapter 3, we calculate the equal time density-density correlation function in the stationary state for several variants of the exclusion process explained in Chapter 2. We also study the behavior of correlation length while approaching the critical point. We obtain the exact analytical expression for the correlation function in the canonical ensemble which we further simplify in the thermodynamic limit [2, 3].

In literature, the asymmetric exclusion process (ASEP) has been studied extensively and its stationary state dynamics have been understood by mapping it to an interface model which is described by the Kardar-Parisi-Zhang equation [30]. Previous studies have shown that the density-density autocorrelation function decays in time with an exponent 2/3 [4]. However, it is well known that an ASEP with periodic boundary conditions does not show a jamming transition. The question of the stationary state dynamics at the critical point for systems having jamming transition is addressed in Chapter 4 by studying the decay of density-density autocorrelation function with time [3].

Besides the stationary state properties of the lattice gas models that exhibit jamming transition, we also study the quench dynamics under slow annealing. In Chapter 5, we study the decay of domain wall density with the inverse quench rate using numerical simulations and analytical arguments [8]. We find that the standard Kibble-Zurek scaling [6, 7] explains our results in the critical region but close to the critical point, we find a new scaling law which also involves the properties of the fast quench dynamics. We also present our preliminary results on slow quench dynamics of a zero range process (which is related to ASEP) in mean field geometry. Finally, in Chapter 6, we summarize our main results.

Chapter 2

Driven systems with jamming transition

2.1 Introduction

As mentioned in Chapter 1, simple models are useful because one can bypass the complex details of the full system and try to understand the system properties in terms of a few parameters. Some of the simple models of nonequilibrium systems that are driven by an external field are well known in literature [1].

An important model in this class is the Zero Range Process (ZRP) in which a particle hops to a neighbouring site with a rate that depends only on the properties of the departure site and has the attractive feature that its steady state distribution can be found exactly [16]. This model has been generalised in various directions in recent years [31–33], and has been used to study the clustering phenomena in traffic flow [34], granular gases [35] and networks [36], avalanche dynamics in sandpiles [37], slow dynamics in glasses [38] and phase separation in nonequilibrium systems [39].

Another class of model, called exclusion process, is defined on a one-dimensional lattice and involves hopping of the hard core particles to an empty site [16, 40]. Our main focus in the thesis is to study the variants of a one-dimensional exclusion process that are closely related to the zero range process [41, 1], or a misanthrope process, whose exact steady state measure can be found in certain cases [42, 33]. Certain models with excluded

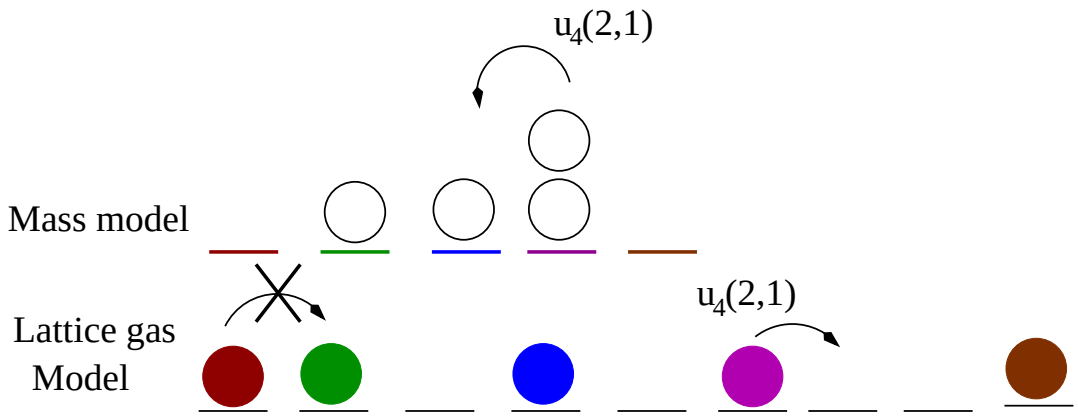

Fig. 2.1 Illustration of the mapping between lattice gas model (bottom) and mass model (top) with short range hop.

volume interaction can also be related to aggregation-fragmentation models [43, 44]. In the following sections, we review these models in detail.

2.2 Stationary states with product measure

In this section, we discuss a class of one-dimensional lattice gas models (exclusion process) defined on a ring. In these models, each site contains at most one particle and a particle hops to an empty nearest neighbor site with a rate $u_i(m,m')$ where m and m' are the number of vacancies in its front and back respectively. Further, the hop rate may also depend on the particle index i.

To understand the lattice gas model analytically, we map it to the so-called *mass model* in which each site can contain multiple particles. As shown in Fig. 2.1, the exclusion process described above with L sites and N particles maps to a mass model with $\mathscr{L} = N$ sites and $\mathscr{M} = L - N$ particles (each of unit mass). A particle hops out of a site with m particles to a target site on right with m' particles at rate $u_i(m,m')$, where the subscript i now refers to the site from which the particle hops out. The density $\varrho = \mathscr{M}/\mathscr{L}$ in the mass model is related to the density $\rho = N/L$ in the exclusion process as

$$\varrho = \frac{1}{\rho} - 1 \,. \tag{2.1}$$

Although we have described the unidirectional case above, it is important to note that the steady state properties for these models are not affected by a bias in the hop rates.

For certain choices of short-range hop rates in the mass model, the stationary state mass distribution is a product measure. More precisely, the stationary state mass distribution of a configuration $C \equiv \{m_1, ..., m_{\mathscr{L}}\}$, where m_i is the number of particles at the ith site is given by

$$\mathscr{P}(m_1, ..., m_{\mathscr{L}}) = \tilde{Z}^{-1}_{\mathscr{L},\mathscr{M}} \prod_{i=1}^{\mathscr{L}} f_i(m_i)\, \delta_{\mathscr{M},\sum_{k=1}^{\mathscr{L}} m_k}\,, \tag{2.2}$$

where $\delta_{\mathscr{M},\sum_{k=1}^{\mathscr{L}} m_k}$ is the Kronecker delta and $\tilde{Z}_{\mathscr{L},\mathscr{M}}$ is the canonical partition function defined as

$$\tilde{Z}_{\mathscr{L},\mathscr{M}} = \sum_{\{m_i\}} \prod_{i=1}^{\mathscr{L}} f_i(m_i)\, \delta_{\mathscr{M},\sum_{k=1}^{\mathscr{L}} m_k}\,. \tag{2.3}$$

Here, $f_i(m_i)$ is the steady state weight factor and can be obtained using the master equation in stationary state, which is given as [1]

$$\sum_{i=1}^{\mathscr{L}} [u_i(m_{i-1}+1, m_i)\mathscr{P}(.., m_{i-1}+1, m_i-1, ...) - u_i(m_i, m_{i+1})\mathscr{P}(..., m_{i-1}, m_i, ...)]\theta(m_i) = 0\,, \tag{2.4}$$

where $\theta(m_i)$ reflects the constraint that the site i must be occupied. Using (2.2) in (2.4) and equating each term, we get the relation between the stationary state weight factor $f_i(m_i)$ and the hop rates $u_i(m, m')$ [1] (as given in Secs. 2.2.1, 2.2.2, and 2.2.3).

Further, we have the exact recursion relation for the canonical partition function (2.3) and is given as [45]

$$\tilde{Z}_{\mathscr{L},\mathscr{M}} = \sum_{k=0}^{\mathscr{M}} f_i(k)\tilde{Z}_{\mathscr{L}-1,\mathscr{M}-k}\,, \tag{2.5}$$

with $\tilde{Z}_{0,m} = \delta_{m,0}$ since $\tilde{Z}_{1,m} = f_i(m)$. For some more properties of the partition function in the canonical ensemble, see Appendices A.1 and A.2.

For clarity, from this point onward, we only consider stationary state properties of homogeneous systems. The steady state properties for the model involving heterogeneity is discussed separately in Sec. 2.2.3. Thus, for homogeneous system, one can also exactly calculate the single site mass distribution in the canonical ensemble for the mass model by

[1]

$$\begin{aligned} p(m) &= \mathscr{P}(m, m_2, ..., m_{\mathscr{L}})\delta\left(\sum_{i=2}^{\mathscr{L}} m_i - (\mathscr{M} - m)\right) \\ &= f(m)\frac{\tilde{Z}_{\mathscr{L}-1,\mathscr{M}-m}}{\tilde{Z}_{\mathscr{L},\mathscr{M}}} . \end{aligned} \tag{2.6}$$

In general, it is difficult to obtain results in the canonical ensemble due to the mass conservation constraint. However, the grand canonical partition function $\mathcal{Z}_{\mathscr{L}}$ can be readily obtained. Using (2.3), we can write it as

$$\mathcal{Z}_{\mathscr{L}}(\omega) = \sum_{n=0}^{\infty} \tilde{Z}_{\mathscr{L},n}\omega^n = g^{\mathscr{L}}(\omega) , \tag{2.7}$$

where $g(\omega)$ is the generating function of $f(m)$ defined as

$$g(\omega) = \sum_{m=0}^{\infty} \omega^m f(m) , \tag{2.8}$$

with a radius of convergence ω^*. In the thermodynamic limit, keeping density fixed, we can determine the fugacity $\omega(\leq \omega^*)$ using the following relation

$$\varrho = \frac{1}{\rho} - 1 = \frac{\omega}{\mathscr{L}} \frac{\partial \ln \mathcal{Z}_{\mathscr{L}}(\omega)}{\partial \omega} = \omega \frac{\partial \ln g(\omega)}{\partial \omega}. \tag{2.9}$$

From (2.6) and (2.9), we have the mass variance $\sigma^2 = \langle m^2 \rangle - \langle m \rangle^2$ in mass model which is given by

$$\sigma^2 = \omega \frac{\partial \varrho}{\partial \omega} = -\frac{\omega}{\rho^2} \frac{\partial \rho}{\partial \omega} . \tag{2.10}$$

Further, in the thermodynamic limit, on summing over the mass on all sites except one site in (2.6), the single site mass distribution is obtained as

$$p(m) = \omega^m \frac{f(m)}{g(\omega)}. \tag{2.11}$$

Equation (2.9) shows that the fugacity ω is an increasing function of the mass-model density ϱ. But, as it is bounded above, it may happen that ω reaches its maximum value at a

finite critical density, ϱ_c. In such a case, the mass distribution $p(m) = \omega^{*m} f(m)/g(\omega^*)$ for all $\varrho \geq \varrho_c$. This implies that the average density in the system is $\mathscr{L}^{-1}\sum_{m=1}^{\infty} m\, p(m) = \varrho_c$. The excess mass $\varrho - \varrho_c$ is then said to be condensed into a single cluster, as shown in Fig. 2.2 for the case of hop rate given by (2.12). This signals the phase transition. In following sections, this phase transition is explained in greater detail for specific choices of the hop rate.

2.2.1 Exclusion process with hole-dependent rates

We consider a model in which the hop rate depends on the number of holes in front of a particle. Specifically, we choose the hop rate to be [1]

$$u(m) = 1 + \frac{b}{m}\,,\ m > 0\,, \tag{2.12}$$

where m denotes the number of vacancies in front of a particle and the parameter $b \geq 0$. When $b = 0$, we obtain the simple exclusion process (SEP) [1, 46] from this model. For nonzero b, the rate $u(m)$ decreases with an increasing number of vacancies, and therefore a particle with many holes in front of it hops at a slower rate and can cause a jam behind it. In fact, it has been shown that for $b > 2$, a phase transition occurs between a homogeneous phase with typical hole cluster of length unity and a jammed phase with a macroscopically large hole cluster, as the total particle density is decreased. To see this result, it is useful to consider a one-dimensional zero range process (ZRP) [1] as described in Sec. 2.2.

For the hop rate (2.12), the steady state weight factor $f(m)$ used in (2.3) for ZRP is given by

$$f(m) = (1 - \delta_{m,0}) \prod_{i=1}^{m} \frac{1}{u(i)} + \delta_{m,0}\,, \tag{2.13}$$

which simplifies to

$$f(m) = \frac{m!}{(b+1)_m}\,, \tag{2.14}$$

where $(a)_m = a(a+1)...(a+m-1)$ is the Pochhammer symbol or rising factorial. In general, it is difficult to obtain results in the canonical ensemble (see however [47, 48, 45]), but one

can do it numerically with the recurrence relation (2.5) for the ZRP partition function $\tilde{Z}_{\mathscr{L},\mathscr{M}}$ with $\mathscr{L}$ sites and $\mathscr{M}$ particles that has been obtained [45].

In the grand canonical ensemble, the generating function (2.8), $g(\omega)$ of $f(m)$ can be written as

$$g(\omega) = {}_2F_1(1,1;1+b;\omega)\,, \tag{2.15}$$

where

$${}_2F_1(a,b;c;\omega) = \sum_{n=0}^{\infty} \frac{(a)_n (b)_n}{(c)_n} \frac{\omega^n}{n!} \tag{2.16}$$

is the Gauss hypergeometric function [49].

It is easy to see that the radius of convergence of $g(\omega)$ in (2.15) is $\omega^* = 1$. Equation (2.9) and the discussion following it then shows that a condensation transition occurs at the critical density in which particles are distributed homogeneously over the system at low densities, but above a critical density, a macroscopic number of particles form a cluster. The exact critical density for ZRP is

$$\varrho_c = \frac{1}{b-2}\,, \tag{2.17}$$

for $b > 2$. In a ZRP, the single site mass distribution is given by

$$p(m) = \omega^m \frac{f(m)}{g(\omega)}. \tag{2.18}$$

One can notice the significant change in the distribution $p(m)$ with density ϱ. For $\varrho < \varrho_c$, the distribution is exponential and at the critical point ϱ_c, the single-site mass distribution (2.18) can be expressed as

$$p(m) = (b-1)\frac{\Gamma(b)\Gamma(m+1)}{\Gamma(m+b+1)}\,, \tag{2.19}$$

which decays algebraically as m^{-b} for large m. For $\varrho > \varrho_c$, the distribution $p(m) \sim m^{-b}$ for density ϱ_c and the excess mass of density $(\varrho - \varrho_c)$ is condensed into a single cluster as shown in Fig. 2.2. Further at the critical point, the algebraic decay of mass distribution signifies that the mass fluctuations (2.10) diverge in the thermodynamic limit when $2 < b < 3$, but remain finite otherwise.

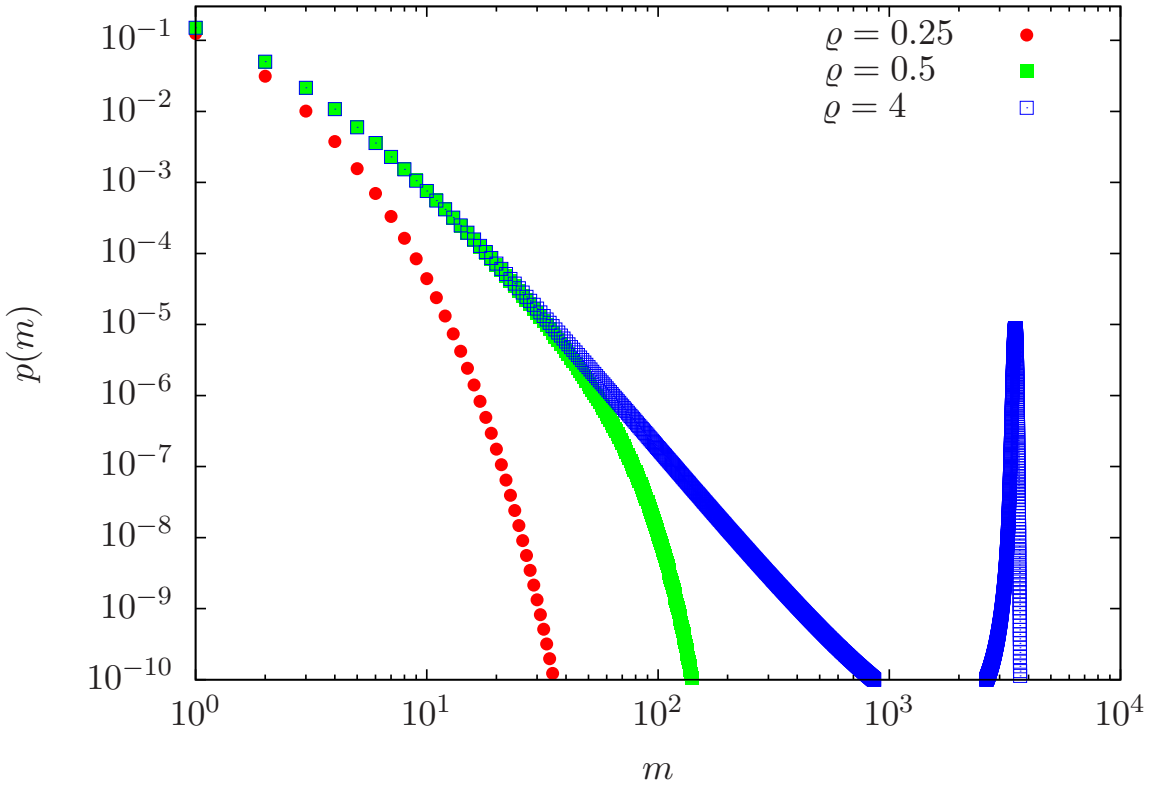

Fig. 2.2 Figure shows the single site mass distribution $p(m)$ versus particles number m for a zero range process from equation (2.18). The result is obtained by iterating the partition function recursion relation (2.5) for a system of size $\mathscr{L} = 1000$ and $b = 4$ at different densities. The density $\varrho = 0.25$ is in fluid phase, $\varrho = 0.5$ is at the critical point and $\varrho = 4$ is in the condensed phase.

2.2.2 Exclusion process with generalised hole-dependent rates

This is a class of driven lattice gas models in which a particle hops to the empty left neighbor at a rate $u(m, m')$ where $m(m')$ denotes the number of vacancies on its left (right). This model can be studied via the mapping described in Sec. 2.2, from a misanthrope process [33] in which a site can be occupied by any number of particles, and a particle hops out of a site with mass m to its right neighbor at a rate $u(m, m')$ when there are m' particles on the landing site. Indeed, it is a generalized extension of ZRP. The misanthrope process was originally used for the hop rate $u(m, m')$ which is increasing in m and decreasing in m' [42]. The general hop rate of this kind is widely used to model rewiring in complex networks [1].

For the misanthrope process, it has been shown that the steady state has product form (2.2) when the hop rate is constrained as [42]

$$u(m,m') = u(m+1,m'-1)\frac{u(1,m')u(m,0)}{u(m+1,0)u(1,m'-1)}\,, \tag{2.20}$$

$$u(m,m') - u(m',m) = u(m',0) - u(m,0). \tag{2.21}$$

Here, $f(m)$ is the steady state weight function which satisfies the following recursion relation

$$f(n) = f(n-1)\frac{f(1)}{f(0)}\frac{u(1,n-1)}{u(n,0)}. \tag{2.22}$$

In this thesis, we are particularly interested in the choice of hop rate for which condensation transition occurs [33]. The hop rate is of factorized form,

$$u(m,m') = (v(m) - v(0))\; v(m')\,, \tag{2.23}$$

where

$$\frac{2}{3} < v(0) < 1, \quad v(m) = 1 + \frac{1}{m+1}\,,\; m > 0\,. \tag{2.24}$$

For the above mentioned hop rate, the steady state weight factor $f(m)$ and its generating function $g(\omega)$ can be worked out to be

$$f(m) = \frac{c}{4}\,\frac{C^{m-1}((m+1)!)^2}{m!(c)_m}\,,\; m \geq 1\,, \tag{2.25}$$

$$g(\omega) = \frac{1}{2}\left[2 - v(0) + v(0)\;{}_2F_1(2,2,c;C\omega)\right]\,, \tag{2.26}$$

where $(a)_m = a(a+1)...(a+m-1)$ is the Pochammer symbol, $f(0) = 1$, and c and C are given by

$$c = \frac{3-2v(0)}{1-v(0)}\,, \tag{2.27}$$

$$C = \frac{c}{2v(0)}\,. \tag{2.28}$$

As for the ZRP discussed in Sec. 2.2.1, the critical density for the misanthrope process is found by setting $\omega = 1/C$ in the density-fugacity relation (2.9), and we find that the critical density is given as

$$\varrho_c = \frac{4v(0)}{c} \frac{{}_2F_1(3,3,c+1;1)}{2-v(0)+v(0){}_2F_1(2,2,c;1)} . \tag{2.29}$$

Note that the expression for the critical density in [33] is incorrect since it is obtained by assuming that $c = 4, C = 1$ (see (45)) which implies that $v(0) = 2$ is in contradiction with (2.24).

At the critical point, the single-site mass distribution is given by

$$p(m) = \frac{v(0)(m+1)(m+1)!}{[2-v(0)+v(0)\ {}_2F_1(2,2,c;1)]\ (c)_m} , \ m > 0 , \tag{2.30}$$

which decays algebraically as m^{3-c}. The mass fluctuations diverge in the thermodynamic limit when $5 < c < 6$ but remain finite otherwise.

2.2.3 Exclusion process with particlewise disorder

We again consider a system of hard-core particles on a ring in which a particle hops to the empty neighbor with the hop rates assigned to the particles being random variables, and are independent of the length of the hole clusters on the either side [25–27]. Here, we consider two cases – a single defect case in which only one particle has slower hop rate than the rest of the particles, and a fully disordered case in which the hop rates are chosen independently from a common distribution. This model can be mapped to a ZRP with sitewise disorder. The site-dependent weight factor for ZRP is given by

$$f_i(m) = u_i^{-m} , \tag{2.31}$$

where u_i is random rate assigned to the site. The generating function of $f_i(m)$ can be calculated as

$$g_i(\omega) = \frac{u_i}{u_i - \omega} . \tag{2.32}$$

As before, the fugacity is determined by the particle conservation equation (2.9),

$$\varrho = \frac{1}{\mathscr{L}} \sum_{i=1}^{\mathscr{L}} \frac{\omega}{u_i - \omega}. \tag{2.33}$$

For some choices of hop rates, the condensation transition occurs between a low-density homogeneous phase and a high-density condensed phase in which a macroscopically large particle cluster forms at the site with minimum hop rate at ϱ_c.

To understand this phase transition in the model, we first consider the case in which one site has hop rate $u_1 = c < 1$ while the rest of the sites have a hop rate $u_i = 1, i > 1$ [26]. The canonical partition (2.3) for the single defect case is given by [1]

$$\tilde{Z}_{\mathscr{L},\mathscr{M}} = \sum_{m=0}^{\mathscr{M}} \binom{\mathscr{M} + \mathscr{L} - m - 2}{\mathscr{L} - 1} c^{-m} . \tag{2.34}$$

For large system sizes, due to (2.33), the mean hop rate increases with increasing particle density till the critical density $\varrho_c = c/(1-c)$. Thus, the mean hop rate in the two phases is given by

$$\langle u \rangle = \frac{\varrho}{1+\varrho} , \ \varrho < \varrho_c , \tag{2.35}$$

$$\langle u \rangle = c , \ \varrho \geq \varrho_c . \tag{2.36}$$

For $\varrho > \varrho_c$, the system is in a condensed phase where the defect site contains all the excess mass density $\varrho - \varrho_c$, and for $\varrho < \varrho_c$, the system is in fluid phase where the mass is uniformly distributed.

In the fully disordered case, the hop rates are chosen independently from a common distribution,

$$q(u) = \frac{1+\gamma}{(1-\tilde{u})^{1+\gamma}} (u - \tilde{u})^{\gamma} , \ \gamma > 0 , \tag{2.37}$$

where $0 < \tilde{u} < u < 1$. Here, the fugacity is bounded above by the minimum hop rate and therefore, as in the previous case, the fugacity increases with increasing particle density until it reaches $\tilde{u}$ (in the thermodynamic limit). The critical density ϱ_c is obtained from

disorder averaged conservation equation [26, 50, 1] as

$$\varrho = \frac{\langle m_{min} \rangle}{\mathscr{L}} + \int_{\tilde{u}}^{\infty} du\, q(u)\, \frac{\omega}{u-\omega}\,, \tag{2.38}$$

where $\langle m_{min} \rangle$ is average number of particles occupied by the slowest site which can take a value of $\mathscr{O}(\mathscr{L})$ in condensed phase.

For a random sequential update the critical density for hop rate distribution (2.37) is known to be [25, 26]

$$\varrho_c = \tilde{u}\frac{1+\gamma}{\gamma(1-\tilde{u})}. \tag{2.39}$$

Furthermore, the averaged single site mass distribution can be obtained by averaging over the disorder distribution, and is given as

$$\overline{p(m)} = \int_{\tilde{u}}^{1} du\, q(u) \frac{\omega^m f(m)}{g(\omega)}\,. \tag{2.40}$$

The asymptotic solution of the single site mass distribution at the critical point shows a power-law decay as $m^{-(2+\gamma)}$ and, similar to previous two models, the mass fluctuations diverge for $0 < \gamma < 1$ but remain finite otherwise.

Interestingly, considering $q(u)$ as the density of states and $\tilde{u}$ as minimum energy state, the condensation phenomenon in this model is related to the phenomena in ideal Bose-Einstein condensation where a finite number of Bosons occupy the lowest energy state.

2.3 Stationary state in mean-field approximation

Unlike in the previous models, both short and long jumps are allowed and the product measure is not exact in the model considered in this section. The specific model studied here is motivated from one-dimensional aggregation-fragmentation model in which either the entire mass cluster or a single particle in the aggregate hop with rate one and w respectively to the nearest neighbor and coalesces. [43]. In the lattice gas picture, these dynamical rules represent hopping of a particle to the farthest (nearest) empty site without

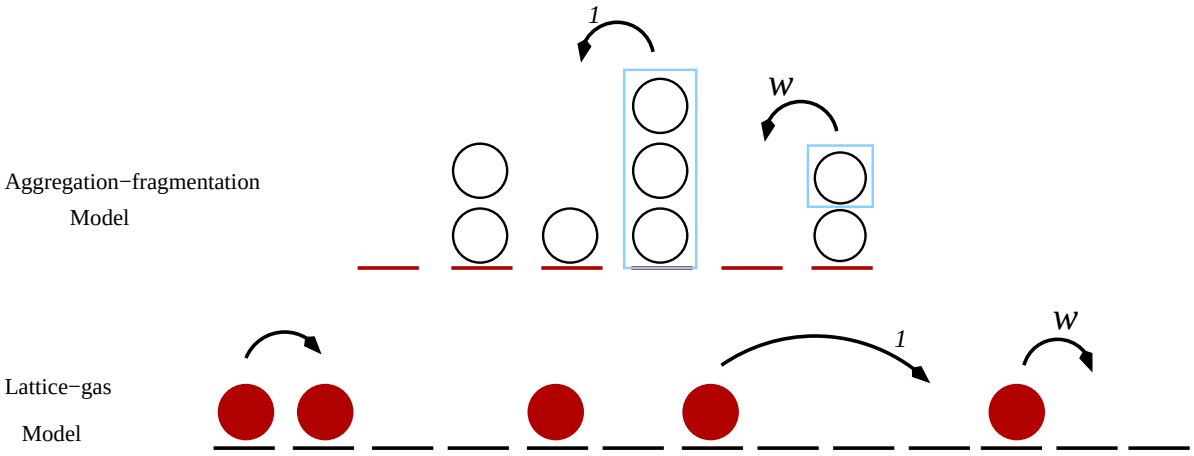

Fig. 2.3 Figure to illustrate the mapping of lattice gas model (bottom) with short and long range hops (bottom) and aggregation-fragmentation model (top).

any preferred direction with rate one (w) as demonstrated in Fig. 2.3. For the aggregation-fragmentation model, it is known that a biased hop rate does not show phase transition [51], so we focus only on the bidirectional case which has a condensation transition at a finite critical point. The steady state of the model is solved within a mean-field approximation [43] which shows very good agreement with the stationary state properties of the one-dimension model [52, 44]. The master equation for the evolution of the probability $p(m,t)$ of any site having mass m at any time t within the mean field approximation is

$$\begin{aligned}\frac{dp(m,t)}{dt} &= -(1+w)[1+\sigma(t)]p(m,t) + wp(m+1,t) + w\sigma(t)p(m-1,t) + p*p\ ,\ m\le 1\ ,\\ \frac{dp(0,t)}{dt} &= -(1+w)\sigma(t)p(0,t) + wp(1,t) + \sigma(t)\ ,\end{aligned} \tag{2.41}$$

where $\sigma(t) = 1 - p(0,t)$ is the occupation probability and $p*p = \sum_{m'=1}^{m} p(m',t)p(m-m',t)$ is a convolution term that describes the coalescence of two masses. To solve the above master equation in stationary state, we use the generating function $Q(y) = \sum_{m=0}^{\infty} p(m)y^m$ for mass distribution which is known to be [43]

$$Q(y) = 1-\sigma+\frac{w+2\sigma+w\sigma}{2} - \frac{w}{2y} - \frac{w\sigma y}{2} + w\sigma\frac{1-y}{2y}\sqrt{(y-y_+)(y-y_-)}\ , \tag{2.42}$$

where $y_\pm = (w+2\pm 2\sqrt{w+1})/w\sigma$. Setting the first derivative of the generating function (2.42) to zero at $y=1$ gives the relation between ρ and σ as

$$2\rho = w(1-\sigma) - w\sigma\sqrt{(y_+-1)(y_--1)}. \tag{2.43}$$

For a fixed w, the above density and occupation probability relation is defined till $y_- \leq 1$. At $y_- = 1$ we obtain the critical density $\rho_c = \sqrt{1+w}-1$ where the mass distribution $p(m)$ changes from an exponential distribution to an algebraic decay as $m^{-5/2}$. For $\rho > \rho_c$, the mass distribution is same as ρ_c, however the excess mass density $\rho-\rho_c$ clusters together to form an aggregate.

Apart from static properties of the model, the steady state dynamics have also been studied and the numerics show that the dynamical exponent is $z=2$ [52]. (In Sec. 4.6.3, we will present a better understanding of this dynamical exponent by calculating the autocorrelation function of the model).

2.4 Dynamics for the model with hole-dependent hop rates

For the hop rate (2.12), extensive studies have been done for the dynamics in the condensed phase in the ZRP both in mean-field approximation [5] and using random walk arguments in one-dimension [53]. These studies mainly focus on the coarsening process in which one drives a system infinitely fast starting from a fluid phase to a condensed phase or to the critical point. The objective of such studies is to determine the timescale for the growth of the condensate. In general, analytical study of the dynamics even in one dimension, is difficult since it requires joint distribution of the mass distribution; however, it is possible to make some analytical progress within a mean-field approximation [54, 55]. In the mean-field system, we allow particles to hop from any site to any other site, with a rate dependent on the number of particles at the departure site. Assuming a factorized steady state, the master equation for the evolution of the single site probability distribution $p(n,t)$ at a given

time t is given by

$$\begin{aligned} \frac{dp(n,t)}{dt} &= u(n+1)p(n+1,t) + \langle u(t)\rangle p(n-1,t) - u(n)p(n,t) - \langle u(t)\rangle p(n,t)\ ,\ n>0\ , \\ \frac{dp(0,t)}{dt} &= u(1)p(1,t) - \langle u(t)\rangle p(0,t)\ , \end{aligned} \tag{2.44}$$

where $\langle u(t)\rangle = \sum_{m=1}^{\infty} u(m)p(m,t)$ is the average value of the hop rate. The equation is non-linear and has been solved for the late time dynamics of both the condensed phase, and at the critical point [5].

2.4.1 In condensed phase

Mean-field analysis by Godréche [5] suggests that the mean condensate size $\langle m(t)\rangle$ grows in time as $t^{1/2}$. This scaling can be understood by a random walk argument in a one dimensional biased ZRP [53]. Moreover, in a symmetric case, mean condensate size grows as $t^{1/3}$ [5, 53].

2.4.2 At the critical point

Dynamical scaling at the critical point has been obtained via exact calculation in the mean-field geometry, and numerical simulations in one dimension. However, the scaling is different in mean-field and one-dimension. In mean-field, the dynamical scaling calculated is the same as in the condensed phase and this work has been analytically done by Godréche [5], which we will briefly explain here. The evolution process at the critical point consists of two regimes:

Regime I: when m is fixed and t is large, the convergence of $p(m,t)$ to stationary state mass distribution $p(m)$ occurs in the following manner

$$p(m,t) = p(m)(1 + v_m t^{-\alpha})\ , \tag{2.45}$$

where $v_m = v_0 + m\ A$, here A is constant, and $p(m) \sim m^{-b}$.

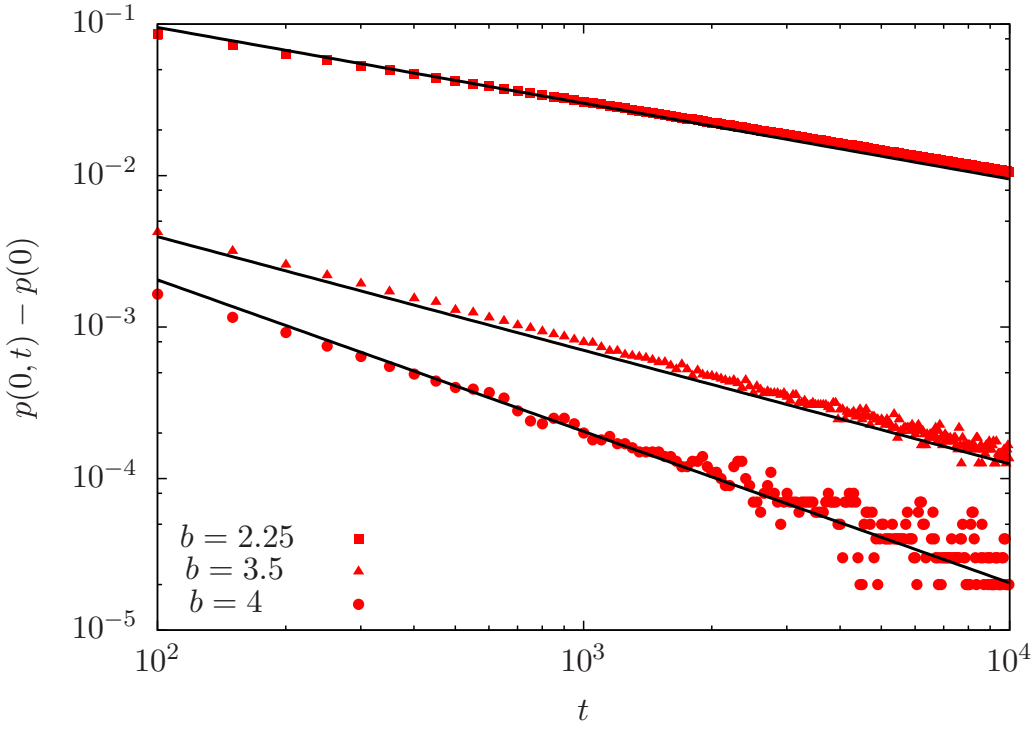

Fig. 2.4 Figure shows the power law decay of the probability $p(0,t) - p(0)$ with time after a fast quench to the critical point, b_c starting from $b = 0$ in mean-field geometry. The line shows the exponent $(b-2)/\hat{z}$ for $b > 3$ and $1/2$ for $b = 2.25$.

Regime II: when m and t are simultaneously large such that the ratio of these two variable is constant, then the similarity solution is given as

$$p(m,t) \approx p(m)F(k)\ ,\ k = m\ t^{-1/\hat{z}}\ , \tag{2.46}$$

where the critical coarsening exponent, $\hat{z} = 2$. Further, the exponent α is calculated from the sum rules $\sum_m p(m,t) = 1$ and $\sum_m m p(m,t) = \varrho$ respectively and for $b > 3$, it is known to be $(b-2)/\hat{z}$ [5, 54]. Moreover, for $2 < b < 3$, due to divergence of the second moment of steady state mass distribution, the sum rule does not hold and, to the best of our knowledge, the exponent α is not known in this case. However, on numerical integration (2.44), we find that for $2 < b < 3$, the exponent $\alpha = 1/\hat{z}$ as shown in Fig. 2.4.

In one dimension, numerical studies show that the coarsening exponents are [5]

$$\hat{z} \simeq \begin{cases} 3 & \text{for bidirectional ZRP ,} \\ 5 & \text{for unidirectional ZRP.} \end{cases} \tag{2.47}$$

2.5 Numerical procedures

Numerical studies are amenable for all the above mentioned lattice gas models and mass models. In particular, dynamical Monte Carlo simulations and numerical evaluation of the partition function (A.1) in the canonical ensemble are useful to study the model behaviour in both phases (fluid phase and jammed/condensed phase) and at the critical point.

In Monte-Carlo simulations, we have followed the random sequential algorithm in which:

- A site is picked at random by generating a random number from 1 to L and selected if it is occupied and the arrival site is unoccupied.
- Then the jump probability $u_i(m,n)/N$ where N is the normalization constant of the hop rate function is calculated which is compared to a random variable between 0 to 1. If the random variable is less than the jump probability, a particle hops to a nearest neighbor.

The algorithm is repeated until the steady state is reached. After reaching steady state, time averages of various quantities of interest are calculated. These time averages are equivalent to the ensemble average, assuming the ergodic hypothesis is valid. In order to overcome finite size effects, simulations are performed for reasonably large systems.

We also solved the recursion relation for the partition function (2.5) numerically to calculate the various quantities in the canonical ensemble.

2.6 Summary

In this Chapter, we introduced various one-dimensional lattice gas models in which particles hop from one site to an empty neighboring site with hop rates that may depend on

the number of vacancies as well as the particle label itself. We reviewed some of the known results for the stationary state and the dynamics of these models which we have used in the present thesis.

Chapter 3

Static density-density correlation function

3.1 Introduction

As discussed in Chapter 2, there exists exhaustive literature on the steady state properties of the Exclusion Process (EP) because of its mapping to the Zero Range Process (ZRP). However, a fundamental question regarding the spatial correlation function in the exclusion process with jamming transition has not been addressed in previous studies. For the one-dimensional totally asymmetric simple exclusion process (TASEP) on a ring which is a special case of the exclusion models studied here, the result for the density-density correlation function is trivial because all configurations are equally likely in the steady state. A non-trivial exact formula for the TASEP with open boundaries where particles enter with rate α at the left end and leave with rate β at the right was given in [56] for arbitrary system size. However, their limiting behaviour has not been calculated to the best of our knowledge, especially at the critical phase line $\alpha = \beta < \frac{1}{2}$. Recently the particle-particle correlation function for the EP with hole-dependent rates was calculated in the laminar phase for certain special choices of hopping rates in the grand canonical ensemble [57].

In this Chapter, we study the two-point correlation function at the critical point in the thermodynamic limit [2, 3] and find a simple analytical formula for the generating function

of two-point function with arbitrary hop rates. This result is applied to the models reviewed in Chapter 2. We also give a result for the two-point function in the canonical ensemble for a system of arbitrary size [2].

The plan of the Chapter is as follows: we show a calculation of the steady state particle-particle correlation function in the canonical ensemble in Sec. 3.2 and obtain an exact expression for it for any system size. We then find an exact expression for the generating function of the correlation function in the thermodynamic limit. In Sec. 3.3, for $u(n) = 1 + (b/n)$, we show that at the critical density, the correlation function decays as a power law with continuously varying exponent. The behaviour of the correlation function in the laminar phase is also studied. In Sec. 3.4, we present a simpler calculation for two-point correlation function in the thermodynamic limit. Later, in Secs. 3.5 and 3.6, we present the results for the two-point function for the models with generalised hole-dependent hop rates and with particlewise disorder respectively. In Sec. 3.7 we extend our calculation to systems with short and long jumps. We finally conclude with a summary of our results and discussion in Sec. 3.8.

3.2 Two-point correlation function in canonical ensemble

In this section, we study a homogeneous system in which the hop rates are such that the stationary state is a product measure (2.2).

3.2.1 Exact formula for finite system

We define the two-point connected correlation function

$$S(r) = \langle \eta_i \eta_{i+r} \rangle - \rho^2 \ , \ r > 0 \ , \tag{3.1}$$

in a system of L sites with N particles. Here, η_i takes a value 1 when site i is occupied and 0 when site is empty. Let us consider a set of configurations in which the r sites from i to $i + r - 1$ contain k holes. Then the contribution to the correlation function $\langle \eta_i \eta_{i+r} \rangle$ comes

from only those configurations in which both the ith and $(i+r)$th sites are occupied. Using the mapping between EP and ZRP described in Sec. 2.2 and summing over all the particle configurations in front of the ith and $(i+r)$th particle, we get

$$\langle \eta_i \eta_{i+r} \rangle = \sum_{k=k_{min}}^{k_{max}} \frac{\tilde{Z}_{r-k,k}\, \tilde{Z}_{N-r+k,L-N-k}}{Z_{L,N}} \tag{3.2}$$

$$= \rho \sum_{k=k_{min}}^{k_{max}} \frac{\tilde{Z}_{r-k,k}\, \tilde{Z}_{N-r+k,L-N-k}}{\tilde{Z}_{N,L-N}}, \tag{3.3}$$

where we have used (A.3) to arrive at the last expression. As the total number of particles is conserved, the maximum number of particles in the first cluster can be $N-1$. In other words, $r-k \leq N-1$ which gives $k_{min} = \max(0, r-N+1)$, as the lower limit k_{min} can not be below zero. Also the local conservation in the first cluster with r sites requires that $k \leq r-1$. Thus we find that $k_{max} = \min(L-N, r-1)$ since k_{max} can not exceed the total number of holes in the system.

3.2.2 Exact expression for infinitely large system

It is evident from (3.3) that the partition function at all densities is required to evaluate the correlation function. However, barring some special cases that are discussed in Appendix B.1 and B.2, it does not seem possible to calculate the exact partition function $\tilde{Z}_{\mathscr{L},\mathscr{M}}$ for all densities. In the following subsections, we will calculate the two-point correlation function in the thermodynamic limit as the problem is analytically tractable in this limit. For $L \to \infty$ and finite r, we first note that the limits in the sum which is appearing in (3.3) simplify to $k_{min} = 0$ and $k_{max} = r-1$. Furthermore, inspired by equilibrium statistical mechanics, we conjecture that there exists a 'free energy' $\tilde{F}(\rho)$ defined as

$$\tilde{F}(\rho) = -\lim_{\mathscr{L}\to\infty} \frac{\ln \tilde{Z}_{\mathscr{L},\mathscr{M}}}{\mathscr{L}}. \tag{3.4}$$

For the hop rate (2.12) and using the recursion equation (2.5), we calculated the partition function $\tilde{Z}_{\mathscr{L},\mathscr{M}}$ as a function of density for various system sizes. Fig. 3.1 shows that the

scaled logarithmic partition function indeed approaches a limiting function with increasing system size.

Thus for large L, using (3.4), we can write [58]

$$\ln\left(\frac{\tilde{Z}_{N-r+k,L-N-k}}{\tilde{Z}_{N,L-N}}\right) = k\mu - (r-k)P\,, \tag{3.5}$$

where the chemical potential μ and the pressure P are given by

$$\mu = \frac{\partial(\mathscr{L}\tilde{F})}{\partial\mathscr{M}}\Big|_{\mathscr{L}} = \tilde{F}'(\varrho)\,, \tag{3.6a}$$

$$P = -\frac{\partial(\mathscr{L}\tilde{F})}{\partial\mathscr{L}}\Big|_{\mathscr{M}} = -\tilde{F}(\varrho) + \varrho\tilde{F}'(\varrho)\,, \tag{3.6b}$$

and the prime stands for derivative with respect to ϱ. Using (3.5) in the expression (3.3) for correlation function $\langle\eta_i\eta_{i+r}\rangle$ and the boundary condition $\tilde{Z}_{0,n} = \delta_{n,0}$ [refer to the discussion after (A.2)], we get

$$\langle\eta_i\eta_{i+r}\rangle = \rho\, e^{-rP}\sum_{k=0}^{r}\tilde{Z}_{r-k,k}\, e^{k(\mu+P)}\,,\ r\geq 0 \tag{3.7}$$

$$= \rho\, e^{r\mu}\sum_{k=0}^{r}\tilde{Z}_{k,r-k}\, e^{-k(\mu+P)} \tag{3.8}$$

$$= \rho\, e^{r\mu}\sum_{k=0}^{r}\frac{k}{r}\, Z_{r,k}\, e^{-k(\mu+P)} \tag{3.9}$$

$$= -\frac{\rho}{r}\, e^{r\mu}\frac{d}{d(\mu+P)}\sum_{k=0}^{r} Z_{r,k}\, e^{-k(\mu+P)}. \tag{3.10}$$

Thus, the correlation function is related to the *grand canonical* partition function of the EP with r sites, which is not known.

However, as explained in Sec. 2.2, the grand canonical partition function for ZRP is known. We therefore define the generating function of the correlation function as $G(y) =$

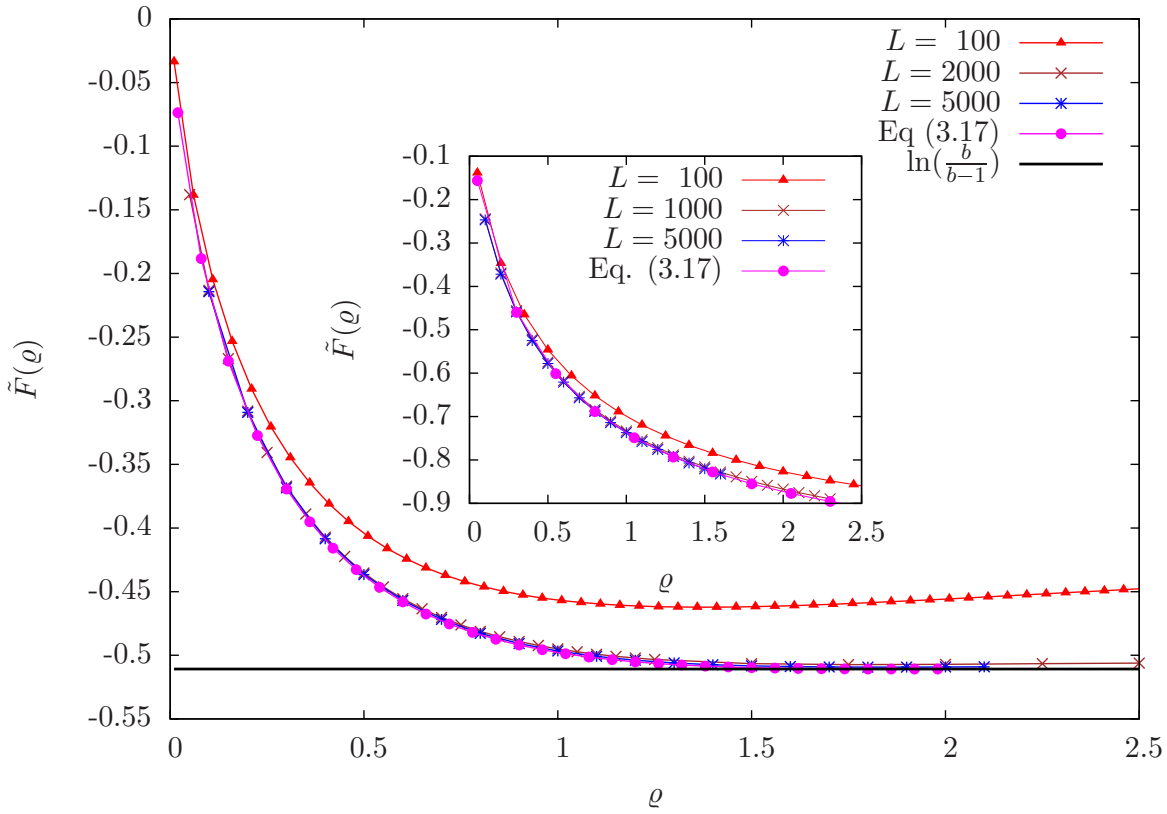

Fig. 3.1 Free energy $\tilde{F}(\varrho)$ for hop rate (3.18) as a function of density ϱ for $b = 3/2$ (inset) and $b = 5/2$ (main) for different system sizes. The data for finite-sized systems is obtained by numerically solving the recursion equation (2.5) and is compared with the result (3.17) for infinitely large system.

$\sum_{r=0}^{\infty} y^r S(r)$ which, on using (3.8), works out to be

$$G(y) = \rho \sum_{l=0}^{\infty} (ye^{-P})^l \sum_{n=0}^{\infty} \tilde{Z}_{l,n} (ye^{\mu})^n - \frac{\rho^2}{1-y} \tag{3.11}$$

$$= \frac{\rho}{1 - ye^{-P} g(y\omega)} - \frac{\rho^2}{1-y}, \tag{3.12}$$

where $\omega = e^{\mu}$. Furthermore, we recall that the equation of state in the grandcanonical ensemble is given by [58]

$$P\mathscr{L} = \ln(\tilde{\mathscr{Z}}_{\mathscr{L}}(\omega)) = \mathscr{L} \ln g(\omega), \tag{3.13}$$

which gives $e^{-P} = 1/g(\omega)$. Thus we arrive at our main result, namely

$$G(y) = \frac{\rho\, g(\omega)}{g(\omega) - y\, g(y\omega)} - \frac{\rho^2}{1-y}\,, \tag{3.14}$$

where the fugacity $\omega(\rho)$ is determined by (2.9). The correlation function is then given by

$$S(r) = \frac{1}{r!}\frac{d^r G(y)}{dy^r}\Big|_{y=0} \tag{3.15}$$

$$= \oint_C \frac{dy}{2\pi i}\frac{G(y)}{y^{r+1}}\,, \tag{3.16}$$

where the integral in the last expression is along the closed curve C around the origin [59]. We check that $S(0) = \rho(1-\rho)$ is obtained from the above expression. The behavior at $r \to \infty$ is obtained by taking the limit $y \to 1$. Expanding (3.14) close to $y = 1$ and using (2.9), we see that $G(y)$ (and hence $S(r)$) vanishes as $r \to \infty$.

Before proceeding further, we note that due to (3.6) and (3.13), the free energy can be written as

$$\tilde{F}(\rho) = \rho\,\mu - \ln g(\omega). \tag{3.17}$$

This expression is also plotted in Fig. 3.1 for hop rate (3.18) with $b = 3/2$ and $5/2$, and we see that it matches well with the results for large systems. We note that $\tilde{F}(\rho)$ is a decreasing function of the density for $b < 2$, but it saturates to $-\ln g(1)$ at high density for $b > 2$.

3.3 Correlation function for hole-dependent hop rates

We consider here the hole-dependent rate which is given as

$$u(m) = 1 + \frac{b}{m}\,,\ m > 0\,, \tag{3.18}$$

where the parameter $b \geq 0$ and m is the number of holes (vacancies) in front of a particle.

Using the approach described in the last section for b = 0, we can obtain the known trivial results of TASEP as described in Appendix B.1. Although we will focus on the rate

(3.18) which models 'attractive interactions' between particles in the ZRP, we also consider the case of free particles in Appendix B.2 for which $u(m) = m$ [60]. In the latter case, each particle is endowed with an exponential clock that ticks at rate one, but since the particles are free and act independently, the total hop out rate is equal to the number of particles at the site.

We now apply the general result (3.14) for the generating function of the correlation function to the choice (3.18) of the hop rates. The correlation function can be easily obtained numerically from (3.14) for an infinitely large system, and these results are shown along with those obtained using the exact result (3.3) for a finite system in Figs. 3.2, 3.3 and 3.4, and see that the latter approaches the result obtained from (3.14) with increasing system size. In the following subsections, we obtain analytical results for $S(r)$ using (3.14).

3.3.1 Laminar phase: $0 < b < 2$

When $b = 0$, we obtain the well known TASEP [16] on a ring for which the steady state is known exactly. This case is discussed briefly in Appendix B.1 using (3.14). For $b = 1$, the generating function $g(\omega)$ given by (2.15) takes a particularly simple form:

$$g(\omega) = -\frac{\ln(1-\omega)}{\omega}. \tag{3.19}$$

Therefore, from (3.14), we get the generating function of the correlation function as

$$G(y) = \frac{\rho \ln(1-\omega)}{\ln(y_0-1) - \ln(y_0-y)} - \frac{\rho^2}{1-y}, \tag{3.20}$$

where $y_0 = 1/\omega > 1$. The density-fugacity relation (2.9) is given by

$$\rho = -\frac{1-\omega}{\omega} \ln(1-\omega), \ \omega < 1. \tag{3.21}$$

To calculate the correlation function, we consider the following integral in the complex-y plane along a closed contour C' of Fig. B.1 wrapped around the branch cut at y_0 which

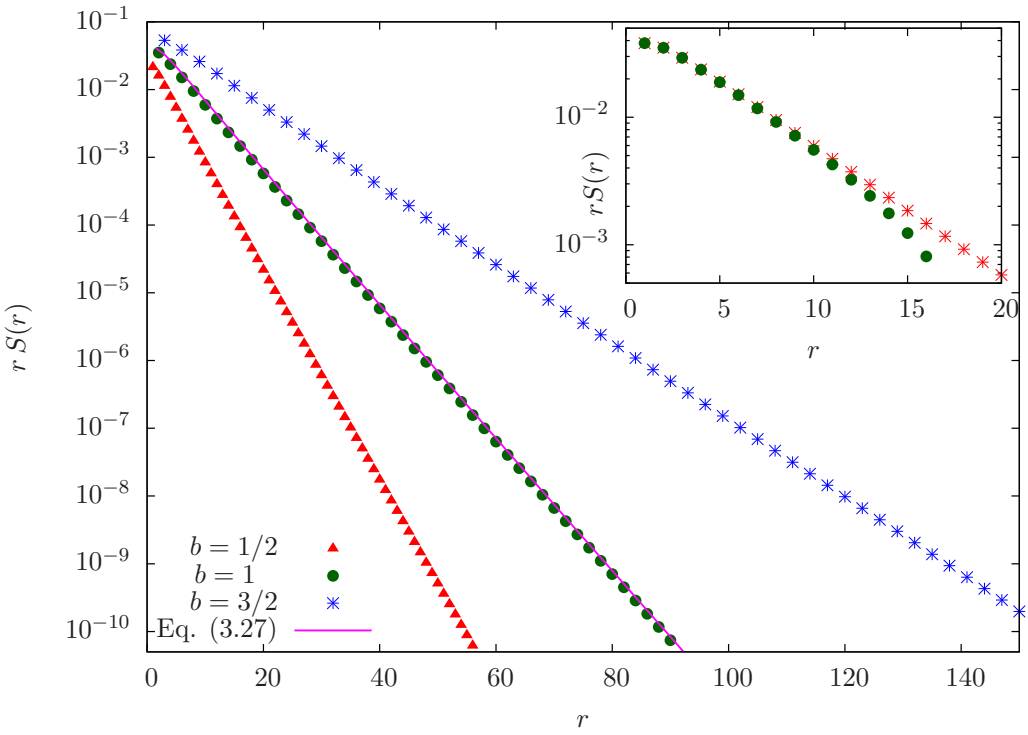

Fig. 3.2 Decay of the correlation function in the laminar phase at $\rho = 0.4$ for various $b < 2$ for hop rate (2.12) in the infinite system. The analytical result (3.27) for $b = 1$ is also shown. The inset compares the correlation function for $b = 1$ obtained using (3.3) for $L = 10^4$ and (3.14) for infinite system.

consists of a large circle of radius R about the origin and a small circle of radius ϵ about y_0:

$$I_1 = \frac{1}{2\pi i} \oint_{C'} \frac{dy}{y^{r+1}} \frac{\rho \ln(1-\omega)}{\ln(y_0-1) - \ln(y_0-y)}. \tag{3.22}$$

As the integrand has a simple pole at $y = 1$ and poles of order $r+1$ at $y = 0$, due to (3.16), the residue at these poles immediately gives $S(r)$. It is easy to check that the contribution from the integrals over the large and the small circle vanishes when $R \to \infty$ and $\epsilon \to 0$. Since the integrand in (3.22) also has a branch cut singularity at $y = y_0$, we finally obtain

$$S(r) = \frac{1}{2\pi i} \left(\int_{AB} \frac{dy}{y^{r+1}} \frac{\rho \ln(1-\omega)}{\ln(y_0-1) - \ln(y_0-y)} + \int_{B'A'} \frac{dy}{y^{r+1}} \frac{\rho \ln(1-\omega)}{\ln(y_0-1) - \ln(y_0-y)} \right), \tag{3.23}$$

where $y - y_0 = x$ along AB and $y - y_0 = xe^{i2\pi}$ along $B'A'$. Since the correlation function is real, writing $-x = xe^{-i\pi}$, we get

$$\begin{aligned} S(r) &= \frac{\rho \ln(1-\omega)}{2\pi i} \int_0^\infty \frac{dx}{(y_0+x)^{r+1}} \left(\frac{1}{\ln(y_0-1) - \ln x + i\pi} - \frac{1}{\ln(y_0-1) - \ln x - i\pi} \right) \\ &= \frac{-\rho \ln(1-\omega)(1-\omega)}{y_0^r} \int_0^\infty \frac{dx}{(1+x(1-\omega))^{r+1}} \frac{1}{(\ln x)^2 + \pi^2}. \end{aligned} \tag{3.24}$$

We are not able to perform the above integral exactly. But an approximate expression can be found for large r as follows:

$$S(r) \approx \frac{-\rho \ln(1-\omega)(1-\omega)}{y_0^r} \int_0^\infty dx \, \frac{e^{-rx(1-\omega)}}{(\ln x)^2 + \pi^2} \tag{3.25}$$

$$\approx \frac{-\rho \ln(1-\omega)(1-\omega)}{y_0^r} \int_0^{\frac{1}{r(1-\omega)}} \frac{dx}{(\ln x)^2 + \pi^2} \tag{3.26}$$

$$\approx \frac{\rho |\ln(1-\omega)|}{r} \frac{e^{-r|\ln\omega|}}{[\ln(r(1-z))]^2 + \pi^2}, \tag{3.27}$$

where the last expression is obtained after an integration by parts and the fugacity is determined in terms of density from (3.21). The last result is plotted against that obtained by solving (3.14) numerically, and we see an excellent agreement. Similar to the $b = 1$ case, the correlation function shows an exponential decay (with power law correction) for $0 < b < 2$, as can be seen in Fig. 3.2.

3.3.2 At the critical density: $b > 2$

We now calculate the correlation function at the critical density (2.17) using (3.14). At the critical density ρ_c, as the fugacity $\omega = 1$, we get

$$G(y) = \frac{\rho_c \, g(1)}{g(1) - y \, g(y)} - \frac{\rho_c^2}{1-y}. \tag{3.28}$$

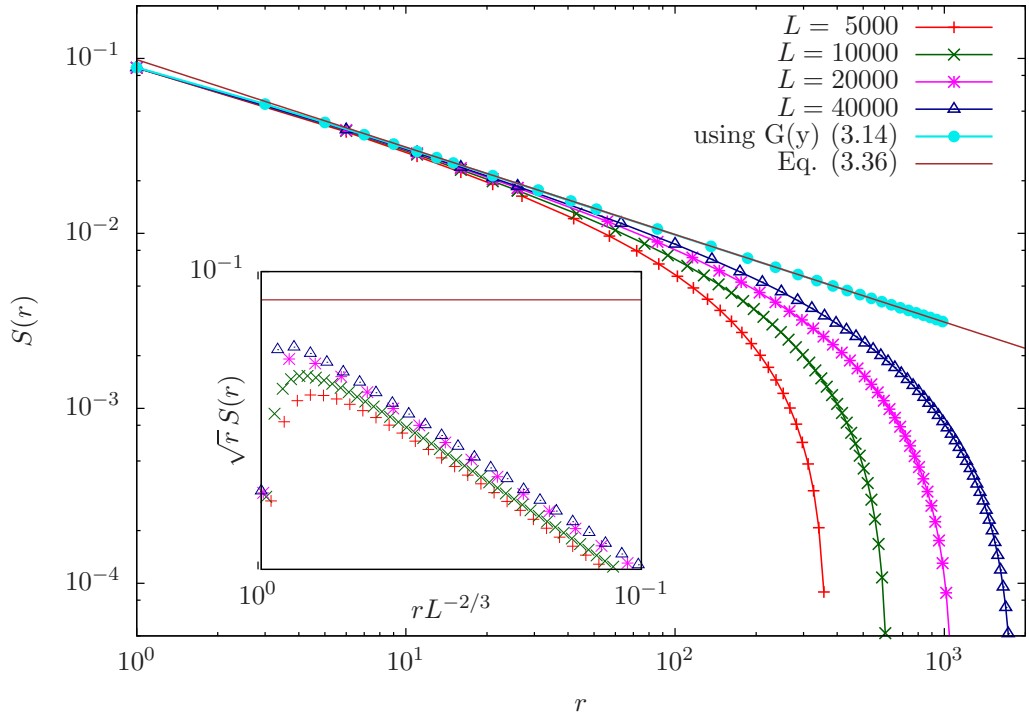

Fig. 3.3 Decay of spatial correlation function with distance at the critical density for hop rate (3.18) for $b = 5/2$. The data for finite-sized systems is obtained by numerically solving (2.5) and (3.3), while the result in the thermodynamic limit is obtained using (3.14). The analytical result (3.36) valid for large inter-particle distances is also shown. The inset shows the data collapse of $S(r,L)$ for different system sizes using (3.47).

We first consider the case when b is not an integer. For large r, we can expand $g(y)$ given by (2.15) about $y = 1$. Using equation (15.3.6) of [49], we obtain

$$g(y) = g(1) - sg'(1) + \frac{s^2}{2!}g''(1) + \ldots + \frac{(-s)^n}{n!}g^{(n)}(1) + \alpha s^{b-1} + \mathcal{O}(s^b)\,, \tag{3.29}$$

where $s = 1 - y$. Here we have retained analytic terms in the Taylor series expansion up to nth order where n is the integer part of $b-1$ and the leading non-analytic term. In the

above expression, $\alpha = b\pi\csc(b\pi)$ and $g(1) = b/(b-1)$. Then we have

$$G(s) = \int_0^\infty dr\ e^{-sr} S(r) \tag{3.30}$$

$$= \frac{\rho_c}{\frac{s}{\rho_c} + c_2 s^2 + \ldots + c_n s^n - \frac{\alpha s^{b-1}}{g(1)}} - \frac{\rho_c^2}{s} \tag{3.31}$$

$$= \frac{\rho_c^2}{s}\left[\frac{\alpha\rho_c s^{b-2}}{g(1)} - \rho_c(c_2 s + \ldots + c_n s^{n-1})\right], \tag{3.32}$$

where the coefficients c_i are writeable in terms of the derivatives of $g(\omega)$ evaluated at one. Since $G(s)$ has a branch cut singularity at $s = 0$, its inverse Laplace transform is given by [59]

$$S(r) = \frac{1}{2\pi i}\int_{-i\infty}^{i\infty} ds\ e^{sr}\ G(s) \tag{3.33}$$

$$= -\frac{\rho_c^3}{2\pi i}\int_{-i\infty}^{i\infty} ds\ e^{sr}\left(c_2 + c_3 s + \ldots + c_n s^{n-2} - \frac{\alpha s^{b-3}}{g(1)}\right). \tag{3.34}$$

An integral similar to above also appears in the calculation of the canonical partition function of the ZRP [47] and we can use those results here. In the above expression, the first integral is $\delta(r)$ and all the integrals (barring the last one) are the derivatives of the delta function. Therefore for large r, these integrals vanish, and we are left with

$$S(r) = \frac{\alpha\rho_c^3}{g(1)}\int_{-i\infty}^{i\infty}\frac{ds}{2\pi i}\ e^{sr}\ s^{b-3}. \tag{3.35}$$

The above integral can be obtained from the integral I_2 calculated in the Appendix B.3 by setting $c = \delta = 0$, and we obtain

$$S(r) = \frac{\rho_c^2\,\Gamma(b-1)}{r^{b-2}}. \tag{3.36}$$

This result is compared against that obtained using (3.14), and we see an excellent match at large r.

When b is an integer, as before, we expand $g(y)$ about $y = 1$ and using (15.3.11) of [49]), we obtain

$$g(1-s) = g(1) - sg'(1) + \frac{s^2}{2!}g''(1) + \ldots + \frac{(-s)^n}{n!}g^{(n)}(1) + \beta s^{b-1}\ln s\,, \tag{3.37}$$

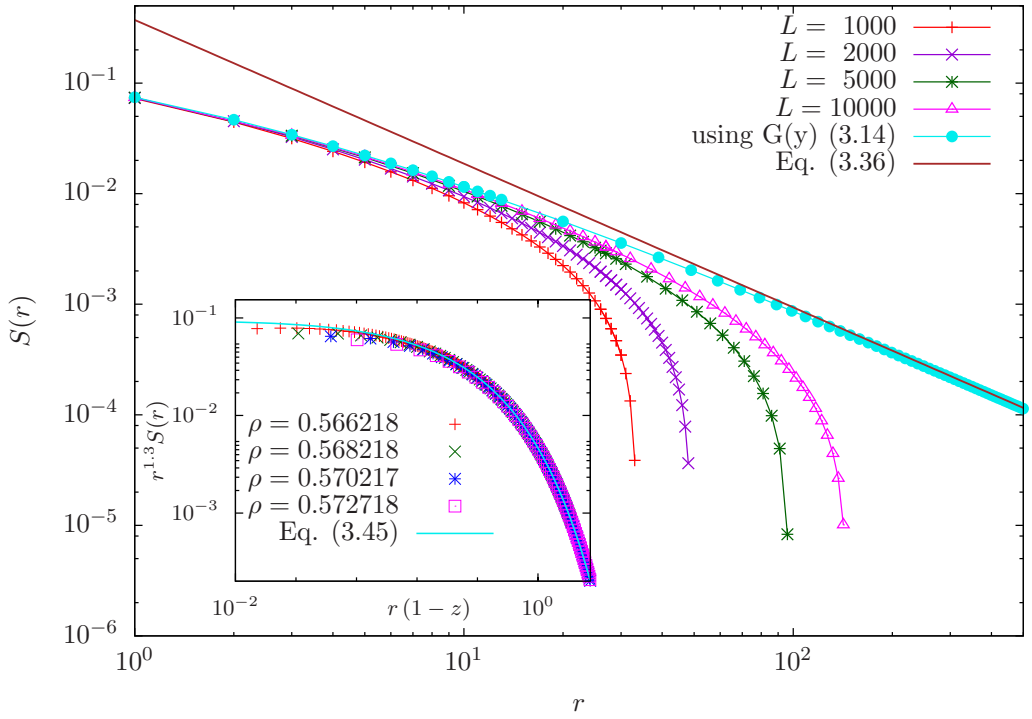

Fig. 3.4 Decay of spatial correlation function with distance at the critical density for hop rate (3.18) for $b = 3.3$. The data for finite-sized systems is obtained by numerically solving (2.5) and (3.3), while the result in the thermodynamic limit is obtained using (3.14). The analytical result (3.36) valid for large inter-particle distances is also shown. The inset shows the data collapse of the correlation function for different densities close to the critical point in the laminar phase for infinite system using (3.45).

where $\beta = (-1)^b b$. Following the same steps as described above, we get

$$S(r) = \frac{\beta\rho_c^3}{g(1)} \int_{-i\infty}^{i\infty} \frac{ds}{2\pi i}\, e^{sr}\, s^{b-3} \ln s \tag{3.38}$$

$$= \frac{\rho_c^3 \beta}{g(1) r^{b-2}} \int_{-i\infty}^{i\infty} \frac{ds}{2\pi i}\, e^s s^{b-3} (\ln s - \ln r) \tag{3.39}$$

$$= \frac{\rho_c^3 \beta}{g(1) r^{b-2}} \int_{-i\infty}^{i\infty} \frac{ds}{2\pi i}\, e^s s^{b-3} \ln s\,, \tag{3.40}$$

where we have used that b is an integer to arrive at the last equation. As the above integrand has a branch cut at $s = 0$, proceeding in a manner similar to that described in Appendix B.3 with $c = t = 0$, we find the above integral to be $(-1)^{b-2}\, \Gamma(b-2)$ which shows that (3.36) is valid for integer b as well.

3.3.3 Above the critical density: $b > 2$

We now consider the behavior of the correlation function in the laminar phase at a density close to the critical point. Since the fugacity is below one here, we write $\delta = 1-\omega$ and expand (2.9) about $\omega = 1$ to find the relationship between δ and ρ. We find that

$$\frac{1}{\rho} = \begin{cases} \frac{1}{\rho_c} - \frac{\alpha(b-1)g'(1)}{g^2(1)}\,\delta^{b-2}\,, & 2<b<3\,, \\ \frac{1}{\rho_c} + \frac{g'(1)}{g(1)}\left(\frac{g'(1)}{g(1)} - \frac{g''(1)}{g'(1)} - 1\right)\delta\,, & b>3. \end{cases} \tag{3.41}$$

The next order corrections to the above expression can also be worked out, and turn out to be of the order δ for $2<b<3$, δ^{b-2} for $3<b<4$ and δ^2 for $b>4$.

For large distances and densities close to the critical density, we now expand the generating function $G(y,\omega)$ in (3.14) about $y=1$ and $\omega=1$. For $b>3$, on using (3.41), we obtain

$$G(s,\delta) = \frac{\alpha\rho^3}{g(1)}\,\frac{(s+\delta)^{b-1}-\delta^{b-1}}{s^2}\,, \tag{3.42}$$

where, as before, $s=1-y$ and we have dropped the analytic terms as they do not contribute to $S(r,\omega)$ for the same reasons as described in the last subsection. We then have

$$S(r,\omega) = \frac{\alpha\rho^3}{g(1)}\int_{c-i\infty}^{c+i\infty}\frac{ds}{2\pi i}\,e^{sr}\,\frac{(s+\delta)^{b-1}-\delta^{b-1}}{s^2}\,, \tag{3.43}$$

where c is a positive real number. The above integral is calculated in Appendix B.3, and we find that in the limit $\delta = 1-\omega \to 0, r\to\infty$ with $r\delta$ finite, the correlation function is of the following scaling form

$$S(r,\omega) = r^{2-b}\,\mathscr{H}(r(1-\omega))\,, \tag{3.44}$$

where the scaling function

$$\mathscr{H}(x) = (b-2)\Gamma(b-1)\rho_c^2\,e^{-x}\left[(x+b-1)e^x E_{b-1}(x) - 1\right]\,, \tag{3.45}$$

is a decreasing function of x. In the above expression, $E_n(x) = \int_1^\infty d\delta\; e^{-x\delta}\delta^{-n}$ is the exponential integral. By carrying out a calculation similar to above, it can be checked that the

results (3.44) and (3.45) hold for $2 < b < 3$ and integer b as well. The inset of Fig. 3.4 shows the data collapse for the correlation function for various densities close to the critical point and the scaling function.

Using the asymptotic properties of the exponential integral $E_n(x)$ [49], we find that the scaling function $\mathscr{H}(x) \overset{x\to 0}{\sim} \Gamma(b-1)\rho_c^2$ which thus reproduces the result at the critical point obtained in the last subsection. At large x, as the scaling function $\mathscr{H}(x) \overset{x\to\infty}{\sim} \Gamma(b)(b-2)\rho_c^2\, e^{-x}/x^2$, the correlation function decays exponentially fast with inter-particle distance r. This analysis yields the correlation length defined by $x = r/\xi$ to be

$$\xi \sim (1-\omega)^{-1} \sim (\rho - \rho_c)^{-\nu}\,, \tag{3.46}$$

which, by virtue of (3.41) gives $\nu = 1/(b-2)$ for $b < 3$ and 1 for $b > 3$.

From the numerical data shown in Figs. 3.3 and 3.4 at the critical point, we note that the finite size effects set in early on. For example, in Fig. 3.3 for $b = 5/2$ and a system size $L = 10^4$, a power law is seen for about a decade only. This makes a numerical determination of the correlation function exponent difficult. Here we have given an expression (3.14) for the generating function of the two-point correlation function for an infinite system which can easily generate several decades of data. For a finite system with L sites, we expect the correlation function to be of the following scaling form:

$$S(r,L) = \frac{1}{r^{b-2}}\,\mathscr{F}(rL^{-z})\,, \tag{3.47}$$

where the scaling function $\mathscr{F}(x)$ is a constant for $x \ll 1$ and decays for $x \gg 1$. In the ZRP, the average mass cluster at the critical point scales as $\mathscr{L}^{1/(b-1)}, b < 3$ and $\sqrt{\mathscr{L}}, b > 3$ [47]. If we make the reasonable assumption that at the critical density, there is a single length scale in the system under consideration and is set by the typical headway, we expect $z = 1/(b-1)$ for $b < 3$. This expectation is consistent with the data shown in the inset of Fig. 3.3 for $b = 5/2$ where we see that the data collapse gets better with increasing L.

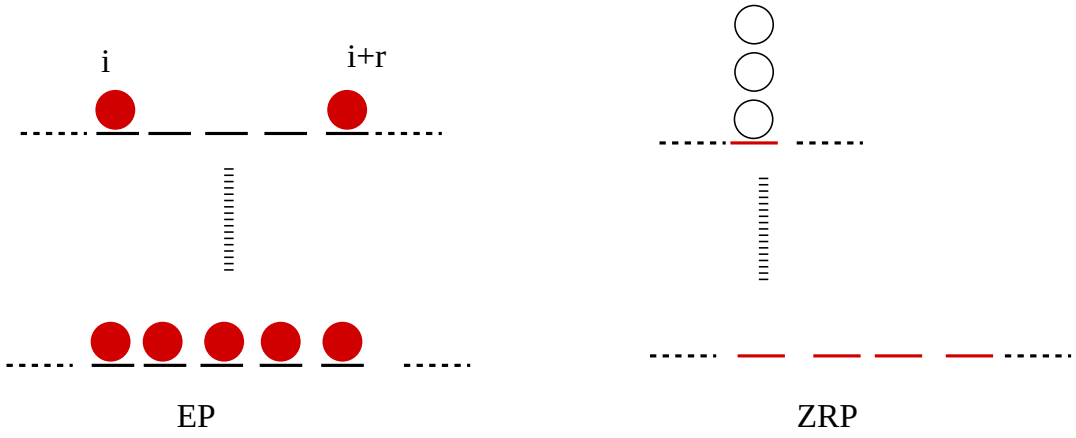

Fig. 3.5 Illustration of the relation between two-point correlation in exclusion process and the single site mass distribution in ZRP. Here, we have shown the two configurations that contribute to calculate the correlation function $S(r)$, where $r = 4$. Provided the sites i and $i + r$ are occupied in EP, we map all the possible configurations of EP between the sites i and $i + r - 1$ to ZRP as described in Sec. 2.2.

3.4 Static correlation function in the thermodynamic limit

Here, we provide a simpler derivation of the result (3.14) in the thermodynamic limit [3]. Consider the probability $P_s(r-s)$ that s consecutive sites in the ZRP have $r-s$ particles. Then, as shown in Fig. 3.5, it is easy to see that in the exclusion process, the probability that two sites at a distance r are occupied is given by

$$\langle \eta_i \eta_{i+r} \rangle = \rho \sum_{s=1}^{r} P_s(r-s) \,. \tag{3.48}$$

The factor ρ on the RHS of the above equation appears because the site i (in the exclusion process) must be occupied. The generating function of the correlation function defined as $G(y) = \sum_{r=0}^{\infty} y^r S(r)$ is then given by

$$G(y) = \rho \sum_{r=0}^{\infty} y^r \sum_{s=1}^{r} P_s(r-s) - \sum_{r=0}^{\infty} y^r \rho^2 \tag{3.49}$$

$$= \rho \sum_{r=0}^{\infty} y^r \sum_{m=0}^{\infty} y^m P_r(m) - \sum_{r=0}^{\infty} y^r \rho^2 \,. \tag{3.50}$$

But due to (2.11), we have

$$\sum_{m=0}^{\infty} y^m P_r(m) = \sum_{m=0}^{\infty} y^m \sum_{m_1,\ldots,m_r} \mathscr{P}(m_1,\ldots,m_r)\, \delta_{\sum_{j=1}^{r} m_j, m} \tag{3.51}$$

$$= \left(\frac{g(y\omega)}{g(\omega)}\right)^r . \tag{3.52}$$

Using the last expression in (3.50), we immediately obtain the result (3.14) for the generating function of the correlation function:

$$G(y) = \frac{\rho}{1 - y\,\frac{g(y\omega)}{g(\omega)}} - \frac{\rho^2}{1-y} . \tag{3.53}$$

The large distance behavior of the correlation function can be found by expanding $G(y)$ about $y = 1$ for the hop rates. For the hop rate (3.18), at the critical point, we obtain the result (3.36)

$$S(r) = \frac{\rho_c^2 \Gamma(b-1)}{r^{b-2}} , \; b > 2 . \tag{3.54}$$

3.5 Correlation function for the model with generalised hole-dependent hop rates

We consider generalised hop rates, where the hop rate depends on the number of empty space in the front and back of the particle as explained in Sec. 2.2.2. The choice of hop rate is given by [33]

$$u(m,m') = (v(m) - v(0))\; v(m') , \tag{3.55}$$

where m (m') is the number of vacancies front (back) of a particles and

$$\frac{2}{3} < v(0) < 1, \quad v(m) = 1 + \frac{1}{m+1} , \; m > 0 . \tag{3.56}$$

Using (2.30) in (3.53) for the generating function of the static density-density correlation function and expanding about $y = 1$, we find that $G(y) \propto (1-y)^{c-6}$ at the critical point,

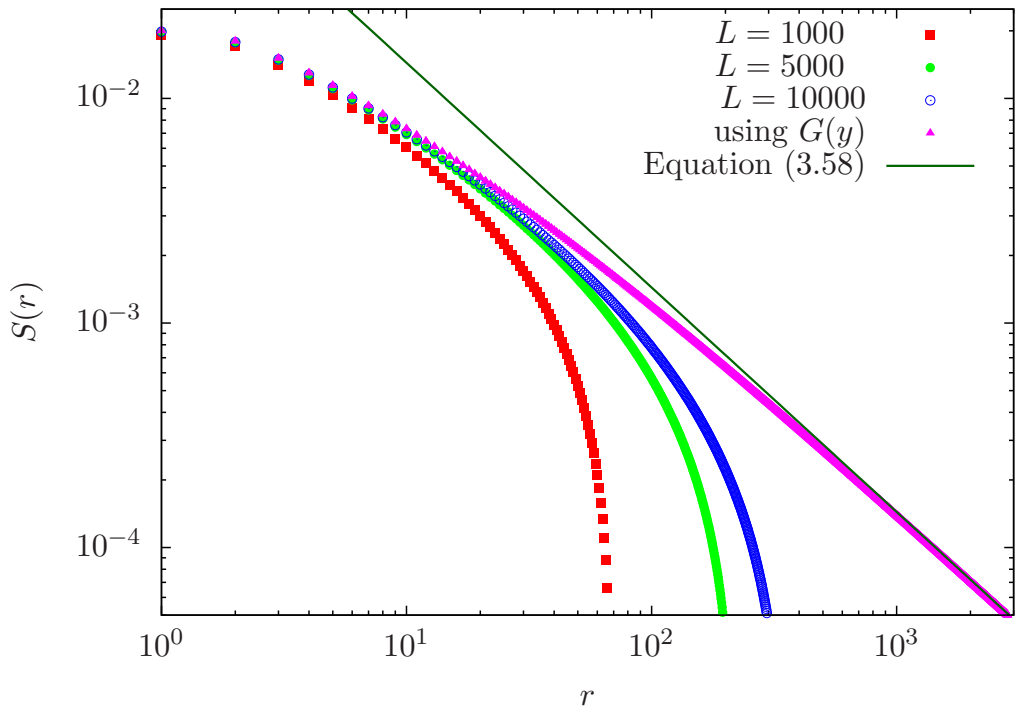

Fig. 3.6 Decay of spatial correlation function with distance at the critical density for hop rate (3.55) for $c = 6$ and $v(0) = 0.75$. The data for finite-size systems is obtained by numerically solving (2.5) and (3.3), while the result in the thermodynamic limit is obtained using (3.53).

where

$$c = \frac{3 - 2v(0)}{1 - v(0)} > 5\,, \tag{3.57}$$

due to (3.56). On inverting the Laplace transform [2], we finally obtain

$$S(r) = \frac{\varrho_c \rho_c^3 (\Gamma(c-2))^2}{4\Gamma(c-3)} \times \frac{1}{r^{c-5}}\,, \tag{3.58}$$

where the critical particle density ρ_c and the related the critical mass density ϱ_c as given in (2.1). The results shows good agreement with numerical simulations as shown in Fig. 3.6.

For correlation length as given in Sec. (3.3.3), we obtain the same scaling form as (3.45) and the correlation length is given as

$$\xi \sim (1-\omega)^{-1} \sim (\rho - \rho_c)^{-\nu}\,, \tag{3.59}$$

which, by virtue, of (3.41) gives $\nu = 1/(c-5)$ for $c < 6$ and 1 for $c > 6$.

3.6 Correlation function for the model with particlewise disorder

The simplest case of a heterogeneous system is one consisting of only a single defect particle, while all other particles are identical. The defect particle hops at a rate smaller than the rest, which can be taken as one. Evidently, the system exhibits a jamming transition. The canonical partition function for such a system is exactly known (see Sec. 2.2.3) which allows us to calculate the exact expressions for the two-point correlation function in both the canonical and grand canonical ensembles. In the canonical ensemble, the two-point correlation function scales with the system size, but approaches a constant value when the size becomes infinitely large. Thus, in the thermodynamic limit, the two-point function is a function of density. For more details on the two-point correlation function of a single defect particle system see Appendix B.4. Additionally in Appendix B.5, we consider another case of a single defect particle system in which the defect particle hop rate is the smallest and dependent on the number of empty spaces in front of it as (3.18).

Further, for a fully disorder system in which the hop rate is different for each particle, analogous to (3.48), we can write the two-point correlation function as

$$\begin{aligned}\langle \eta_i \eta_{i+r} \rangle &= \sum_{\alpha=1}^{N} \text{Prob(site } i \text{ is occupied by particle } \alpha) \\ &\quad \times \sum_{s=1}^{r} P_s(r-s; \{u_\alpha, ..., u_{\alpha+s-1}\}) \,, \end{aligned} \tag{3.60}$$

where $P_s(r-s;\{u_\alpha,...,u_{\alpha+s-1}\})$ denotes the distribution of mass $r-s$ on s consecutive sites in the ZRP when the sites have a hop rate $\{u_\alpha,...,u_{\alpha+s-1}\}$. Similar to (3.52), this distribution is given by

$$P_s(r-s;\{u_\alpha,...,u_{\alpha+s-1}\}) = \sum_{m_1,..,m_s} \prod_{j=\alpha}^{\alpha+s-1} \frac{\omega^{m_j} f_j(m_j)}{g_j(\omega)} \delta_{\sum_{k=\alpha}^{\alpha+s-1} m_k, r-s} \,. \tag{3.61}$$

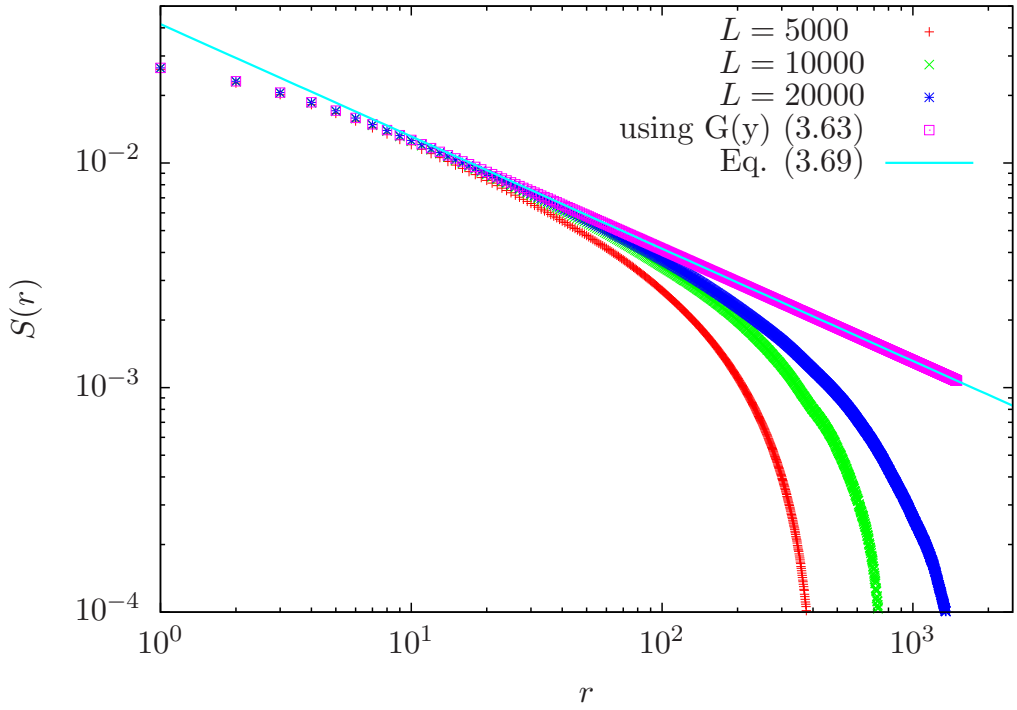

Fig. 3.7 Decay of spatial correlation function with distance at the critical density for disordered hop rate (2.37) for $\gamma = 0.5$, $\tilde{u} = 0.5$. The data for finite-sized systems is obtained by numerical simulations, while the result in the thermodynamic limit is obtained using (3.63). The analytical result (3.69) valid for large inter-particle distances is also shown.

On averaging over the particle hop rates, we get

$$\overline{\langle \eta_i \eta_{i+r} \rangle} = \rho \sum_{s=1}^{r} \sum_{\{m_j\}} \overline{p(m_1)} \ldots \overline{p(m_s)}\, \delta_{\sum_{j=1}^{s} m_j, r-s}\,, \tag{3.62}$$

where $\overline{p(m)}$ is the single site mass distribution obtained after disorder averaging given by (2.40). Some of the stationary state properties are briefly given in Sec. 2.2.3, and at the critical point for the power-law distributed hop rate (2.37), the fugacity ω takes the value of the lowest hop rate $\tilde{u}$. Therefore, we find the disorder averaged generating function $\overline{G(y)}$ of the correlation function at the critical point by

$$\overline{G(y)} = \frac{\rho_c}{1 - \frac{\overline{y\, g(y\ \tilde{u})}}{g(\tilde{u})}} - \frac{\rho_c^2}{1-y}\,. \tag{3.63}$$

Exact solution of the disorder averaged correlation function in thermodynamic limit require expansion of ratio $\overline{\frac{g(\tilde{u}\ y)}{g(\tilde{u})}}$ around $y=1$ and for non-integer γ we have,

$$\overline{\frac{g(\tilde{u}y)}{g(\tilde{u})}} = 1-\left(\frac{1+\gamma}{\gamma}\right)\left(\frac{\tilde{u}}{1-\tilde{u}}\right)s+.....+c_n\frac{(-s)^k}{k!}+\alpha\ s^{\gamma+1}\,, \tag{3.64}$$

where $s=1-y$. Using above expansion, (3.63) becomes

$$\overline{G(s)} = \frac{\rho_c}{\frac{s}{\rho_c}+c_2s^2+...\alpha\ s^{n+1}}-\frac{\rho^2}{s} \tag{3.65}$$

$$= \frac{\rho^2}{s}\left[\alpha\ s^{\gamma}+\rho_c(c_2\ s+..)\right]\,. \tag{3.66}$$

Now the correlation function can be evaluated using contour integration,

$$\overline{S(r)} = \frac{1}{2\pi\,\imath}\int_{\imath\infty}^{\imath\infty} ds\ e^{sr}\ \overline{G(s)}. \tag{3.67}$$

Note that the integrand has a branch cut singularity at $s=0$. The integral with an analytic term is a delta function, and it vanishes upon integration. Thus we just need to solve the following integral

$$\overline{S(r)} = \alpha\rho_c\int_{-\imath\infty}^{\imath\infty}\frac{ds}{2\pi\,\imath}\ e^{sr}\ s^{\gamma-1}\,, \tag{3.68}$$

where $\alpha = \pi\gamma\csc(\gamma\pi)(1+\gamma)\left(\frac{\tilde{u}}{1-\tilde{u}}\right)^{1+\gamma}$. Finally, we get

$$\overline{S(r)} = \rho_c^3(1+\gamma)\left(\frac{\tilde{u}}{1-\tilde{u}}\right)^{1+\gamma}\frac{\Gamma(\gamma)}{r^{\gamma}}\,, \tag{3.69}$$

For integer γ, the expansion of $\overline{\frac{g(\tilde{u}\ y)}{g(\tilde{u})}}$ around $y=1$ results,

$$\overline{\frac{g(cy)}{g(c)}} = 1-\left(\frac{1+\gamma}{\gamma}\right)\left(\frac{c}{1-c}\right)s+...+\beta s^{\gamma+1}\ln s\,, \tag{3.70}$$

where $\beta=\rho_c^2(-1)^{\gamma}(1+\gamma)\left(\frac{c}{1-c}\right)^{1+\gamma}$. For a non-integer γ, we follow the same procedure and obtain the same result as (3.69). The results (3.63) and (3.69) are consistent with numerical simulations shown in Fig. 3.7.

3.7 Correlation function for exclusion process with short and long range hops

The model, considered here is defined in Sec. 2.3 where a particle hops to the farthest (nearest) empty site with rate one (w). Using (3.48), the generating function $G(y)$ of the correlation function can be expressed in terms of the generating function $Q(y)$ of mass distribution $p(m)$ and is given by

$$G(y) = \rho \sum_{r=0}^{\infty} y^r \sum_{s=1}^{r} P_s(r-s) - \sum_{r=0}^{\infty} y^r \rho^2 \tag{3.71}$$

$$= \rho \sum_{l=0}^{\infty} y^l \prod_{j=1}^{l} \left(\sum_{m=0}^{\infty} m p(m) \right) \tag{3.72}$$

$$= \rho \sum_{l=0}^{\infty} [yQ(y)]^l \tag{3.73}$$

$$= \frac{\rho}{1-yQ(y)} - \frac{\rho^2}{1-y}. \tag{3.74}$$

At critical point the generating function $Q(y)$ of single site mass distribution in mean-field approximation is given by (2.42) which on expanding about $y = 1$ and $\sigma = \sigma_c$ and retaining the terms which are linear in σ and nonanalytic terms to lowest order in the deviation of $s = 1 - y$, and $\delta = (\sigma_c - \sigma)$, we get

$$Q(s,\delta) = 1 - s\varrho_c + \ldots + \frac{ws\sigma_c}{2} \sqrt{(y_+(\sigma_c) - 1)\left(s + \frac{\delta}{\sigma_c}\right)}, \tag{3.75}$$

where we have used that $y_-(\sigma_c) = 1$. This gives the generating function of correlation function as

$$G(s,\delta) = \frac{\rho_c^3 w \sigma_c \sqrt{y_+(\sigma_c) - 1}}{2} \frac{\sqrt{s + \delta/\sigma_c}}{s}. \tag{3.76}$$

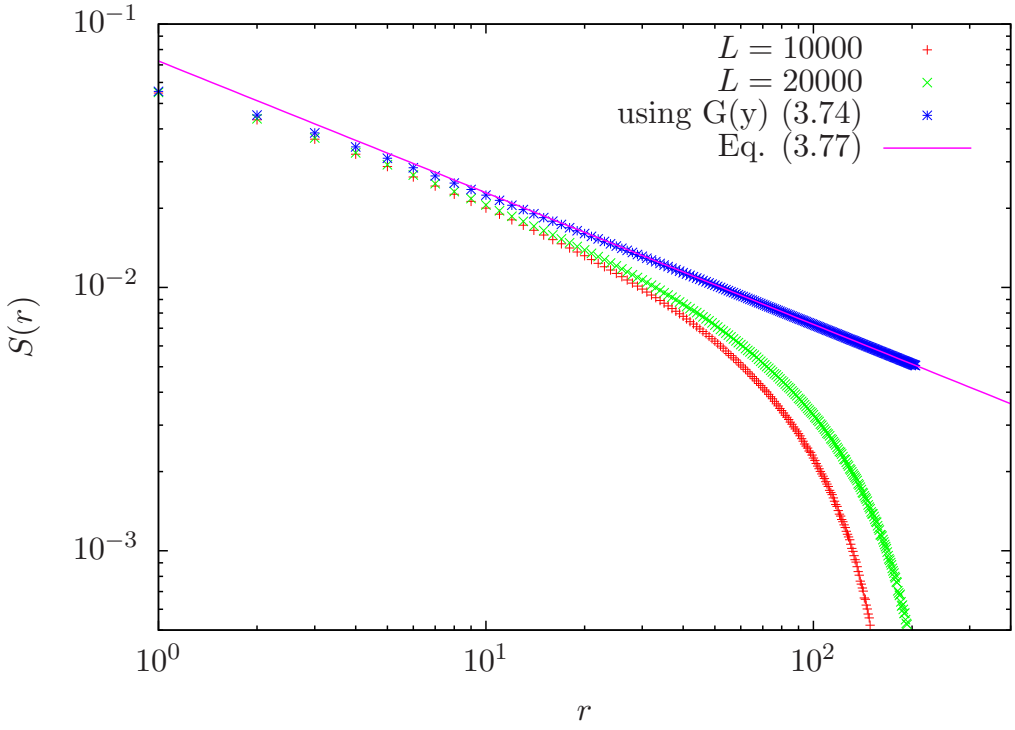

Fig. 3.8 Decay of spatial correlation function with distance at the critical density for short and long range hop model for $w = 8$. The data for finite-sized systems is obtained by numerical simulation, while the result in the thermodynamic limit is obtained using (3.74). The analytical result (3.77) valid for large inter-particle distances is also shown.

On inverting the Laplace transform using a contour that includes the branch cut at $-t/\sigma_c$, we finally get

$$S(r) = \frac{\rho_c^3 w \sigma_c \sqrt{y_+(\sigma_c) - 1}}{2} \frac{1}{\sqrt{\pi r}} \mathscr{H}(\delta r/\sigma_c) \,, \tag{3.77}$$

where $\mathscr{H}(x) = e^{-x} + \sqrt{\pi x}\,\mathrm{erf}(x)$. The decay of the two-point function is compared with numerical simulations as shown in Fig. 3.8.

3.8 Summary

In this Chapter, we studied several exclusion process on a ring in which a particle hops to a empty neighbour with a rate assigned to it. Although we assumed that the hops are unidirectional, the results obtained here also hold for the bidirectional case, in which a par-

ticle may hop to either left or right empty neighbour with nonzero rate. This is because the general exclusion models maps to some of the mass models whose partition function is independent of the bias in the hop rates [1]. Then our exact equation (3.3) for the correlation function, holds for any bias in the hop rates.

Although most of the results for the ZRP and hence the exclusion process have been obtained in the grand canonical ensemble [1], some studies in the canonical ensemble have also been carried out [47, 48, 61, 45]. In particular, an expression for the partition function $\tilde{Z}_{\mathscr{L},\mathscr{M}}$ in the canonical ensemble at and in the vicinity of the critical point has been calculated for finite systems [47], and it has been shown that for the weight $f(m)$ with the same asymptotic behavior as (2.15), $\tilde{Z}_{\mathscr{L},\mathscr{M}}$ depends exponentially on system size for $\varrho < \varrho_c$, but sublinearly on $\mathscr{L}$ for $\varrho \geq \varrho_c$. This implies that the free energy (3.4) changes with the density ϱ in the homogeneous phase but becomes a constant equal to $-\ln g(1)$ (which is chosen to be zero in [47]) for all $\varrho \geq \varrho_c$, as seen here in Fig. 3.1. Due to the latter property, our analysis can not be carried over to the jammed phase. However, since we are mainly concerned with critical exponents here, it suffices to consider the system in the infinite size limit.

For an infinitely large system, we have derived an exact expression (3.14) for the generating function of the steady state two-point correlation function in the canonical ensemble. This result was applied to the several choices of hop rate for $\rho \geq \rho_c$ to find the relevant critical exponents. The case of $b = 1$ in hop rate (3.18), where the system is in laminar phase for all densities, has been considered in [57], but an explicit expression for the correlation function was not provided.

Interestingly, at the critical point, we find the exponent characterising the power law decay of the two-point correlation function changes continuously with the hop parameter. Equilibrium systems in two dimensions that show continuously varying exponents at the critical point are known [62], and their behavior is understood in terms of conformal field theories with central charge one [63]. We do not know if the behavior found here has any such deeper significance.

We also found that for the correlation function, exponent is always of 2 orders less than the hole cluster distribution exponent. We have also given a general result regarding the ex-

ponent ν associated with correlation length. The exponent ν in (3.46) is constant except in the parameter regime where mass variance diverges. This scaling for the correlation length has been obtained in a previous study as well [64]. In addition, we have also derived the scaling function for the correlation function in the high density phase here and found that when the steady state is of product form, the scaling is universal. However, for the exclusion process corresponding to aggregation-fragmentation model, we find that the static correlation function decays as $1/\sqrt{r}$ and the scaling function is also different from the other hop rates we have used.

Chapter 4

Critical dynamics of the jamming transition in driven lattice-gas models

4.1 Introduction

This Chapter focuses on the stationary state dynamics of several driven lattice-gas models in one dimension that exhibit a jamming transition; most of the work discussed in this Chapter has been published in [3]. A special case of the models studied here is the totally asymmetric simple exclusion process (TASEP) in which a particle hops to the left neighbor with rate one if it is empty. It is known that the jamming transition does not occur in this model and its steady state dynamics can be understood using its relationship to the Kardar-Parisi-Zhang equation for interface growth; specifically, the density-density autocorrelation function decays with time as $t^{-2/3}$ [46, 65]. The models of interest here are driven lattice-gas models with hard-core particle interaction and in which the hop rates are chosen such that jamming transition can occur. In the fluid phase and at the critical point, the hole clusters are not macroscopically long as in the TASEP. Then it is natural to ask if the dynamical properties in the fluid phase and especially at the critical point differ from those in the TASEP.

The class of models that we consider are related to a zero range process [41, 1], a misanthrope process [42, 33] and an aggregation-fragmentation model [43, 52]. In these models,

a jamming transition appears as a condensation transition where a macroscopically large mass cluster forms on a single site at high densities but at low densities, the mass is distributed uniformly. The coarsening dynamics in the condensate phase have been studied for these models quite extensively [25, 53, 5, 27, 66, 33], but the stationary state dynamics are largely unexplored (however, see [27, 67]). It should be noted that in this picture, the questions relate to the properties of hole *clusters*, whereas here we are concerned with the holes themselves.

The relation to the mass model allows us to find the static density-density correlation function analytically. In Chapter 3, we studied the equal time density-density correlation function in the stationary state in a class of models where the product measure is exact and a model within mean-field approximation. It was shown that at the critical point, the two-point function decays as a power law in distance with a continuously varying exponent in the former [2], and a constant exponent in the latter. Using this result and numerical simulations, in models with exact product measure, we find that at the critical point, when the static correlation function decays slower than the inverse distance, the exact autocorrelation function decays as a power-law in time with a continuously varying exponent. However, the TASEP behavior for the autocorrelation function, *viz.*, $t^{-2/3}$ decay holds otherwise. Moreover, for a model studied using mean-field approximation, we find the decay of autocorrelation function slower than $t^{-1/2}$, as for symmetric exclusion process.

In the following section, we describe the mapping of our basic model to an interface growth model. We then discuss the results for the static and dynamic correlation function in Secs. 4.4 and 4.5 respectively. Sec. 4.6 is devoted to a discussion of three other models that exhibit a jamming transition. Later, in Sec. 4.7, we discuss preliminary results on calculation of the variance of a tagged particle at the critical point. We conclude with a summary of results and open questions in Sec. 4.8.

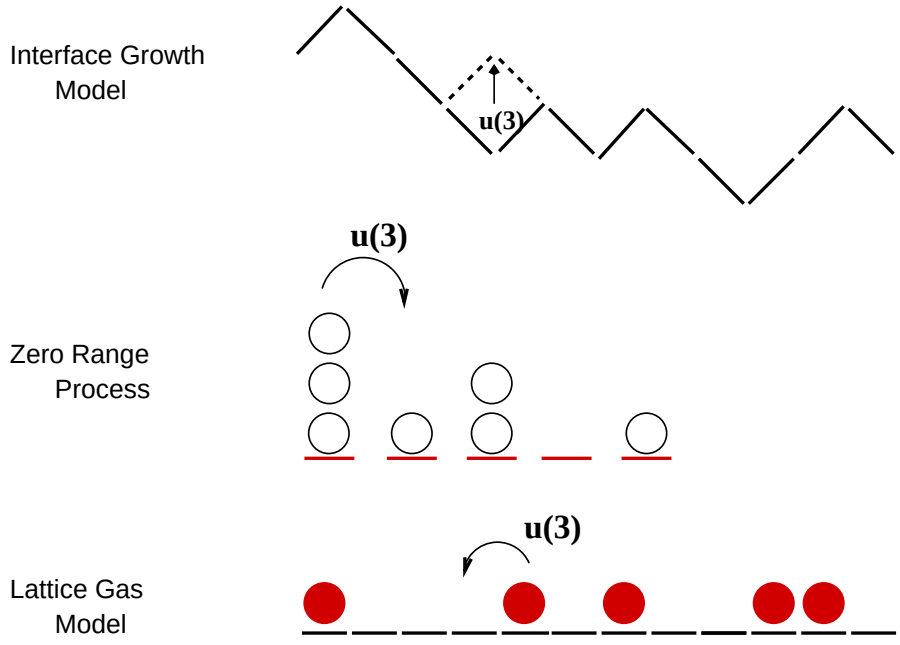

Fig. 4.1 Figure to illustrate the mapping between the lattice gas model (bottom), zero range process (middle) and interface growth model (top).

4.2 Models

We consider a system of hard core particles on a ring with L sites in which the total N number of particles is conserved. As described in Sec. 2.2.1, a particle attempts to hop to a left neighbor with hop rate $u(m)$. For the rate $u(m) = 1 + b/m$, where $m > 0$ are the number of vacancies in front of it, the occupancy variable $\eta_i(t)$ at site i and time t evolves according to the following equation:

$$\frac{d\langle\eta_i\rangle}{dt} = \langle \sum_{m=0}^{\infty} \eta_{i+1}\eta_{i-(m+1)}\, u(m+1) \prod_{k=0}^{m}(1-\eta_{i-k}) - \sum_{m=1}^{\infty} \eta_i\eta_{i-(m+1)}\, u(m) \prod_{k=1}^{m}(1-\eta_{i-k})\rangle\,, \quad (4.1)$$

where the angular brackets denote averaging over initial conditions and independent stochastic trajectories.

The exclusion process described can also be related to an interface growth model. As shown in Fig. 4.1, an interface height profile can be obtained by associating an upward (downward) slope with a particle (hole) in the exclusion process. The interface evolves in time by flipping a local valley to a hill with a rate that depends on the number of upward

slopes on the left. It is convenient to work with a height profile with zero average slope, and we therefore define the height $h_j(t)$ of the interface at the substrate site j and time t as

$$h_j(t) = \sum_{i=1}^{j} \eta_i(t) - \rho\, j \ . \tag{4.2}$$

4.3 Density-density correlation function

Consider the unequal time density-density correlation function defined as

$$S(r,t) = L^{-1} \sum_{i=1}^{L} \left[\langle \eta_i(0) \eta_{i+r}(t) \rangle - \rho^2 \right] , \tag{4.3}$$

where the angular brackets denote an average over initial conditions that are chosen from the *stationary state ensemble* and independent stochastic histories. We already studied the equal time correlation function $S(r,0) \equiv S(r)$ in Chapter 3 and we will study the autocorrelation function $S(0,t)$ in Sec. 4.5. The correlation function $S(r,t)$ is related to the height-height correlation function defined as [46, 65]

$$C(r,t) = L^{-1} \sum_{i=1}^{L} \left[\langle (h_{i+r}(t) - h_i(0))^2 \rangle \right] , \tag{4.4}$$

via the relation [68]

$$S(r,t) = \frac{1}{2} \frac{\partial^2 C(r,t)}{\partial r^2} , \tag{4.5}$$

which can be obtained on using (4.2) in the derivative of $C(r,t)$ with respect to r.

The correlation function $C(r,t)$ has been studied for several interface growth models, and found to grow with time as $t^{2\beta}$ initially and saturate to $r^{2\alpha}$ over a time scale that grows as r^z. In other words, it is of the scaling form [68]

$$C(r,t) = t^{2\beta}\, \mathscr{C}\left(\frac{r}{t^{1/z}} \right) , \tag{4.6}$$

where the scaling function $\mathscr{C}(x)$ is a constant when $x \gg 1$ and $x^{2\alpha}$ for $x \ll 1$, and $\alpha = \beta z$. Correspondingly, for the density-density correlation function, we have

$$S(r,t) = t^{-\frac{2(1-\alpha)}{z}}\, \mathscr{S}\left(\frac{t}{r^z}\right), \tag{4.7}$$

where the scaling function $\mathscr{S}(x)$ is a constant for $x \ll 1$ and decays to zero for $x \gg 1$.

The height model corresponding to the TASEP is known to obey the Kardar-Parisi-Zhang (KPZ) equation [30], for which it is known that the dynamic exponent $z = 3/2$, the roughness exponent $\alpha = 2 - z = 1/2$, and the growth exponent $\beta = 1/3$ (see Appendix C.1), and therefore $S(0,t) \propto t^{-2/3}$ for large systems as indeed verified in recent numerical simulations [69]. Further for a TASEP, the full scaling form is known to be

$$S(r,t) \approx \left(\frac{1}{2}\right)^{1/3} \left(\frac{A}{2\lambda t}\right)^{2/3} \mathscr{Q}\left(\frac{r}{(2\lambda^2 A t^2)^{1/3}}\right), \tag{4.8}$$

where $\mathscr{Q}(x) \sim \exp(-0.295x^3)$ [4, 68], A is the prefactor of static height-height correlation function calculated in Sec. 4.4 and λ is a function of the moments of the mass distribution and is given by (C.6). Our objective here is to study the exclusion process with hole-dependent hop rates at the critical point and determine if the dynamics differ from that in the TASEP case. The autocorrelation function is mostly studied by simulating the driven lattice gas model via sequential updating. In most cases, we worked with large systems of size $L = 10^4$ or larger, and the data were averaged over more than 10^4 independent initial conditions in the stationary state. Our results for $S(r,0)$ and $S(0,t)$ are described in the following two sections. Although in most of the Chapter, we focus on the exclusion process, with hop rate $u(m) = 1 + b/m$, we also discuss other models that exhibit a jamming transition in Sec. 4.6.

4.4 Height-height correlation function and roughness exponent

We now use the result obtained in the Chapter 3 to find the equal time height-height correlation function $C(r,0)$ defined in (4.4) which grows as $r^{2\alpha}$ [46, 65]. Using (4.2) in (4.4), we have

$$C(r,0) = \rho(1-\rho)r + 2\sum_{k=1}^{r}(r-k)S(k,0)\,, \tag{4.9}$$

where $S(k,0) \equiv S(k)$, which has been calculated in Chapter 3. For TASEP, as $S(k,0)$ vanishes for all $k > 0$ in the thermodynamic limit, the above correlation function increases linearly with r and therefore the roughness exponent α equals $1/2$ [46, 65]. For $u(m) = 1 + b/m$, $b > 2$, at the critical point, we get

$$C(r,0) = \rho_c(1-\rho_c)r + 2\rho_c^2\Gamma(b-1)\left(rH_r^{(b-2)} - H_r^{(b-3)}\right)\,, \tag{4.10}$$

where we have used (3.36). In the above equation, $H_n^{(x)} = \sum_{i=1}^{n} i^{-x}$ is a harmonic number of order x and whose large n behavior is given by [49]

$$H_n^{(x)} = \frac{n^{1-x}}{1-x} + \zeta(x) + \mathcal{O}(n^{-x}), \tag{4.11}$$

where $\zeta(x) = \sum_{k=1}^{\infty} k^{-x}$ is the Riemann zeta function. Using the above equation in (4.10), we find the leading and two subleading terms in the height-height correlation function to be

$$C(r,0) = \begin{cases} c_1 r^{4-b} + c_2 r + c_3 & , b \neq 3,4, \\ \left[2\rho_c^2\Gamma(b-1)\right] r\ln r + c_2' r & , b = 3, \\ c_2 r - 2\rho_c^2\Gamma(b-1)\ln r & , b = 4\,, \end{cases} \tag{4.12}$$

where the coefficients $c_1 = 2\rho_c^2\Gamma(b-1)((3-b)(4-b))^{-1}, c_2 = \rho_c(1-\rho_c) + 2\rho_c^2\Gamma(b-1)\zeta(b-2), c_2' = \rho_c(1-\rho_c) + 2\rho_c^2\Gamma(b-1)(\gamma_{EM}-1), c_3 = -2\rho_c^2\Gamma(b-1)\zeta(b-3)$ and $\gamma_{EM} \approx 0.577$ is the

Euler-Mascheroni constant. It can be verified that the correlation function $S(r,0)$ in (3.36) is obtained using the above result in (4.5).

Equation (4.12) shows that for large r, the height variance grows as r^{4-b} for $2 < b < 3$ and linearly for $b > 3$. Thus the interface is rougher in the former case, and the growth of the interface width with distance can be characterised by the roughness exponent given by

$$\alpha = \begin{cases} (4-b)/2 & , 2 < b < 3 \, , \\ 1/2 & , b > 3 \, . \end{cases} \tag{4.13}$$

The subleading terms in the correlation function $C(r,0)$ are useful in understanding the dynamical behavior of the correlation function which we discuss in the next section.

4.5 Unequal time correlation function

We now study the autocorrelation function at the critical point. The results of our numerical simulations are shown in the inset of Fig. 4.2 for the autocorrelation function defined in (4.3), and we find that it oscillates in time. This is because the density fluctuations move with a nonzero speed $v = \partial J/\partial \rho$ [70] (also, see Appendix C.1) where J is the stationary state current. These oscillations (with time period L/v) can be eliminated by working in the rest frame of the density fluctuations [66], and we therefore consider

$$S(r,t) = \langle \eta_i(0) \eta_{i+vt+r}(t) \rangle - \rho^2 \, . \tag{4.14}$$

4.5.1 Current-density relation for the exclusion process with hole-dependent rates

To find the speed v, we first calculate the stationary state current as follows. Since a particle hops to the left empty neighbor with a rate that depends on the number of vacancies in front of it, the stationary state current in the bond connecting the sites $i-1$ and i is given

by

$$J(\rho) = \langle u(1)\eta_{i-2}(1-\eta_{i-1})\eta_i + u(2)\eta_{i-3}(1-\eta_{i-2})(1-\eta_{i-1})\eta_i + ...\rangle \tag{4.15}$$

$$= \langle \sum_{m=1}^{\infty} u(m)\eta_i\eta_{i-(m+1)} \prod_{k=1}^{m}(1-\eta_{i-k})\rangle. \tag{4.16}$$

Upon mapping the particle configurations appearing on the RHS of the above equation to the ZRP as described in Sec. 2.2.1, we find that

$$J(\rho) = \rho \sum_{m=1}^{\infty} u(m)p(m) \tag{4.17}$$

$$= \rho \sum_{m=1}^{\infty} u(m)\frac{\omega^m f(m)}{g(\omega)} \tag{4.18}$$

$$= \rho\, \omega(\rho)\,, \tag{4.19}$$

since $p(m)$ is given by (2.6) and $f(m)$ obeys (2.13). As shown in the inset of Fig. 4.2, the current is a nonmonotonic function of density: it increases linearly in the jammed phase and reaches a maximum at $\rho \geq \rho_c$.

For the current (4.19), the speed $v = \partial J/\partial\rho = \omega + \rho\partial\omega/\partial\rho$. In the high density phase where $\omega < 1$, using (2.10), we obtain

$$v = \omega - \frac{\omega}{\rho\sigma^2}\,. \tag{4.20}$$

However, in the low density phase, since the fugacity equals one, the current is simply given by ρ and thus the speed of the density fluctuations for $\rho < \rho_c$ is unity for all $b > 2$. Moreover, in high density phase, this speed changes sign and vanishes at $b^* = 3 + \sqrt{2}$ for $b > 3$. For $b < b^*$, since the slope $v_+(\rho_c)$ of the current at ρ_c from the high density side is positive, the current continues to increase beyond the critical density. The density $\rho^* > \rho_c$ where the current is maximum can be found by setting the derivative of the current equal to zero and using the density-fugacity relation (2.9). For $b = 2.5$ for which $\rho_c = 1/3$, we find that $\rho^* \approx 0.65$ as shown in Fig. 4.2. For $b > b^*$, the current must decrease as the critical density is crossed since the speed v_+ is negative. But as the slope v_- is positive, the maximum current

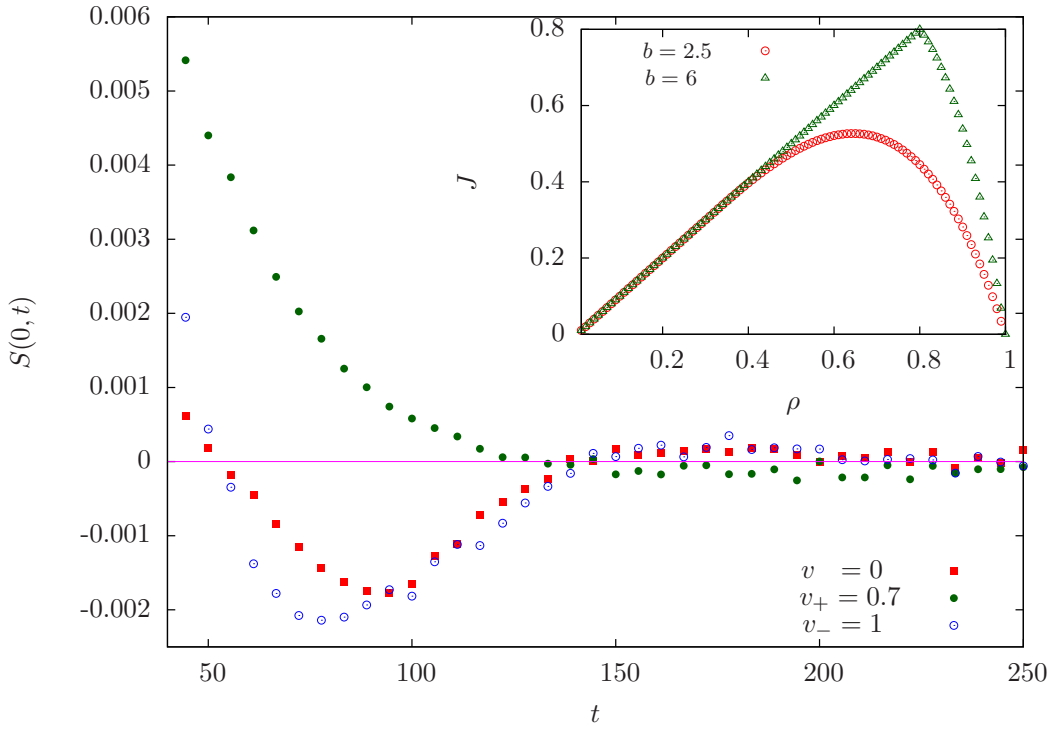

Fig. 4.2 Autocorrelation function $S(0,t)$ defined in (4.14) at the critical point for $b = 7/2$ and $L = 100$ to show that the density fluctuations move with the speed v_+ given by (4.21). The inset shows the stationary state current (4.19) as a function of the particle density for two values of the parameter b. The critical density $\rho_c = 1/3$ and $4/5$ for $b = 5/2$ and 6 respectively.

is obtained at the critical density. Note that the derivative of the current does not exist at the critical point for $b > 3$. At the critical point, since the mass distribution $p(m) \sim m^{-b}$, the variance σ^2 diverges when $2 < b < 3$ and remains finite otherwise. As a result, the speed is not a continuous function of density for $b > 3$ since

$$v_+(\rho_c) = \begin{cases} 1 & , 2 < b < 3 \,, \\ 1 - \frac{(b-2)(b-3)}{b-1} & , b > 3 \,, \end{cases} \tag{4.21}$$

whereas, as mentioned above, $v_-(\rho_c) = 1$ for $b > 2$ [66]. Thus, for $b > 3$, it is not clear whether one should use v_+ or v_- in (4.14) at the critical point. Our numerical simulations show that the correlation function $S(0,t)$ does not oscillate in time when v_+ is used, see

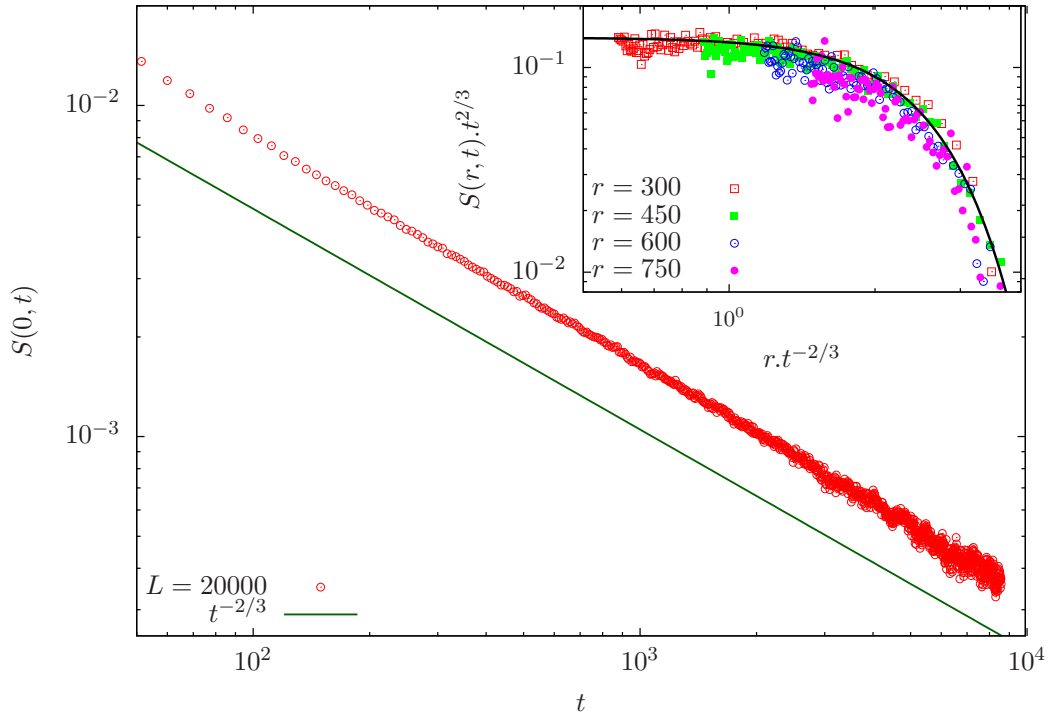

Fig. 4.3 Temporal decay of the autocorrelation function $S(0,t)$ defined in (4.14) in the fluid phase for $b = 5/2$ at $\rho = 1/2$ for the exclusion process with hop rate $u(m) = 1 + b/m$. The inset shows the scaled unequal time two-point correlation function for hop rate (2.12) where, $b = 2.5$ at density $\rho = 1/2$ in fluid phase. The straight line in inset shows the scaling function given in (4.8) where $A = \rho(1-\rho)$ and $\lambda = 3.27$.

Fig. 4.2. To rationalize this observation, we note that the speed v is determined by a steady state property (namely, the first derivative of the steady state current). But in the stationary state, a typical hole cluster is not macroscopically long (see Sec. 4.2) and therefore the properties of the critical state are similar to that in the fluid phase. In the following, we will set $v = v_+$ which is given by (4.21).

4.5.2 Autocorrelation function when $b > 3$

To get an insight into the dynamics, we write down an equation for the height of the interface model (explained in Sec. 4.2) in Appendix C.1 using a standard prescription for $\rho \geq \rho_c$. The coefficients appearing in this equation are related to the second and third cumulants of

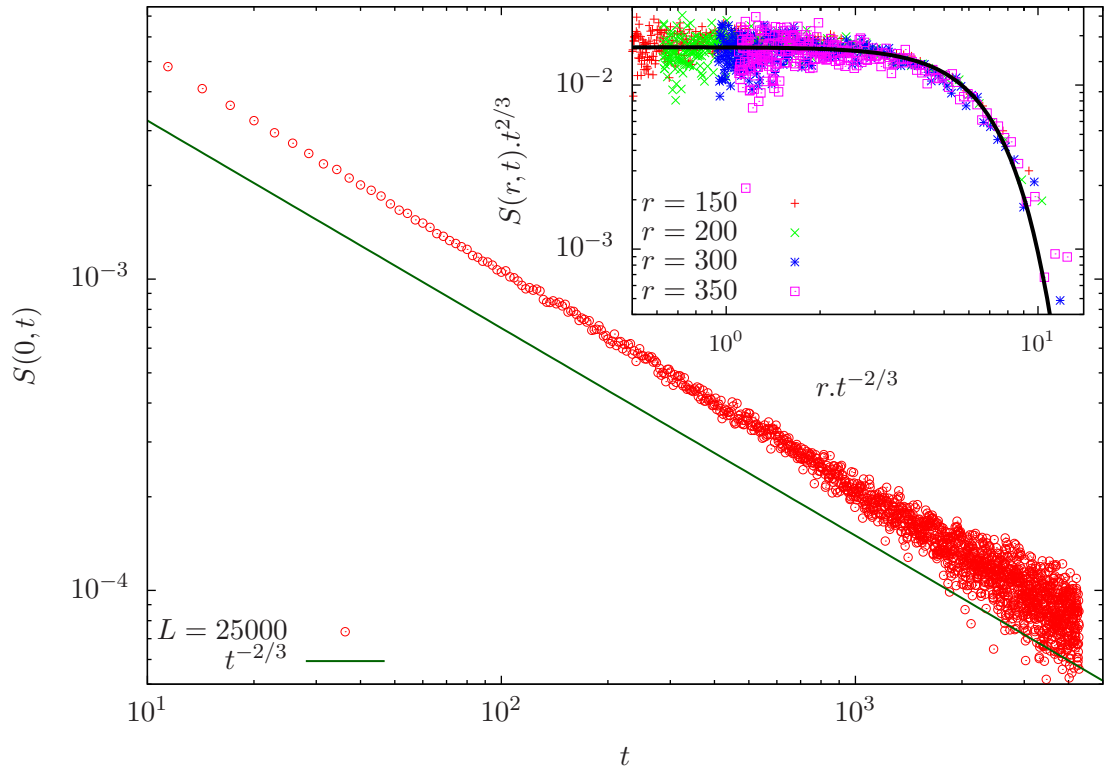

Fig. 4.4 Temporal decay of the autocorrelation function $S(0,t)$ defined in (4.14) at critical point for $b = 6$ for the exclusion process with hop rate (2.12). The inset shows the scaled unequal time two-point correlation function at critical density for hop rate (2.12) where, $b = 6$. The straight line in inset shows the scaling function given in (4.8) where $A = \rho(1-\rho)/2$ and $\lambda = 25.28$.

the hole cluster distribution $p(m)$ in (2.18). In the fluid phase where the distribution of the hole clusters is an exponential, we find that the KPZ equation is obtained for all $b > 2$ and therefore the autocorrelation function $S(0,t) \propto t^{-2/3}$, as shown in the Fig. 4.3. We have also compared the scaling form (4.8) of the TASEP with the scaling function in the fluid phase and have found good agreement with numerics as shown in the inset of Fig. 4.3.

However, at the critical point where the hole cluster distribution $p(m) \sim m^{-b}$, we find that the interface height profile obeys the KPZ equation when $b > 4$. We thus expect that the density-density autocorrelation function $S(0,t)$ decays as $t^{-2/3}$ as in the standard KPZ case. Our numerical results shown in Fig. 4.4 for $b = 6$ are indeed consistent with this expectation.

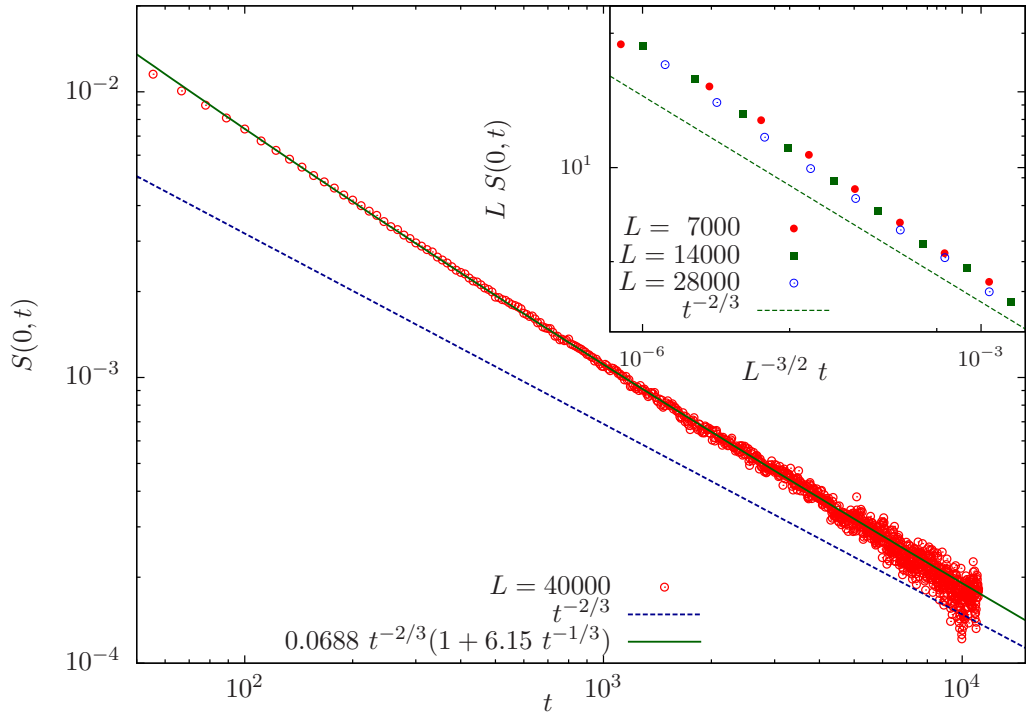

Fig. 4.5 Temporal decay of the autocorrelation function $S(0,t)$ defined in (4.14) at the critical point for the exclusion process with hop rate (2.12) and $b = 7/2$. The inset shows the data collapse for various system sizes for $b = 3.8$ at the critical density.

On comparing the unequal time correlation function with that for TASEP, we find a good agreement up to a constant factor as shown in inset of Fig. 4.4.

We next turn to the case when $3 < b < 4$. Although the roughness exponent in (4.13) is $1/2$ in this parameter regime, as the third cumulant of $p(m)$ diverges for $b < 4$, our hydrodynamic description in Appendix C.1 breaks down. However, our numerical data for the autocorrelation function shown in Fig. 4.5 is consistent with the $t^{-2/3}$ decay at large times which means that the dynamic exponent $z = 3/2$ here as well. This is also verified by writing (4.7) as $r\,S(r,t) = x^{-2/3}\mathscr{S}(x)$, $x = t\,r^{-3/2}$ and obtaining a data collapse for three system sizes as shown in the inset of Fig. 4.5. The slow convergence of $S(0,t)$ to the asymptotic behavior indicates that the subleading corrections to the leading behavior may be strong. From (4.12) for the static correlation function, we see that the subleading correction grows

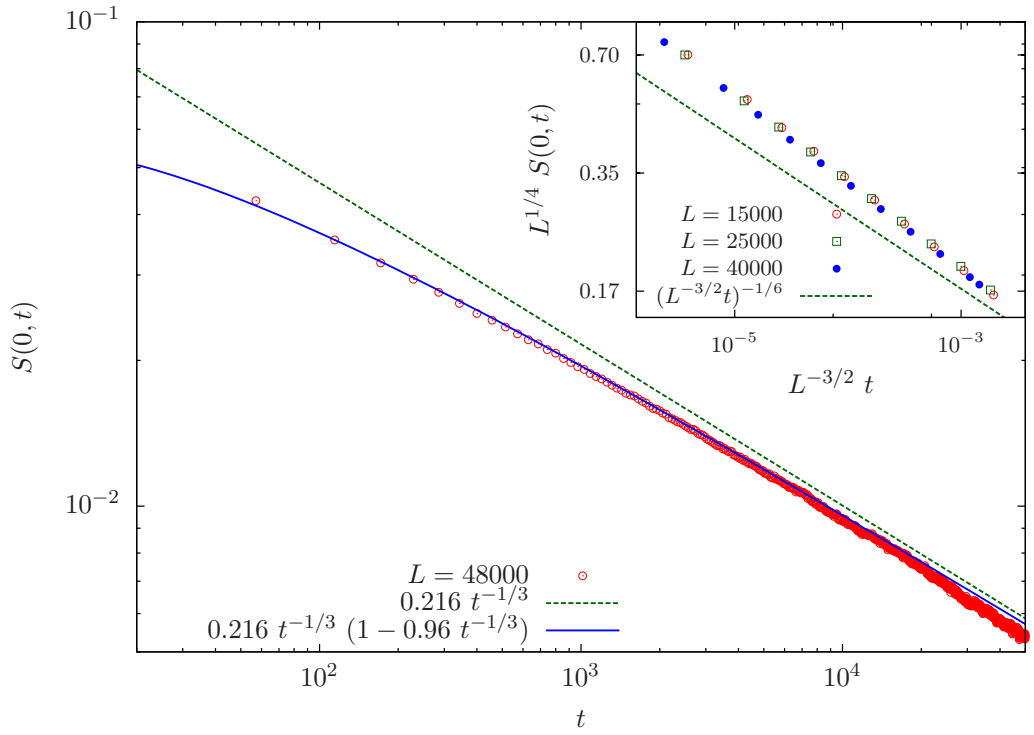

Fig. 4.6 Temporal decay of the autocorrelation function $S(0,t)$ defined in (4.14) at the critical point for the exclusion process with hop rate (2.12) and $b = 5/2$. The inset shows the data collapse for various system sizes for $b = 9/4$ at the critical density.

as r^{4-b} for $b > 3$. On using this result and the discussion in Sec. 4.3, we find that

$$S(0,t) \propto \frac{1}{t^{\frac{2}{3}}}\left(1 + \frac{A}{t^{\frac{2(b-3)}{3}}}\right), \tag{4.22}$$

where A is a constant. Thus for $b = 7/2$, the correction to the leading order behavior is expected to decay slowly as $t^{-1/3}$; the numerical data fits well to the above equation as shown in Fig. 4.5.

4.5.3 Autocorrelation function when $2 < b < 3$

As in the $3 < b < 4$ case, here our hydrodynamic description also breaks down, the reason for which can be traced to the slow decay of the hole cluster distribution. In addition, the static correlation function $C(r,0)$ increases superlinearly, see (4.12). As shown in the inset of

Fig. 4.6, we obtain a good data collapse for various system sizes using $\alpha = (4-b)/2$ and $z = 3/2$ in (4.7). Thus, here the autocorrelation function decays with time as a power law with a continuously varying exponent given by $2(b-2)/3$. Moreover, on taking the subleading corrections to the static correlation function into account, we obtain

$$S(0,t) \propto \frac{1}{t^{\frac{2(b-2)}{3}}}\left(1+\frac{A'}{t^{\frac{2(3-b)}{3}}}\right), \tag{4.23}$$

which provides a good fit to the numerical data as shown in Fig. 4.6 for $b = 5/2$.

4.6 Critical dynamics in other models

The main conclusions so far are that at the critical point, in a certain parameter regime, the roughness exponent is different from that in the TASEP but the dynamic exponent $z = 3/2$ holds throughout. Below we discuss three more models that show a similar jamming transition and for which the above results continue to hold. In Sec. 4.6.3, we also discuss a model for which the above conclusions are not valid.

4.6.1 Generalised exclusion process with hole-dependent rates

We now discuss a class of driven lattice gas models in which a particle hops to the empty left neighbor at a rate $u(m,m')$ where $m(m')$ denotes the number of vacancies on its left (right). This model is obtained, via the mapping described in Sec. 2.2, from a misanthrope process [33] in which a site can be occupied by any number of particles and a particle hops out of a site with mass m to its right neighbor at a rate $u(m,m')$ when there are m' particles on the landing site. When the hop rate does not depend on the mass at the target site, we obtain a ZRP as already discussed in Sec. 2.2.

Here we consider such a case with hop rates given by [33]

$$u(m,m') = (v(m) - v(0))\; v(m')\,, \tag{4.24}$$

where

$$\frac{2}{3} < v(0) < 1, \quad v(m) = 1 + \frac{1}{m+1}\,,\ m > 0\,. \tag{4.25}$$

Thus a particle hops to the left empty site with a lower rate if there are large empty regions on either side. For the range of $v(0)$ mentioned above, a jamming transition occurs, see detail in Sec. 2.2.2. The static density-density correlation function at the critical point is calculated in Sec. 3.5 and given by

$$S(r,0) = \frac{\varrho_c \rho_c^3 (\Gamma(c-2))^2}{4\Gamma(c-3)} \times \frac{1}{r^{c-5}}\,, \tag{4.26}$$

where the critical particle density ρ_c and the related mass density ϱ_c are given in Sec. 2.2.2. On comparing this result with those in Sec. 4.4, we immediately see that the roughness exponent is equal to $(7-c)/2$ for $5 < c < 6$ and $1/2$ for $c > 6$.

Further, the speed of the density fluctuations $v = \partial J/\partial\rho$ where the stationary state current expression J in lattice gas model with hop rates (4.24) and (4.25) can be written as

$$\begin{aligned}
J(\rho) &= \langle u(1,0)\eta_{i-2}(1-\eta_{i-1})\eta_i\eta_{i+1} + u(2,0)\eta_{i-3}(1-\eta_{i-2})(1-\eta_{i-1})\eta_i\eta_{i+1} \\
&\quad + \ldots + u(1,1)\eta_{i-2}(1-\eta_{i-1})\eta_i(1-\eta_{i+1})\eta_{i+2} + \ldots\rangle \\
&= \langle \sum_{m=1}^{\infty}\sum_{m'=0}^{\infty} u(m,m')\eta_{i-(m+1)}\eta_i\eta_{i+(m'+1)} \prod_{k=1}^{m}(1-\eta_{i-k}) \prod_{j=1}^{m'}(1-\eta_{i+j})\rangle \qquad (4.27) \\
&= \rho \sum_{m=1}^{\infty}\sum_{m'=0}^{\infty} (v(m)-v(0))\,v(m')\,p(m)\,p(m') \qquad (4.28) \\
&= \rho\omega \frac{v(1)-v(0)}{v(0)} \left(\frac{2v(0)\,{}_2F_1(1,3,c,C\omega)}{2-v(0)+v(0)\,{}_2F_1(2,2,c,C\omega)}\right)^2 . \qquad (4.29)
\end{aligned}$$

Furthermore, assuming that the dynamic exponent $z = 3/2$ here as well, we expect that the autocorrelation function behaves as

$$S(0,t) \propto \begin{cases} t^{-\frac{2(c-5)}{3}}\left(1 + \alpha_1\, t^{-\frac{2(6-c)}{3}}\right) & ,\ 5 < c < 6\,, \\ t^{-\frac{2}{3}}\left(1 + \alpha_2\, t^{-\frac{2(c-6)}{3}}\right) & ,\ 6 < c < 7\,, \\ t^{-\frac{2}{3}}\left(1 + \alpha_3\, t^{-\frac{2}{3}}\right) & ,\ c > 7\,, \end{cases} \tag{4.30}$$

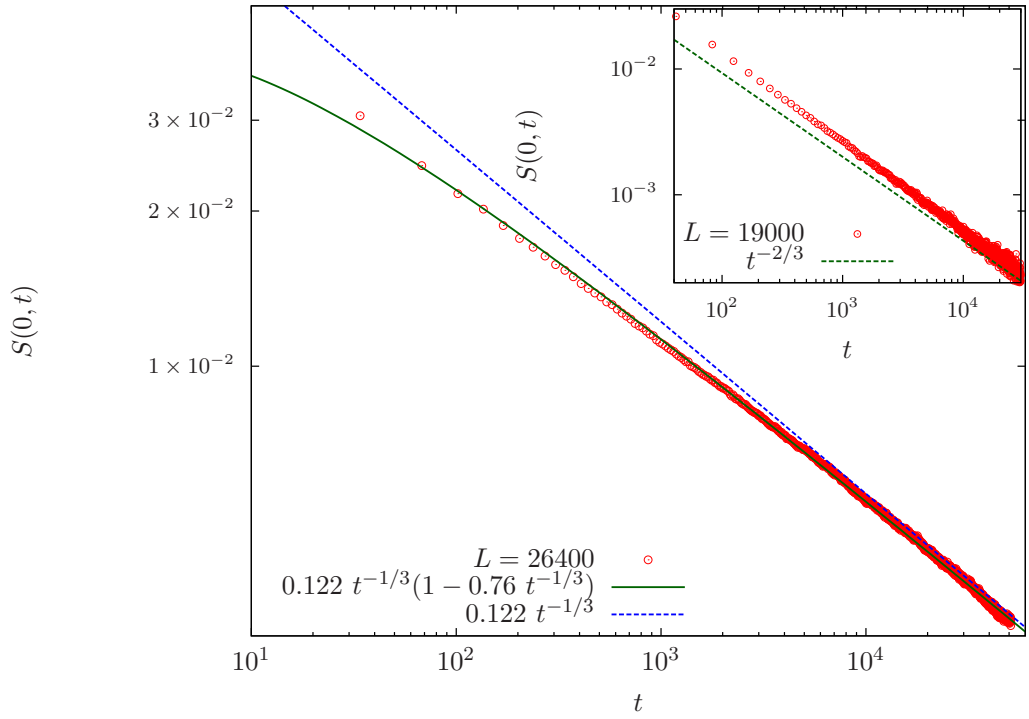

Fig. 4.7 Autocorrelation at the critical point for the generalised exclusion process discussed in Sec. 4.6.1 for $c = 5.5$ with $\rho_c = 5/33$, $\nu = 0.285714$ (main) and $c = 9$ with $\rho_c = 12/19$, $\nu = -0.00846192$ (inset).

where α_i's are constants. Our numerical results for the autocorrelation function shown in Fig. 4.7 for $c = 5.5$ and 9 in the rest frame of the density fluctuations are in agreement with these expectations.

4.6.2 Exclusion process with particlewise disorder

We again consider a system of hard core particles on a ring in which a particle hops to the empty left neighbor. However, the hop rate of a particle is now a random variable, and it is independent of the length of the hole clusters on either side [25–27]. The hop rates are chosen independently from a common distribution,

$$q(u) = \frac{1+\gamma}{(1-\tilde{u})^{1+\gamma}}(u-\tilde{u})^{\gamma}\ ,\ \gamma > 0\ , \tag{4.31}$$

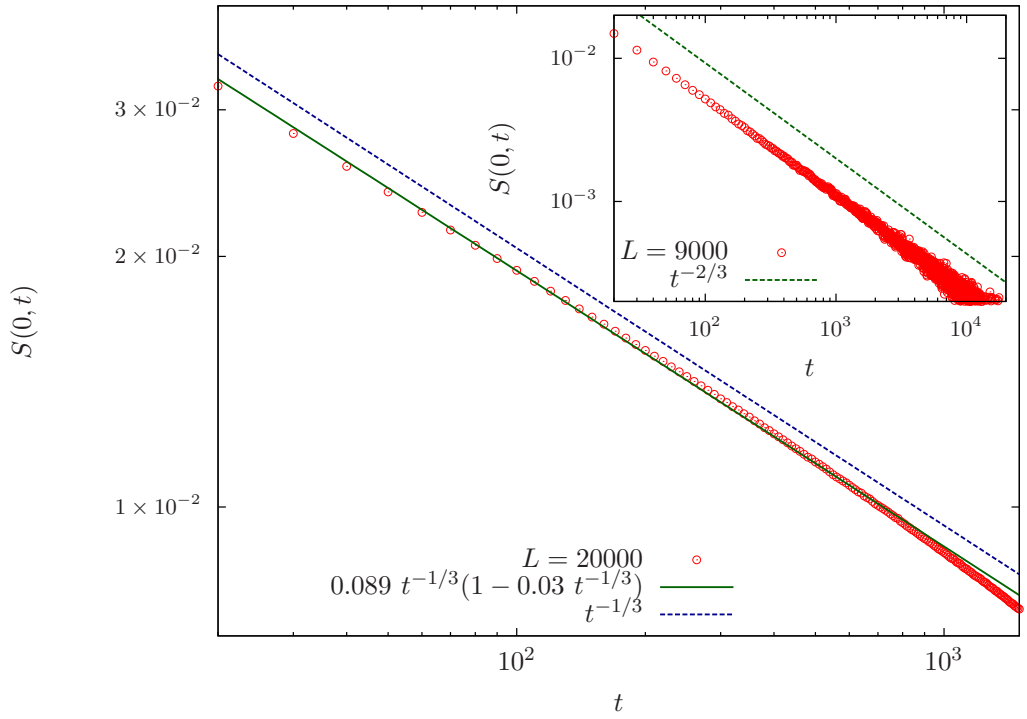

Fig. 4.8 Autocorrelation function at the critical point for the disordered exclusion process discussed in Sec. 4.6.2 for $\gamma = 0.5$ (main) and $\gamma = 4$ (inset). The data are averaged over 2000 independent disorder configurations for the rates chosen from (4.31) with $\tilde{u} = 1/2$.

where $0 < \tilde{u} < u < 1$. This model can be mapped to a ZRP with sitewise disorder as explained in Sec. 2.2.3 and shows a jamming transition at $\rho_c = \gamma\frac{1-\tilde{u}}{\tilde{u}+\gamma}$ [25, 26]. On using the result from Sec. 3.6, the static two-point correlation function turns out to be

$$\overline{S(r,0)} = \rho_c^3(1+\gamma)\left(\frac{\tilde{u}}{1-\tilde{u}}\right)^{1+\gamma}\frac{\Gamma(\gamma)}{r^\gamma}\,. \tag{4.32}$$

Using this expression in (4.9), we find that the roughness exponent is given by $(2-\gamma)/2$ when $0 < \gamma < 1$ but is $1/2$ for $\gamma > 1$.

Following similar steps to the models considered before, the stationary state current for a given configuration of particle hop rates is found to be $J = \rho\omega$, and the speed of the density fluctuations can be calculated using (2.33) and its derivative with respect to ω. In numerical simulations, for a given set of u_i's, we calculated the speed and measured the

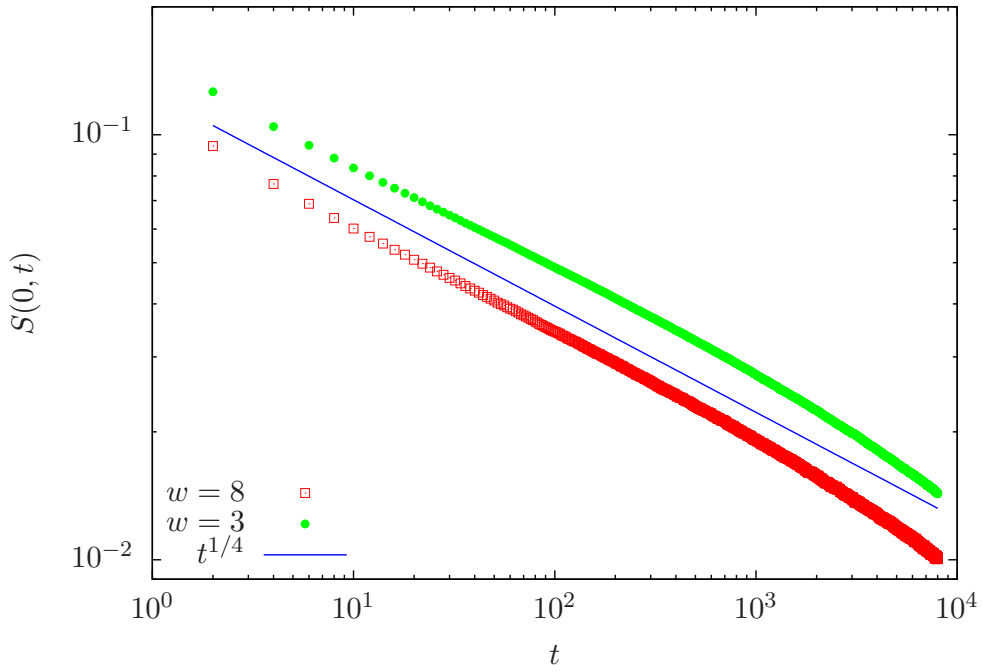

Fig. 4.9 Autocorrelation function at the critical point for the process with short and long jumps for two values of parameter w. The data are shown here for system size ~ 15000 and averaged over 2000 independent histories. The plot confirms that the autocorrelation function decay is independent of hop parameters and decays with exponent 1/4.

autocorrelation function in (4.14). The numerical data were averaged over many disorder configurations to yield $\overline{S(0,t)}$ which is shown in Fig. 4.8, and we find that our numerical results are consistent with (4.7) where the roughness exponent is as quoted above and the dynamic exponent $z = 3/2$.

4.6.3 Exclusion process with short and long jumps

The model of our interest is already explained in Sec. 2.3. It is known to show jamming transition only in the bidirectional case when the current in the system is zero. From the hydrodynamic agreements, one would expect it to fall in Edwards-Wilkinson (EW) universality class [71] and therefore, the dynamic exponent $z = 2$. Using the static two-point correlation function decay exponent from (3.77) in (4.9), we calculate the roughness exponent α to be 0.75 which is very different from standard prediction of $\alpha = 1/2$ by EW. Further, us-

ing the two-point correlation function scaling given by (4.7), the autocorrelation function is given as

$$S(0,t) \sim t^{-1/4}\,, \tag{4.33}$$

and is consistent with the numerical simulation as shown in Fig. 4.9.

4.7 Tagged particle correlation for the model with hole-dependent hop rate

Another way to understand the stationary state dynamics is through the study of the displacement of a tagged particle. Here, we study the growth of the variance of the displacement of a tagged particle with time. The variance is studied at the critical point for exclusion process with hole-dependent hop rate (3.18), in stationary state. The details of some of the known stationary state properties of this model have already been discussed in Sec. 2.2.1. The time growth of the fluctuation for a tagged particle in the steady state for ASEP [72–74] as well as that for the hole-dependent hop rate (3.18) [66] has been well studied. However, a detailed analysis at the critical point is still lacking.

The study of the fluctuation by measuring the variance of a tagged particle displacement in time can be approached in two ways: (a) by calculating the variance $\sigma^2(t)$, averaged over different stationary state initial configurations and (b) by calculating variance $s^2(t)$, which is only averaged over stochastic histories starting from the same initial condition.

Earlier studies on ASEP show that the fluctuation, $\sigma^2(t)$, grows linearly in time with a diffusion constant, D_0 which is a function of density and the bias [73] in the thermodynamic limit; for TASEP, it is given by $D_0 = (1-\rho)$. Further, it has been observed that the growth of the variance is sensitive to ensemble averaging, i.e., the variance decay scaling changes if the variance is averaged over different stochastic histories starting from same initial condition. In the thermodynamic limit, the variance, s^2 with same initial condition, shows a constant growth in time with exponent 2/3 ($s^2(t) \sim t^{2/3}$) [74]. This difference in the expo-

nent can be explained by arguing that in the stationary state, the displacement of the n^{th} tagged particle, $y(n,t) - y(n,0)$, has contributions from three different terms: drift, sliding density fluctuations, and dissipation. Thus, one can write the displacement as

$$d(t) = y(n,t) - y(n,0) = D_0 t + W_n t^{\alpha} + t^{\beta} \mathscr{G}_n(t) \,, \tag{4.34}$$

where α is the roughness exponent and β is the growth exponent of the KPZ equation. Presently, we will not go into the detailed observation of (4.34) (see [74] for details) and use it to explain briefly how the exponents for σ^2 and s^2 are different. Two different scenarios are considered –

(i) When the displacement is averaged with respect to the different stationary initial conditions, we get

$$\overline{d(t)} = \overline{\langle y(n,t) - y(n,0) \rangle} = D_0 t + \overline{W_n} t^{\alpha} + t^{\beta} \langle \mathscr{G}_n \rangle \,, \tag{4.35}$$

where the angular bracket denotes averaging over the stochastic histories, and the over-bar denotes ensemble averaging of initial conditions. Now, taking the variance of displacement, $\sigma^2(t)$ becomes

$$\sigma^2(t) = ((W_n - \overline{W_n}) t^{\alpha} + t^{\beta} (\mathscr{G}_n - \langle \mathscr{G}_n \rangle))^2 \sim t^{2\alpha} \,, \tag{4.36}$$

where $\alpha = 1/2$ for TASEP.

(ii) When the displacement is averaged over different stochastic histories while keeping the initial condition fixed, we get

$$\langle d(t) \rangle = \langle y(n,t) - y(n,0) \rangle = D_0 t + W_n t^{\alpha} + t^{\beta} \langle \mathscr{G}_n \rangle \,, \tag{4.37}$$

Thus, the variance of the displacement becomes

$$s^2(t) = t^{\beta} (\mathscr{G}_n - \langle \mathscr{G}_n \rangle) \sim t^{2\beta} \,, \tag{4.38}$$

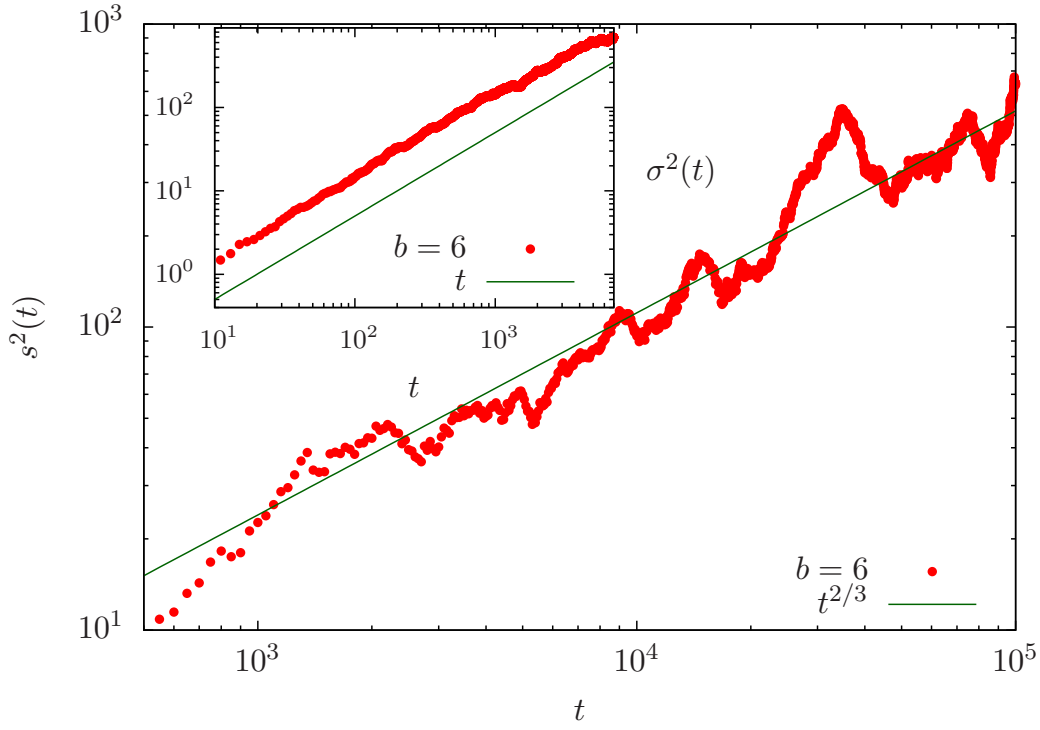

Fig. 4.10 Growth of the variance of the displacement in time at critical point is shown for hop rate (3.18) when $b = 6$ for the system size $L = 16000$. The main figure shows the growth of the variance s^2 as $t^{2/3}$ same as in TASEP given by (4.38). The inset shows the linear growth of the variance σ^2 (4.36) when average is taken over several initial conditions.

where $\beta = 1/3$ for TASEP. Hence, we recover two different scaling of $\sigma^2(t)$ and s^2 (see ref. [74] for details).

Note that although, there is fair amount of literature for hop rate (3.18), but the result is not very clear at critical point [66]. Here, we do not comprehensively analyse this, rather, we carry out some numerical simulations to understand the growth of the displacement fluctuation of a tagged particle at the critical point. Following the study of TASEP given earlier in this section, we require knowledge of the roughness exponent α and the growth exponent β at the critical point [3]. In Sec. 4.4, we have found two different regimes for the roughness exponent and growth exponent. For $2 < b < 3$, we have continuously varying exponents, and for $b > 3$, we have exponents as that for the KPZ equation. Therefore, for $b > 3$, the variance of displacement is expected to show the same result as TASEP.

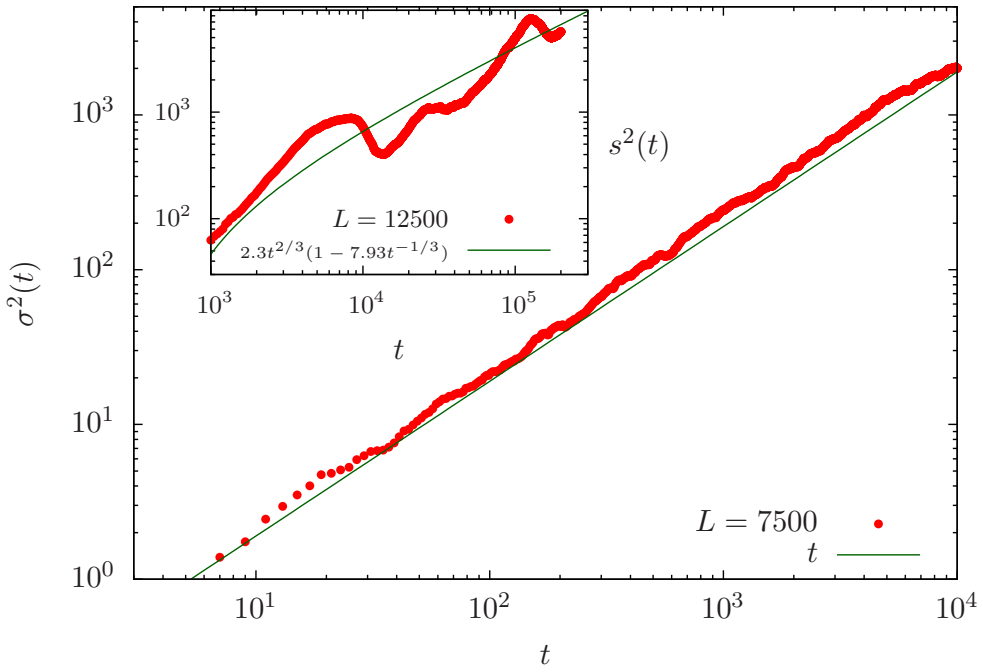

Fig. 4.11 Growth of the variance of the displacement in time at the critical point is shown for the hole-dependent hop rate (3.18) when $b = 3.5$ for the system of size $L = 12000$. The main figure shows the linear growth (4.36) for the variance, σ^2 which is averaged over several initial conditions. The inset shows the growth of the variance, s^2 with next order correction when averaged over stochastic histories only.

The results obtained from numerical simulations for the hop rate (3.18) are compared with the known TASEP results [66]. On the basis of the result of roughness exponents (4.13) and growth exponents α/z where $z = 3/2$, the fluctuation in the tagged particle displacement is calculated from (4.36) and (4.38).

4.7.1 Variance of a tagged particle displacement when $b > 3$

For $b > 3$, the exponents α and β are $1/2$ and $1/3$ respectively, same as in TASEP. Therefore, the results for the variance s^2 and σ^2 are same as in TASEP case and are given by equations (4.38) and (4.36) respectively. This has been confirmed by the numerical simulations as shown in Figs. 4.10 and 4.11. In Fig. 4.11, we consider next order correction of the variance $s^2(t)$ similar to the correction incorporated for the autocorrelation function (4.22).

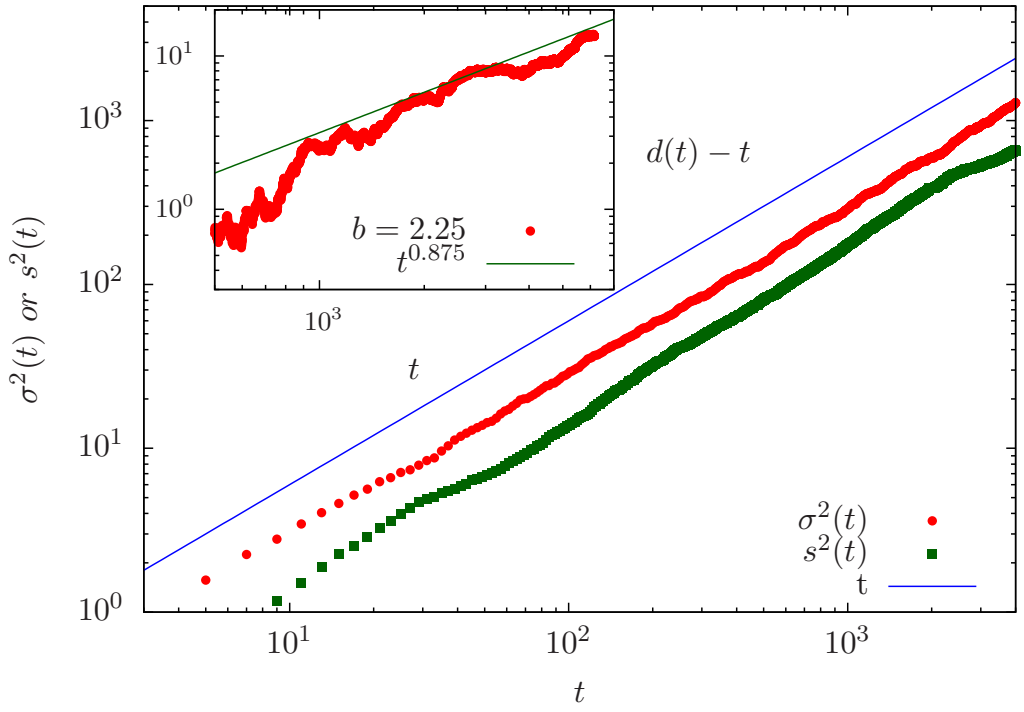

Fig. 4.12 Growth of the variance of the displacement in time at the critical point is shown for the hole-dependent hop rate (3.18) when $b = 2.25$ for the system of size $L = 15000$. The main figure shows the linear growth for both variance σ^2 and s^2. The inset shows the next-order term of the displacement given in (4.35) which represent the value of roughness exponent α.

4.7.2 Variance of a tagged particle displacement when $2 < b < 3$

In this case, the static correlation function suggests that the roughness exponent α is continuously varying with hop parameter, $\alpha = (4-b)/2$. Hence the growth exponent β is also continuously varying with exponent $(4-b)/2z$. Using these values of exponents in (4.36), and (4.38), we get the variance of the displacement as

$$\sigma^2(t) \sim t^{(4-b)}, \text{ when averaged over different initial configurations}, \tag{4.39}$$

$$s^2(t) \sim t^{(4-b)/z}, \text{ when averaged over stochastic histories only}. \tag{4.40}$$

This suggests that the growth of $\sigma^2(t)$ and $s^2(t)$ are faster compared to that for $b > 3$. However the numerics suggest that the growth of the fluctuation is linear for both σ^2 (when the

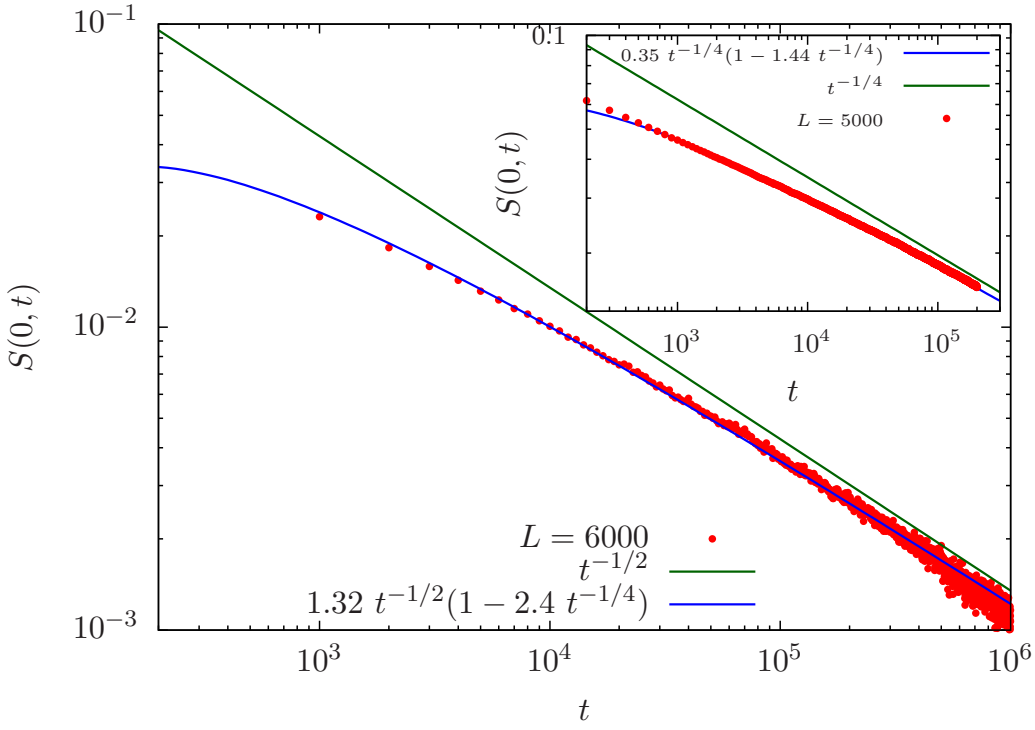

Fig. 4.13 Autocorrelation function at the critical point for the bidirectional case for hop rate $u(m) = 1 + b/m$ discussed in Sec. 2.2.1 for $b = 3.5$ (main) and 2.5 (inset). The results of autocorrelation function is consistent with numerical simulation with dynamical exponent $z = 2$.

initial configuration is averaged) and s^2 (with fixed initial condition) as shown in main figure of Fig. 4.12. The exponent for variance s^2 is same as given by (4.40) while σ^2 is different from (4.39). We do not know the reason for this difference yet, and would like to revisit it in future. Moreover, we have checked the second leading order term for the displacement of a tagged particle and it is consistent with the exponent given by roughness exponent α as shown in the inset of Fig. 4.12.

4.8 Summary

Although the critical dynamics of some nonequilibrium phase transitions such as absorbing state transitions [75] have been rather well studied, such questions have not been addressed for the condensation transition and the related jamming transition barring some

exceptions [27, 67]. The dynamical behavior in the stationary state for the latter class of transitions is the subject of this Chapter.

Here we studied several one-dimensional models in which the particles have hard core interactions and always hop in one direction. Our main finding is that when the equal time density-density correlation function decays faster than the inverse of the distance, the autocorrelation function decreases with time in the same way as in the TASEP. However for slower decaying $S(r,0)$, the autocorrelation function $S(0,t)$ also decays slower than $t^{-2/3}$ and with an exponent that varies continuously with a model parameter. In a driven system of hard core particles with nonlocal hop rates, the static correlation function is found to decay as r^{-2} and the dynamic exponent has been shown to be one [76], unlike here where $z = 3/2$ is found to be robust.

For a generalisation of the hop rate (2.12) given by $u(n) = 1 + (b/n^{\lambda})$, the jamming transition occurs when $0 < \lambda < 1, b > 0$ (besides the case considered here, namely, $\lambda = 1, b > 2$) [77]. In the former case, at the critical point, the single site mass distribution $p(m) \propto \exp\left[-b(1-\lambda)^{-1} m^{1-\lambda}\right]$ decays faster than a power law as in the fluid phase. As a consequence, the roughness exponent remains one half [2] and the dynamical behavior is the same as in the TASEP for all $0 < \lambda < 1, b > 0$. We have also studied a bidirectional version of the model in Sec. 4.2 in which a particle may hop to either side with equal probability at a rate that depends on the number of holes in the direction toward which it chooses to hop. This model can be mapped to a symmetric ZRP whose steady state is the same as in Sec. 4.2. As a result, the roughness exponent does not change from the driven model. However, since the steady state current vanishes, the dynamic exponent $z = 2$ here [46, 65] as shown in Fig. 4.13. Our numerical simulations for the autocorrelation function given by (4.7) are consistent with these values of the roughness exponent and the dynamic exponent.

We note that the Galilean invariance which holds for the KPZ equation and yields the scaling relation $\alpha + z = 2$ is violated for the models studied here at the critical point when the static correlation function decays slower than $1/r$. Precisely what is responsible for this breakdown is not understood. We have been able to obtain an understanding of the KPZ dy-

namic exponent $z = 3/2$ in the models discussed here using a hydrodynamic theory when the third cumulant of the hole distribution is finite, but an extension of the hydrodynamic description to the complete range of parameters at the critical point is desirable.

Chapter 5

Critical dynamics of classical systems under slow quench

5.1 Introduction

In the past few decades, extensive studies have been carried out to understand the phase ordering dynamics of classical systems with equilibrium [78] and nonequilibrium steady states [54, 67, 53] when the system is quenched infinitely fast from a disordered state to an ordered one. Slow quench (or annealing) dynamics have also attracted some attention in the recent years, and have been invoked to understand the defect structures in the early universe [6, 79] and more generally, to systems exhibiting second order phase transitions [7, 80] in both classical [81–87] and quantum [88–92] settings. Moreover, a number of experiments investigating the relationship between defect density and quench rates have also been performed in variety of systems such as liquid crystals, superfluid ^{3}He, superconductors, Bose-Einstein condensates and colloidal systems, see [93] for a recent review. The defect density at the end of the quench is generally found to decay as a power law in the inverse quench rate (although some systems such as 2D XY model exhibit non-algebraic decay [94, 95]).

Much of the body of work on slow quench dynamics appeals to the Kibble-Zurek argument [6, 7] which states that if the control parameter is varied slowly across the criti-

cal point, the system stays close to the steady state (*adiabatic regime*) until its relaxation time becomes longer than the quench time after which the dynamics are hypothesised to remain “frozen" (*impulse regime*) until the critical region is crossed. Thus the argument applies only for quench processes near the critical point, but recent works have elucidated the slow annealing dynamics when the system is quenched far from the critical point to an ordered phase and argued that the defect density is determined by coarsening dynamics [85, 94]. However the question about the dynamical behavior when the system is quenched slowly *in the critical region* has not been addressed in previous investigations. Moreover, all the studies mentioned above deal with systems with equilibrium steady state (but, see [96] that considers a nonequilibrium quantum system).

Here we consider the slow quench dynamics of the jamming transition that occurs in diverse settings such as vehicular traffic [20], cellular traffic [19] and granular media [23]. We study a classical nonequilibrium system in one dimension which shows a jamming transition in the stationary state [47]. The steady state of this model is known exactly [1], and some results for the coarsening dynamics [5, 53] and stationary state dynamics [3] have also been obtained. However the dynamics of this model under slow annealing have not been studied and here we address this problem using numerical simulations and analytical arguments. We find that the standard Kibble-Zurek scaling explains our results in the critical region but close to the critical point and for quenches deep in the jammed phase, the defect density decay can be understood using the corresponding results for rapid quench dynamics [85].

5.2 Model

We consider an exclusion process with hole-dependent rates given by

$$u(n) = 1 + \frac{b}{n}\,,\ n > 0\,. \tag{5.1}$$

The stationary state properties of this model and its mapping to a Zero Range Process (ZRP) have been described in Sec. 2.2.1. Here we recall that for this hop rate, a jamming transition

occurs at

$$b_c = \frac{2-\rho}{1-\rho}\,, \tag{5.2}$$

where $\rho = N/L$ is the total particle density. For $b < b_c$, the typical hole cluster length is of order unity (fluid phase) while for $b > b_c$, a macroscopically long hole cluster coexists with gaps that are power law distributed as n^{-b} (jammed phase) [1]. As shown in Appendix D.1, close to the critical point, the static correlation length $\xi \sim (b_c - b)^{-\nu}$, diverges with an exponent ν that varies continuously with b_c when $2 < b_c < 3$ but is a constant otherwise [2],

$$\nu = \begin{cases} (b_c-2)^{-1} & ,\ 2 < b_c < 3, \\ 1 & ,\ b_c \geq 3\,. \end{cases} \tag{5.3}$$

The stationary state dynamics have also been studied and it has been found that at the critical point, the steady state density fluctuations decay on a time scale that grows as L^z where the dynamic exponent $z = 3/2$ [3].

In the following, we also consider a *bidirectional model* in which the particle first chooses either the left or the right neighbor with equal probability and then hops with a rate that depends on the vacancies in the chosen direction provided the target site is empty. The steady state obeys detailed balance and is the same as that in the unidirectional model [1]. As a result, the correlation length exponent ν is given by (5.3); however, the dynamic exponent $z = 2$ in this case [3].

To study the slow quench dynamics, we introduce time-dependence in the hop rates and write

$$u(n,t) = 1 + \frac{b(t)}{n}\,,\ n > 0\,, \tag{5.4}$$

where, for simplicity, we work with linearly varying b given by

$$b(t) = \frac{b_\tau\, t}{\tau}\,,\ 0 \leq t \leq \tau\,. \tag{5.5}$$

The quench protocol was carried out by changing the parameter b from zero (in the fluid phase) to a final value $b_\tau = b_c$ (critical point) and $2b_c$ (jammed phase) keeping the density

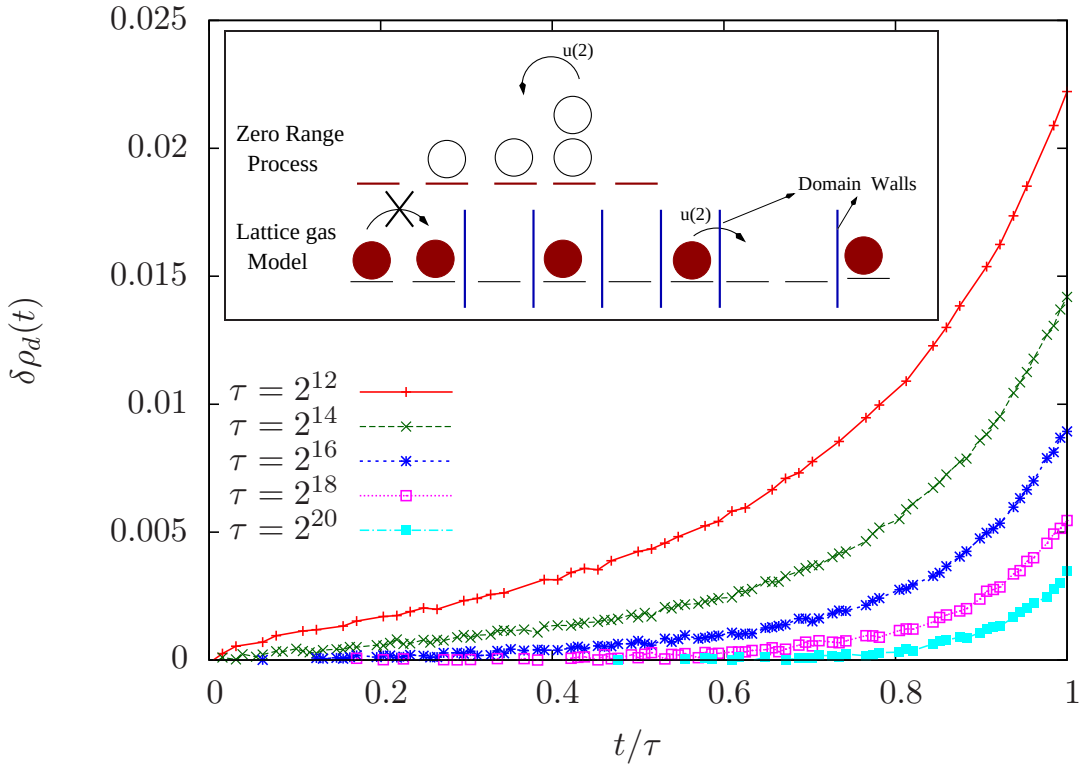

Fig. 5.1 Inset shows the unidirectional lattice gas model studied in this article and the related zero range process. Main figure shows the dynamics of the excess defect density defined in (5.6) for $b_\tau = b_c = 2.3$ in the unidirectional model.

fixed at ρ_c which is given by (5.2). Our quantity of interest is the domain wall density (which is the interface between the particle and hole) in the lattice gas model. From the inset of Fig. 5.1, we see that the number of domain walls is equal to two times the number of occupied sites in the ZRP. For finite inverse quench rate τ, as the system is far from its steady state and has more domain walls than at stationarity, we consider the excess defect density given by

$$\delta\rho_d(t) = 2\rho_c[p(0,t) - p(0)]\,, \tag{5.6}$$

where $p(0,t)$ is the probability that a site is empty at time t in ZRP when the parameter b is time-dependent and $p(0)$ is given by (2.6). In Monte-Carlo simulations of the mod-

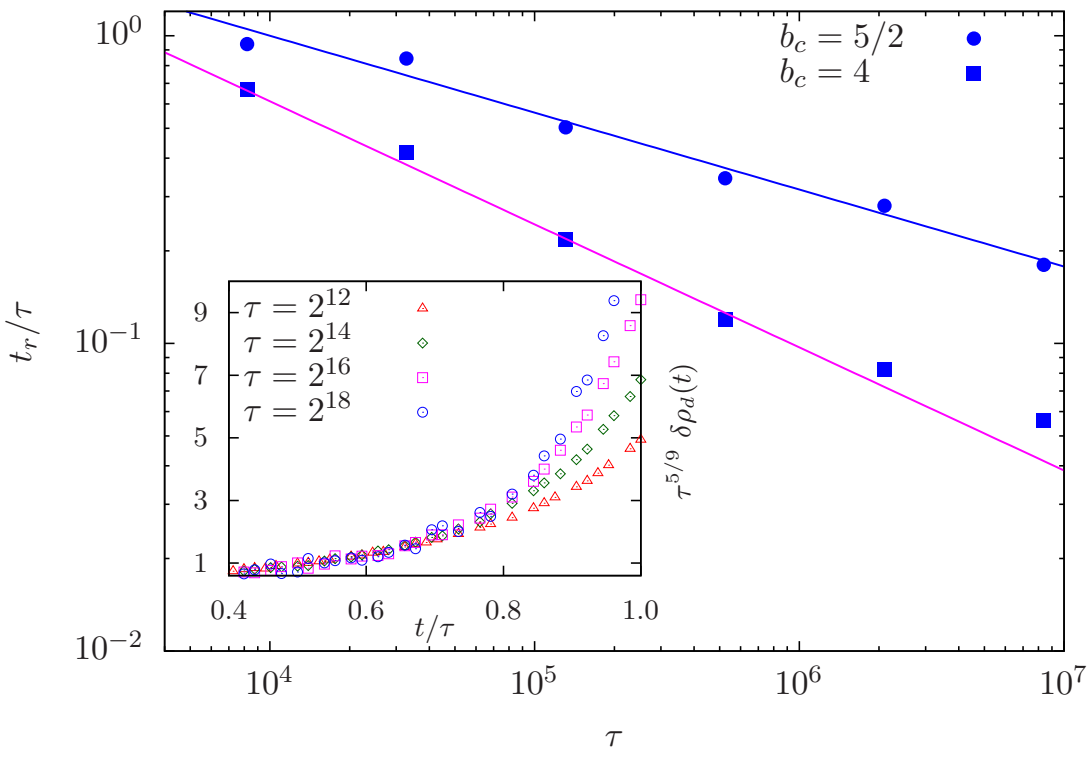

Fig. 5.2 Main figure shows that the remaining time t_r to the critical point obeys the Kibble-Zurek prediction (5.7) for the unidirectional model when $b_\tau = b_c$. Inset shows the collapse of excess defect density with the Kibble-Zurek scaling (5.8) for time $t_* < t < \tau$ when the system is quenched to $b_\tau = b_c = 2.3$.

els described above, we measured $\delta\rho_d(t)$ for system sizes in the range 15000 – 20000 and averaged the data over 2000 – 4000 independent initial conditions.

5.3 Results

When the quench rate τ^{-1} is very small, the parameter b changes very slowly allowing the system to relax to the stationary state. But for faster quench, the system is farther from the steady state. Indeed, as Fig. 5.1 shows, the excess defect density $\delta\rho_d(t)$ decreases with increasing τ. Our objective here is to understand how $\delta\rho_d(\tau)$ decays with τ when the system is quenched slowly to b_τ.

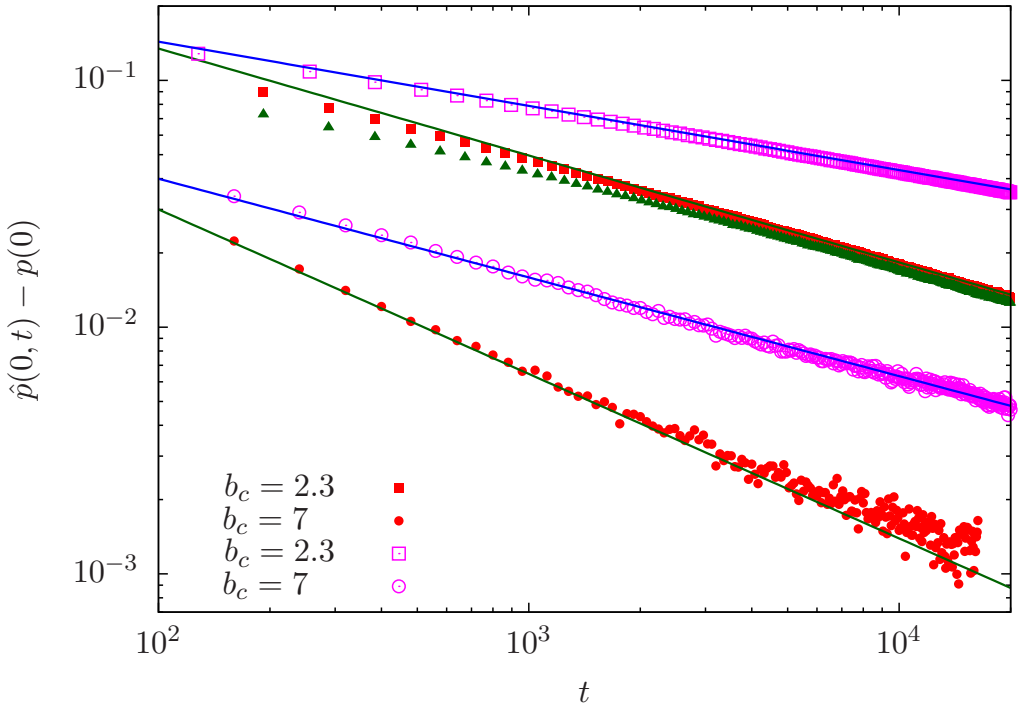

Fig. 5.3 Power law decay of the probability $\hat{p}(0,t) - p(0)$ with time after a fast quench to the critical point starting from $b = 0$ to b_c with density ρ_c in the unidirectional model (closed symbols) and bidirectional model (open symbols). The lines show the scaling (5.9) and the triangular closed symbols show the numerical data when the system is quenched instantaneously to $b_c = 2.3$ from the initial value one.

5.3.1 Dynamics in the critical region

When the system is far from the critical point, it relaxes quickly. But as the critical point is approached, the relaxation time increases and at time t_*, the remaining time $t_r = \tau - t_*$ to reach the critical point becomes comparable to the relaxation time in the stationary state which can be expressed as [6, 7]

$$\tau - t_* \sim \xi_*^z \sim (b_c - b(t_*))^{-z\nu} \sim \left(1 - \frac{t_*}{\tau}\right)^{-z\nu}, \tag{5.7}$$

so that $t_r \sim \tau^{\frac{z\nu}{1+z\nu}}$. As the system falls out of equilibrium at t_*, in numerical simulations, we picked the time t_* to be the one where the excess domain wall density is 10^{-3} and found the time t_r. Using the exponents ν and z quoted in the last section, we find that for the

unidirectional model, the time $t_r \sim \tau^{3/(2b_c-1)}$ for $2 < b_c < 3$ and as $\tau^{3/5}$ for $b_c \geq 3$ which is in good agreement with the numerical data in Fig. 5.2. (We have checked that our scaling results are not affected if t_* is determined by the criteria that excess defect density $\lesssim 10^{-3}$).

Assuming that the system does not evolve after time t_*, the defect density *after* crossing the critical point is posited to be $\delta\rho_d(\tau) \sim \xi_*^{-1} \sim \tau^{-\nu/(1+\nu z)}$ [6, 7]. However, we find that the Kibble-Zurek scaling works well for times $< \tau$ but not at or after the critical point is crossed (see below). Our simulation results for the unidirectional model shown in the inset of Fig. 5.2 for a quench to the critical point demonstrate that the excess defect density is of the form,

$$\delta\rho_d^{(\mathrm{uni})}(t) = \begin{cases} \tau^{-\frac{2}{2b_c-1}} f(t/\tau) & , \ 2 < b_c < 3 \, , \\ \tau^{-2/5} f(t/\tau) & , \ b_c \geq 3 \, , \end{cases} \tag{5.8}$$

where $f(x)$ is the scaling function and $t_* < t < \tau$. We also find that the above scaling form breaks down at times of order t_*.

Close to the critical point, the system undergoes critical coarsening during the time interval t_r [85]. We therefore turn to a discussion of the fast quench dynamics of the ZRP in which the system initially in the fluid phase is quenched instantaneously to the critical point. To distinguish between the quantities obtained using slow and fast quench, in the following, we use $\hat{}$ to refer to quantities obtained using the fast quench protocol. In [5], critical coarsening dynamics of the ZRP have been investigated in mean-field geometry and in one dimension. In the latter case, numerical simulations indicate that a measure of the domain length grows with time as $t^{1/\hat{z}}$ with the coarsening exponent $\hat{z} = 3$ (5) for unidirectional (bidirectional) model and a scaling argument suggests that the probability $\delta\hat{p}(0,t) \sim t^{-\hat{\alpha}}$ with the exponent $\hat{\alpha} = (b-2)/\hat{z}$ for $b > 3$. While our numerical results for $\hat{z}$ are in agreement with those of [5], the distribution of empty sites does not obey the scaling law claimed by Godréche. Instead, our numerical results shown in Fig. 5.3 suggest that $\delta\hat{p}(0,t) \sim t^{-\hat{\alpha}}$ where,

$$\hat{\alpha} = \begin{cases} (b_c-1)/\hat{z} & , \ 2 < b_c < 3 \, , \\ 2/\hat{z} & , \ b_c \geq 3 \, . \end{cases} \tag{5.9}$$

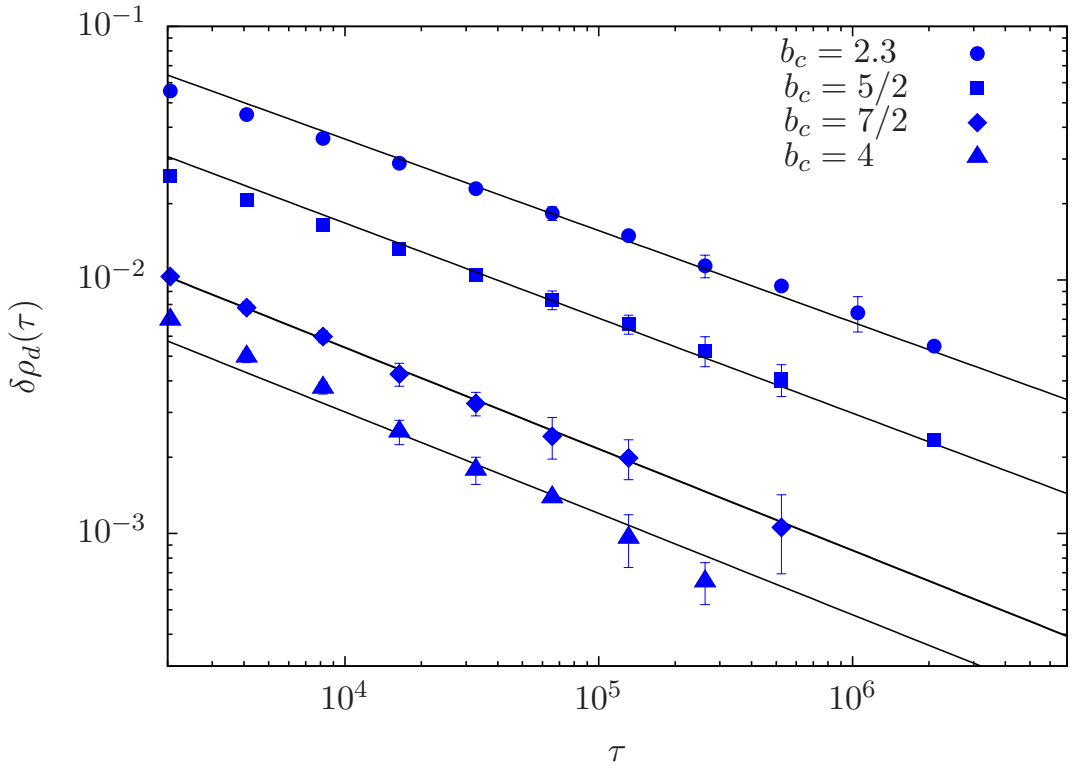

Fig. 5.4 Decay of the excess defect density when the system is quenched slowly to the critical point ($b_\tau = b_c$) in the unidirectional model. Our scaling prediction (5.12) is compared with numerical data for several values of b_c and the errorbars for some representative points are also shown.

In the stationary state, using the fact that the mass distribution $p(n) \sim n^{-b}$ at the critical point and extreme value theory [97], it can be seen that in a system of size L, the largest mass is of the order $L^{1/(b-1)}$ for $b > 2$. These considerations also show that

$$p(0,L) - p(0) \sim \int_{L^{\frac{1}{b-1}}}^{\infty} dn\, n^{-b} \sim L^{-1}\,, \tag{5.10}$$

and the mass fluctuation ℓ grows as [47]

$$\ell \sim \begin{cases} L^{1/(b-1)} & ,\ 2 < b < 3\,, \\ \sqrt{L} & ,\ b \geq 3\,. \end{cases} \tag{5.11}$$

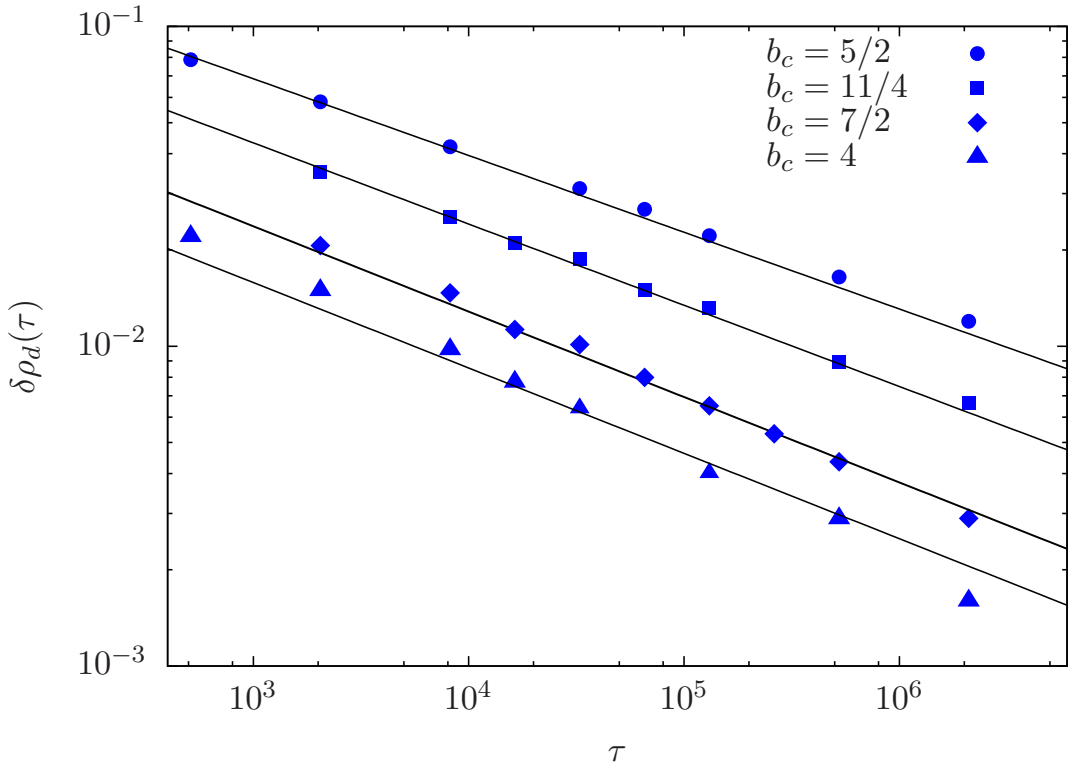

Fig. 5.5 Decay of the excess defect density when the system is quenched slowly to the critical point ($b_\tau = b_c$) in the bidirectional model. Our scaling prediction (5.13) is compared with numerical data for several values of b_c; the errorbars in this case are smaller than the point size.

However, as mentioned above, on rapid quench, the mass fluctuation $\hat{\ell}(t) \sim t^{1/\hat{z}}$ [5] on using which in (5.11) yields a relationship between time and system size thence leading to $\delta\hat{p}(0,t) \sim t^{-\hat{\alpha}}$ with $\hat{\alpha}$ given by (5.9).

Using the above results and recalling that the coarsening process initiates at time of order t_*, we obtain $\delta\rho_d(\tau) \sim t_r^{-\hat{\alpha}} \sim \tau^{-z\nu\hat{\alpha}/(1+z\nu)}$ when the system is quenched to the critical point. Here we have ignored the dependence on the quench depth (*i.e.*, $b_c - b(t_*)$) since our numerical results in Fig. 5.3 suggest that the long time dynamics are independent of it. More explicitly, for the unidirectional model, we have

$$\delta\rho_d^{(\mathrm{uni})}(\tau) \sim \begin{cases} \tau^{-\frac{b_c-1}{2b_c-1}} & , \ 2 < b_c < 3 \,, \\ \tau^{-2/5} & , \ b_c \geq 3 \,, \end{cases} \tag{5.12}$$

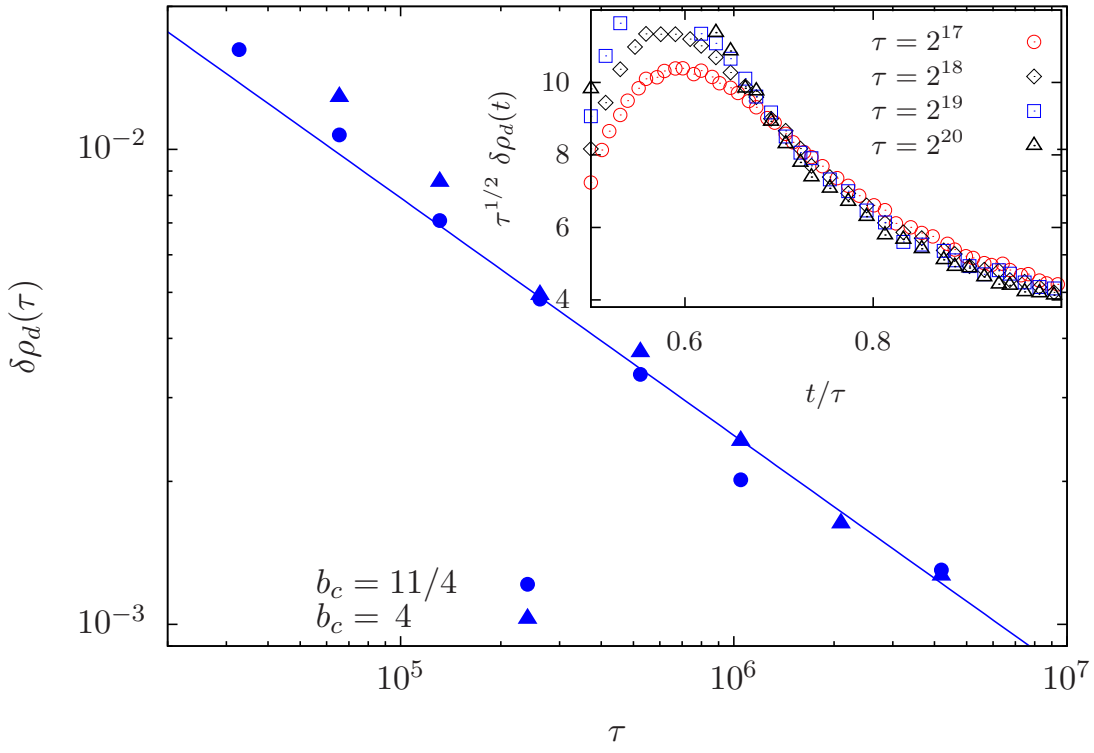

Fig. 5.6 Decay of the excess defect density in the unidirectional model when the system is quenched slowly to $b_\tau = 2b_c$. The lines in the main figure show (5.14) and the data collapse with the coarsening exponents in the jammed phase is shown in the inset for $b_\tau = 2b_c, b_c = 2.3$.

while, for the bidirectional model, we get

$$\delta\rho_d^{(\mathrm{bi})}(\tau) \sim \begin{cases} \tau^{-\frac{2(b_c-1)}{5b_c}} & , \ 2 < b_c < 3\,, \\ \tau^{-4/15} & , \ b_c \geq 3\,. \end{cases} \tag{5.13}$$

The above predictions for the excess defect density are consistent with the numerical results shown in Figs. 5.4 and 5.5 when $b_\tau = b_c$. We have also checked that the above scaling predictions hold when the system is quenched in the vicinity of b_c.

5.3.2 Dynamics in the jammed phase

For $b_\tau \gg b_c$, the system undergoes coarsening in the jammed phase after the time $t_c + t_r$ where $b(t_c) = b_c$ [85]. As the time scale $t_c \sim \tau$ but t_r is sublinear in τ, the time left until the quench is of order τ. Thus we expect the defect density to simply decay as

$$\delta\rho_d(\tau) \sim \tau^{-1/\hat{z}}\,,\; b_c > 2\,, \tag{5.14}$$

where the coarsening exponent $\hat{z} = 2$ ($\hat{z} = 3$) for unidirectional (bidirectional) model [53, 1]. Fig. 5.6 shows that our numerical results for $b_\tau = 2b_c$ are consistent with the above scaling prediction. Moreover, the excess defect density $\delta\rho_d(t)$ is of a scaling form similar to (5.8) as attested by the data collapse shown in the inset of Fig. 5.6.

5.4 Slow quench dynamics of zero range process in mean field geometry

Here, we consider a zero range process (ZRP) in mean-field geometry, in which, a particle hops to any other site with a rate depending on the number of particles at the departure site which is given in (5.1). For this choice of hop rate, in the mean-field, one obtains a condensation transition at

$$b_c = \frac{1}{\varrho} + 2\,, \tag{5.15}$$

where ϱ is a finite density. The stationary state is specified by a product measure (as reviewed in Sec. 2.2.1). Along with the stationary state properties, the model has well studied coarsening dynamics both at the critical point and in the condensed phase [5](see Sec. 2.4). Here, our intention is to extend the study of slow quench dynamics in the mean-field geometry [9]. For slow quench process in mean-field geometry, a particle hops to any other site with time dependent hop rates (5.4). To perform study, we compute the excess probability of a site having zero mass, in comparison with its probability at stationary state

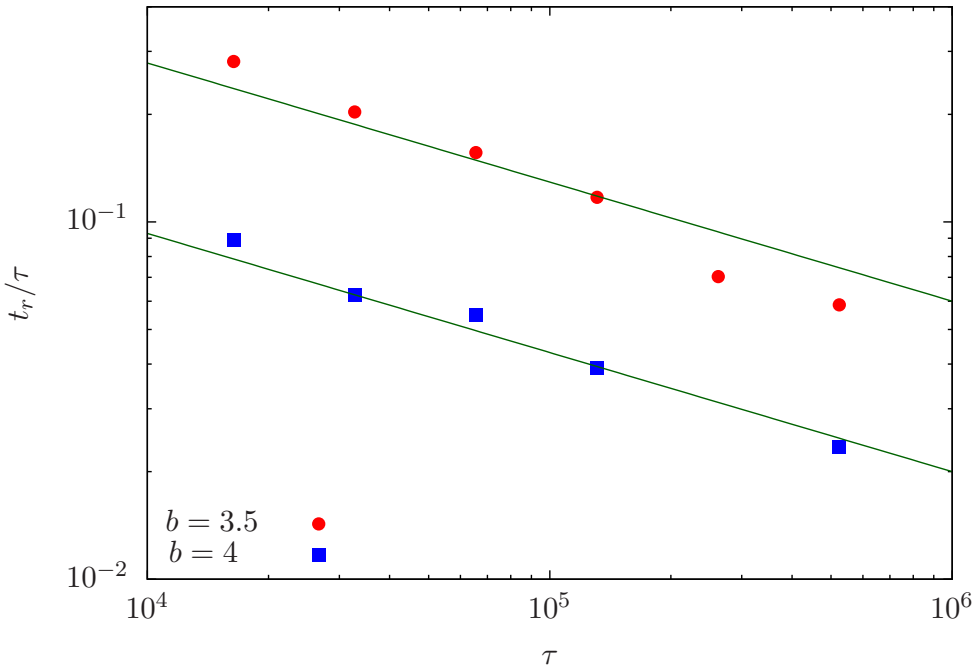

Fig. 5.7 The Kibble-Zurek prediction (5.7) for the remaining time t_r to reach the critical point is shown in the figure for $b > 3$.

$$\delta p(t) = p(0,t) - p(0)\,, \tag{5.16}$$

where $p(0,t)$ is the probability of a site having zero mass at time t. Similar to one dimension, we start the analysis with the help of Kibble-Zurek argument, and therefore, we expect the decay of the excess probability of a site having zero mass, at the critical point to be $\tau^{-\nu z\alpha/(1+\nu z)}$, with appropriate exponents. In order to determine this excess probability we need information of the unknown exponents z, α and ν. The exponents α and ν are already known from the previous studies [5, 2]. The correlation length ξ which scales as $\xi \sim (b_c - b)^{-\nu}$ diverges at the critical point with exponent ν is given in (5.3). The exponent α is decay exponents of the probability of a site having zero mass in time at the critical point due to fast quench process and is explained in Sec. 2.4. Further, we need to know about the nature of the stationary state fluctuation in order to determine the exponent z. The simplest way is to get an understanding of the fluctuation via hydrodynamic equation in higher dimensions. Earlier studies on the KPZ equation have shown that above the upper

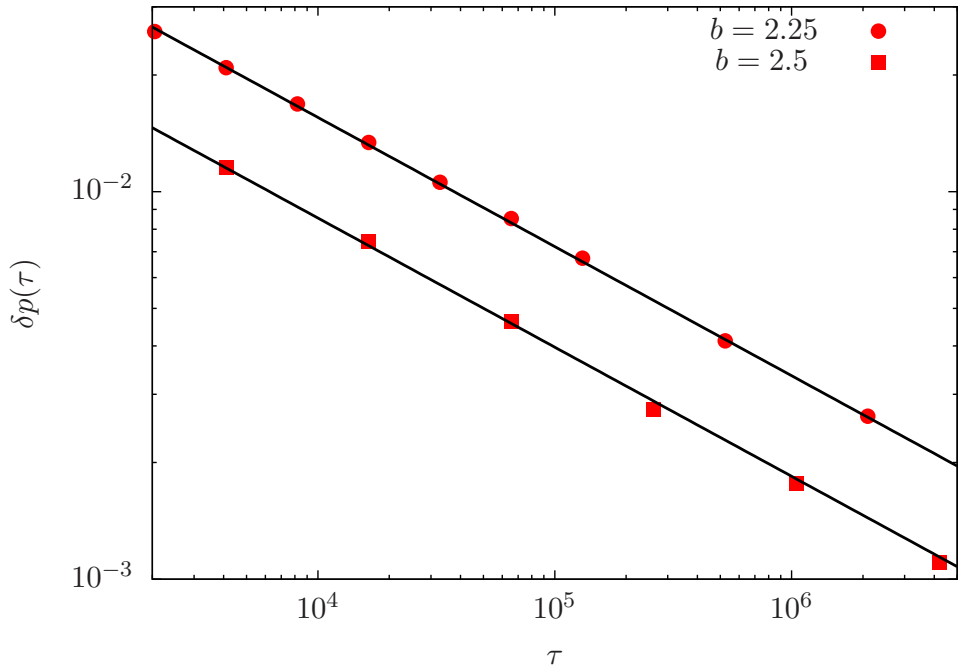

Fig. 5.8 Decay of defect density when the system is quenched slowly to the critical point ($b_\tau = b_c$) in mean-field geometry of ZRP for $2 < b < 3$. The numerical results show the decay of excess probability of a site having zero mass in comparison to its stationary state in τ with an exponent $1/3$, for two values of b.

critical dimension, the dynamical exponent z changes from $3/2$ to 2 [98]. Therefore, we consider the dynamical exponent $z = 2$ for this case. Nevertheless, it is worth mentioning that a more comprehensive understanding of the stationary state fluctuation in mean-field is still needed and is one of the goals for the future work. Below, we briefly describe the results obtained so far for this model.

5.4.1 Dynamics in the critical region

Using the above mentioned exponents for mean-field, we have first checked for the Kibble-Zurek scaling (5.7) of the remaining time t_r, to reach the critical point and find good agreement with numerical simulations for $b_c > 3$, as shown in Fig. 5.7.

Close to the critical point, system undergoes critical coarsening during the remaining time in the same manner as given for one dimension in Sec. 5.3.1 but with different expo-

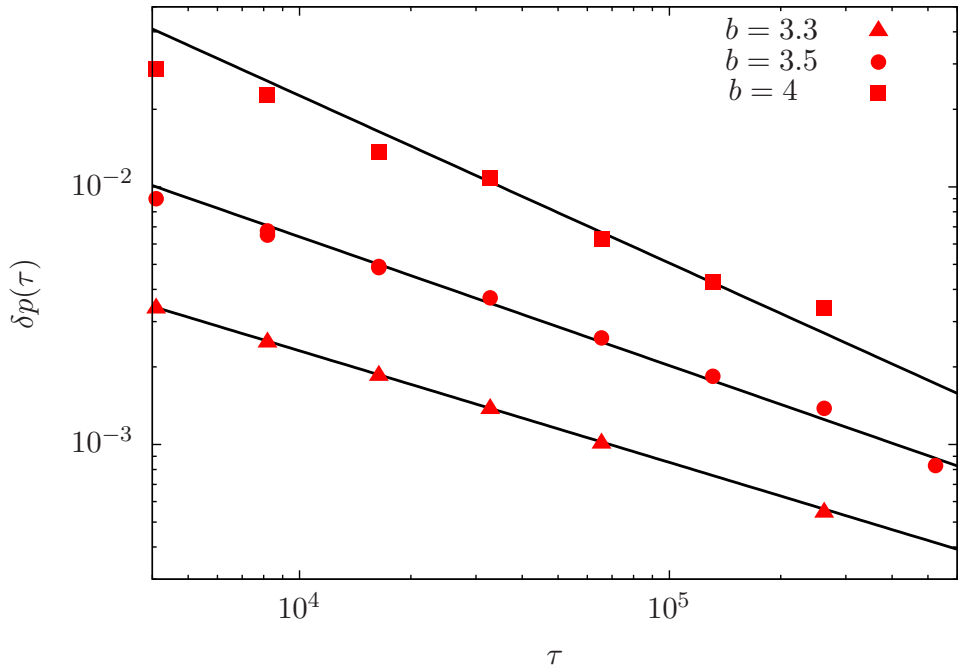

Fig. 5.9 Decay of defect density when the system is quenched slowly to the critical point ($b_\tau = b_c$) in mean-field geometry of ZRP. Our prediction (5.17) is compared with numerical data for several $b_c > 3$ in mean-field geometry.

nent. Using the known results of the critical coarsening for mean-field [5] (as described in Sec. 2.4) and remaining time t_r, the excess probability of a site having zero mass in comparison to the stationary state can be shown to algebraically decay with τ at the critical point. For $2 < b_c < 3$, the excess probability $\delta p(\tau)$ decays in τ with a exponent $1/3$, whereas for $b_c > 3$, the exponent is continuously varying with the hop parameter as shown in Figs. 5.8 and 5.9. However, the analytical results in the mean-field picture, suggest the decay of excess probability as

$$\delta p(\tau) \sim \begin{cases} \tau^{-\frac{1}{b_c}} & , \ 2 < b_c < 3 \, , \\ \tau^{-(b_c-2)/3} & , \ b_c \geq 3. \end{cases} \tag{5.17}$$

For $b_c > 3$, the numerical simulations are consistent with the result (5.17) which is shown in Fig. 5.9, whereas, for $2 < b_c < 3$, we find a disagreement with the predicted exponent of $1/b_c$ shown in Fig. 5.8.

Further, we are also trying to understand the slow quench dynamics of the mass distribution analytically by analysing the modified master equation. The dynamical equation for the evolution of the single site mass distribution with the time-dependent hop rates is given as

$$\begin{aligned}\frac{\partial p_\tau(n,t)}{\partial t} &= u(n+1,t)\,p_\tau(n+1,t) + \bar{u}(t)\,p_\tau(n-1,t) - u(n,t)\,p_\tau(n,t) - \bar{u}(t)\,p_\tau(n,t), n>0\,,\\ \frac{\partial p_\tau(0,t)}{\partial t} &= u(1,t)\,p_\tau(1,t) - \bar{u}(t)\,p_\tau(0,t)\,, \end{aligned} \tag{5.18}$$

where $u(n) = 1 + b(t)/n$ and $b(t) = \delta\frac{t}{\tau}$. The $\bar{u}(t)$ is the mean hop rate in the model given by $\bar{u}(t) = \sum_n u(n,t)\,p(n,t)$. We perform exact integration of the equation (5.18) for different τ values and find that the results obtain by integration are consistent with the simulation results and same as shown in Figs. 5.8 and 5.9. The detailed analysis is in progress [9].

5.5 Summary

Slow quench dynamics have been studied extensively when the control parameter is changed across the critical point of a second order phase transition in equilibrium systems [7, 80] and recent works have considered slow quenches deep into the ordered phase [85, 94]. Here we have performed, to our knowledge, first quantitative study for the slow quench dynamics when the system is quenched in the critical region.

The Kibble-Zurek argument assumes that in the critical region, the dynamics are frozen since the relaxation times are much longer than the time available. Here, we find that the defect density decays as a power law even within the so called frozen regime although with an exponent smaller than or equal to the Kibble-Zurek prediction. While the dynamics outside the critical region involve only the stationary state dynamic exponent (z) and the deep quench in the ordered phase is determined by the coarsening exponent ($\hat{z}$), the critical point quench dynamics are more complex involving both static fluctuations and critical coarsening.

For the class of models considered here, a comparison of the decay exponents shows that the excess defect density decays faster in the unidirectional model which has a nonequilibrium steady state than in the bidirectional model with equilibrium steady state. We also obtain continuously varying exponents for $2 < b < 3$ where the mass fluctuations are anomalous but constant otherwise [1].

A detailed exploration of other nonequilibrium and equilibrium systems with critical point annealing should inform us better about the dynamics in the impulse regime and is a goal for the future.

Chapter 6

Summary

In this Chapter, we summarise our main findings and give a brief outlook of future research. We have considered several stochastic models that exhibit jamming and condensation transitions. Although, in the recent past, several authors have studied stationary state properties and dynamics of condensates, a complete and coherent picture at the critical point has been lacking. This thesis has made some efforts in this regard; it provides a detailed study of nonequilibrium stationary states and dynamical properties at the critical point within the scope of certain one-dimensional driven lattice gas models. In particular, we have focused on models whose stationary measures are either of a product form or given by the mean-field approximation. Mostly, the emphasis is on the study of the two-point correlation function which describes the statistical fluctuation of density at critical point.

In Chapter 3, exact static two-point correlation functions in the canonical ensemble and in the thermodynamic limit which are valid in the fluid phase and at the critical point are calculated. The main results obtained from this Chapter are:

(i) At the critical point, the exponent characterizing the power-law decay of the two-point correlation function changes continuously with the hop parameter when stationary state partition function of the model is given by a product measure.

(ii) The correlation length diverges with an exponent ν which changes continuously for the parameter regime where mass variance diverges, whereas it is constant otherwise.

(iii) Our calculation of two-point correlation function in the thermodynamic limit is valid even in a mean-field approximation. In the aggregation model, the correlation function decays with an exponent 1/2, and the correlation length decays with exponent $\nu = 1$.

The stationary state dynamical behavior for the jamming transition is the subject of Chapter 4. Our main findings in this regard are:

(i) The autocorrelation function decreases with time in the same way as in the TASEP when the equal time density-density correlation function decays faster than the inverse of the distance.

(ii) When the static correlation function decays slower than the inverse of the distance, the autocorrelation function decays slower than $t^{-2/3}$.

(iii) The Galilean invariance which holds for the KPZ equation and yields the scaling relation $\alpha + z = 2$ is violated at the critical point for the case when mass variance diverges.

Chapter 5 is devoted to understanding the role of cooling or annealing mechanism in the equilibration of the classical systems in the critical regime, especially via slow quench process. To the best of our knowledge, we have performed the first quantitative study of the slow quench dynamics when the system is quenched in the critical region. The main results we obtain from our study of slow quench dynamics are:

(i) The defect density decays as a power-law even within the so called “frozen regime ”of Kibble-Zurek scaling.

(ii) The critical point quench dynamics are more complex involving both static fluctuations and critical coarsening.

(iii) We obtain the exponents that are continuously varying in the region where the mass fluctuations are anomalous, and are constant otherwise.

The continuously varying critical exponents for the regime where the variance of the hole or mass clusters distribution diverges is key universal feature observed in our work. The

power-law distribution of clusters is hallmark of a phase transition and is observed in many scenarios. For this reason, we expect our results to hold in more general settings and we hope that this thesis would initiate further enquiry in this direction.

References

[1] M. R. Evans and T. Hanney. Nonequilibrium statistical mechanics of the zero-range process and related models. *J. Phys. A: Math. Gen.*, 38:R195, 2005.

[2] Priyanka, A. Ayyer, and K. Jain. Two-point correlation function of an exclusion process with hole-dependent rates. *Phys. Rev. E*, 90:062104, 2014.

[3] Priyanka and K. Jain. Critical dynamics of the jamming transition in one-dimensional nonequilibrium lattice-gas models. *Phys. Rev. E*, 93:042104, 2016.

[4] M. Prähofer and H. Spohn. Current fluctuations for the totally asymmetric simple exclusion process. In *In and Out of Equilibrium: Probability with a Physics Flavor*, pages 185–204. Birkhäuser Boston, Boston, MA, 2002.

[5] C. Godréche. Dynamics of the condensation in zero-range processes. *J. Phys. A: Math. Gen.*, 36(23):6313–6328, 2003.

[6] T. W. B. Kibble. Topology of cosmic domains and strings. *J. Phys. A: Math. Gen.*, 9(8):1387, 1976.

[7] W. H. Zurek. Cosmological experiments in superfluid-helium. *Nature*, 317:505–508, 1985.

[8] Priyanka and K. Jain. Critical dynamics of classical systems under slow quench. *arXiv:1607.00617*, 2016.

[9] Priyanka. Slow quench dynamics of zero range process in mean field geometry. *in preparation*, 2016.

[10] N.G. Van Kampen. *Stochastic Processes in Physics and Chemistry (Third Edition)*. Elsevier, 2007.

[11] K. Mallick. The exclusion process: A paradigm for non-equilibrium behaviour. *Physica A: Statistical Mechanics and its Applications*, 418:17 – 48, 2015. Proceedings of the 13th International Summer School on Fundamental Problems in Statistical Physics.

[12] B. Schmittmann and R. K.P. Zia. *Statistical Mechanics of Driven Diffusive Systems Vol 17*. Academic Press Inc., San Diego, CA, 1995.

[13] G. M. Schütz. Exactly solvable models for many-body systems far from equilibrium. In C. Domb and J. Lebowitz, editors, *Phase transitions and Critical Phenomena*, pages 3–242. Academic Press, London, 2000.

[14] W. Lenz. Beitrag zum Verständnis der magnetischen Erscheinungen in festen Körpern. *Z. Phys.*, 21:613–615, 1920.

[15] C. T. MacDonald, J. H. Gibbs, and A. C. Pipkin. Kinetics of biopolymerization on nucleic acid templates. *Biopolymers*, 6(1):1–25, 1968.

[16] F. Spitzer. Interacting markov processes. *Adv. Math.*, 5(2):246–290, 1970.

[17] S. Katz, J. L. Lebowitz, and H. Spohn. Phase transitions in stationary nonequilibrium states of model lattice systems. *Phys. Rev. B*, 28:1655–1658, 1983.

[18] S. Katz, J. L. Lebowitz, and H. Spohn. Nonequilibrium steady states of stochastic lattice gas models of fast ionic conductors. *J. Stat. Phys.*, 34(3):497–537, 1984.

[19] C. Leduc, K. Padberg-Gehle, V. Varga, D. Helbing, S. Diez, and J. Howard. Molecular crowding creates traffic jams of kinesin motors on microtubules. *Proc. Natl. Acad. Sci.*, 17:6100–5, 2012.

[20] D. Chowdhury, L. Santen, and A. Schadschneider. Statistical physics of vehicular traffic and some related systems. *Phys. Rep.*, 329:199–329, 2000.

[21] T. Chou. How fast do fluids squeeze through microscopic single-file pores? *Phys. Rev. Lett.*, 80(1):85–88, 1998.

[22] T. Karzig and F. von Oppen. Signatures of critical full counting statistics in a quantum-dot chain. *Phys. Rev. B*, 81:045317, 2010.

[23] A. J. Liu and S. R. Nagel. Nonlinear dynamics: Jamming is not just cool any more. *Nature*, 396:21–22, 1998.

[24] O. J. O'Loan, M. R. Evans, and M. E. Cates. Jamming transition in a homogeneous one-dimensional system: The bus route model. *Phys. Rev. E*, 58:1404–1418, 1998.

[25] J. Krug and P. A. Ferrari. Phase transitions in driven diffusive systems with random rates. *J. Phys. A: Math. Gen.*, 29(18):L465, 1996.

[26] M. R. Evans. Bose-Einstein condensation in disordered exclusion models and relation to traffic flow. *Europhys. Lett.*, 36(1):13–18, 1996.

[27] K. Jain and M. Barma. Dynamics of a disordered, driven zero-range process in one dimension. *Phys. Rev. Lett.*, 91:135701, 2003.

[28] A. John, A. Schadschneider, D. Chowdhury, and K. Nishinari. Trafficlike collective movement of ants on trails: Absence of a jammed phase. *Phys. Rev. Lett.*, 102:108001, 2009.

[29] E. Heisler, N. J. Suematsu, A. Awazu, and H. Nishimori. Swarming of self-propelled camphor boats. *Phys. Rev. E*, 85:055201, 2012.

[30] M. Kardar, G. Parisi, and Y. C. Zhang. Dynamic scaling of growing interfaces. *Phys. Rev. Lett.*, 56:889–892, 1986.

[31] A. G. Angel, M. R. Evans, E. Levin, and D. Mukamel. Criticality and condensation in a non-conserving zero-range process. *J. Stat. Mech.: Theor. Exp.*, 2004(08):P08017, 2004.

[32] S. Großkinsky and G. M. Schütz. Discontinuous condensation transition and nonequivalence of ensembles in a zero-range process. *J. Stat. Phys.*, 132(1):77–108, 2008.

[33] M. R. Evans and B. Waclaw. Condensation in stochastic mass transport models: beyond the zero-range process. *J. Phys. A: Math. Theor.*, 47(9):095001, 2014.

[34] J. Kaupužs, R. Mahnke, and R. J. Harris. Zero-range model of traffic flow. *Phys. Rev. E*, 72:056125, 2005.

[35] J. Török. Analytic study of clustering in shaken granular material using zero-range processes. *Physica A*, 355:374–382, 2005.

[36] P. K. Mohanty and S. Jalan. Analytical results for stochastically growing networks: Connection to the zero-range process. *Phys. Rev. E*, 77:045102, 2008.

[37] K. Jain. Simple sandpile model of active-absorbing state transitions. *Phys. Rev. E*, 72:017105, 2005.

[38] A. Ryabov. Zero-range process with finite compartments: Gentile's statistics and glassiness. *Phys. Rev. E*, 89:022115, 2014.

[39] Y. Kafri, E. Levine, D. Mukamel, G. M. Schütz, and J. Török. Criterion for phase separation in one dimensional driven systems. *Phys. Rev. Lett.*, 89:035702, 2002.

[40] T. M. Liggett. *Interacting Particle Systems*. Springer-Verlag, New York, 1985.

[41] E. D. Andjel. Invariant measures for the zero range process. *The Annals of Probability*, 10(3):525–547, 1982.

[42] C. Cocozza-Thivent. Processus des misanthropes. *Zeitschrift für Wahrscheinlichkeitstheorie und Verwandte Gebiete*, 70(4):509–523, 1985.

[43] S. N. Majumdar, S. Krishnamurthy, and M. Barma. Nonequilibrium phase transitions in models of aggregation, adsorption, and dissociation. *Phys. Rev. Lett.*, 81:3691–3694, 1998.

[44] R. Rajesh and S. N. Majumdar. Exact phase diagram of a model with aggregation and chipping. *Phys. Rev. E*, 63:036114, 2001.

[45] P. Chleboun and S. Großkinsky. Finite size effects and metastability in zero-range condensation. *J. Stat. Phys.*, 140:846–872, 2010.

[46] T. Kriecherbauer and J. Krug. A pedestrian's view on interacting particle systems, KPZ universality and random matrices. *J. Phys. A: Math. Theor.*, 43(40):403001, 2010.

[47] M. R. Evans, S. N. Majumdar, and R. K. P. Zia. Canonical analysis of condensation in factorised steady states. *J. Stat. Phys.*, 123:357–390, 2006.

[48] M. Kanai. Exact solution of the zero-range process: fundamental diagram of the corresponding exclusion process. *J. Phys. A: Math. Theor.*, 40(26):7127, 2007.

[49] M. Abramowitz and I.A. Stegun. *Handbook of Mathematical Functions with Formulas, Graphs, and Mathematical Tables*. Dover, New York, 1964.

[50] M. R. Evans. Exact steady states of disorder hopping particle models with parallel and ordered sequential dyanamics. *J. Phys. A: Math. Gen.*, 30(16):5669, 1997.

[51] R. Rajesh and S. Krishnamurthy. Effect of spatial bias on the nonequilibrium phase transition in a system of coagulating and fragmenting particles. *Phys. Rev. E*, 66:046132, 2002.

[52] S. N. Majumdar, S. Krishnamurthy, and M. Barma. Nonequilibrium phase transition in a model of diffusion, aggregation, and fragmentation. *J.Stat. Phys.*, 99(1):1–29, 2000.

[53] S. Großkinsky, G. M. Schütz, and H. Spohn. Condensation in the zero range process: Stationary and dynamical properties. *J. Stat. Phys.*, 113(3):389–410, 2003.

[54] C. Godréche and J. M. Luck. Nonequilbrium dynamics of the zeta urn model. *Eur. Phys. J. B*, 23:473–486, 2001.

[55] C. Godréche and J. M. Luck. Nonequilibrium dynamics of urn models. *J. Phys: Cond. Mat.*, 14(7):1601, 2002.

[56] B. Derrida, M. R. Evans, V. Hakim, and V. Pasquier. Exact solution of a 1D asymmetric exclusion model using a matrix formulation. *J. Phys. A: Math. Gen.*, 26(7):1493, 1993.

[57] U. Basu and P. K. Mohanty. Particle ordering in zero range process : Exact spatial correlations of the corresponding exclusion models. *J. Stat. Mech.: Theor. Exp.*, 2010(03):L03006, 2010.

[58] K. Huang. *Statistical Mechanics*. John Wiley and sons, 2000.

[59] J. Mathews and R. L. Walker. *Mathematical methods of physics*. Addison-Wesley Publishing Company, Inc., 1969.

[60] K. Jain and M. Barma. Phases of a conserved mass model of aggregation with fragmentation at fixed sites. *Phys. Rev. E*, 64:16107, 2001.

[61] M. R. Evans and S. N. Majumdar. Condensation and extreme value statistics. *J. Stat. Mech.: Theor. Exp.*, 2008(05):P05004, 2008.

[62] R. J. Baxter. *Exactly Solved Models in Statistical Mechanics*. Academic Press, 1982.

[63] J. L. Cardy. Continuously varying exponents and the value of the central charge. *J. Phys. A: Math. Gen.*, 20:L891–L896, 1987.

[64] Y. Kafri, E. Levine, D. Mukamel, G. M. Schütz, and R. D. Willmann. Phase-separation transition in one-dimensional driven models. *Phys. Rev. E*, 68:035101, 2003.

[65] T. Halpin-Healy and K. A. Takeuchi. A KPZ cocktail-shaken, not stirred... *J. Stat. Phys*, 140:794–814, 2015.

[66] S. Gupta, M. Barma, and S. N. Majumdar. Finite-size effects on the dynamics of the zero-range process. *Phys. Rev. E*, 76:06010, 2007.

[67] C. Godréche and J. M. Luck. Dynamics of the condensate in zero-range processes. *J. Phys. A: Math. Gen.*, 38(33), 2005.

[68] M. Prähofer and H. Spohn. Exact scaling functions for one-dimensional stationary KPZ growth. *J. Stat. Phys.*, 115(1-2):255–279, 2004.

[69] G. L. Daquila and U. C. Täuber. Slow relaxation and aging kinetics for the driven lattice gas. *Phys. Rev. E.*, 83:051107, 2011.

[70] M. J. Lighthill and G. B. Whitham. On kinematic waves. i. flood movement in long rivers. *Proceedings of the Royal Society of London. Series A, Mathematical and Physical Sciences*, 229(1178):281–316, 1955.

[71] S. F. Edwards and D. R. Wilkinson. The surface statistics of a granular aggregate. *Proceedings of the Royal Society of London A: Mathematical, Physical and Engineering Sciences*, 381(1780):17–31, 1982.

[72] S. N. Majumdar and M. Barma. Tag diffusion in driven systems, growing interfaces, and anomalous fluctuations. *Phys. Rev. B*, 44:5306–5308, 1991.

[73] B. Derrida, M. R. Evans, and D. Mukamel. Exact diffusion constant for one-dimensional asymmetric exclusion models. *J. Phys. A: Math. Gen.*, 26(19):4911, 1993.

[74] S. Gupta, S. N. Majumdar, C. Godrèche, and M. Barma. Tagged particle correlations in the asymmetric simple exclusion process: Finite-size effects. *Phys. Rev. E*, 76:021112, 2007.

[75] H. Hinrichsen. Non-equilibrium critical phenomena and phase transitions into absorbing states. *Adv. Phys.*, 49(7):815–958, 2000.

[76] V. Popkov and G. M. Schütz. Transition probabilities and dynamic structure function in the ASEP conditioned on strong flux. *J. Stat. Phys.*, 142:627–639, 2011.

[77] S. Armendariz, I. Großkinsky and M. Loulakis. Zero range condensation at criticality. *Stoch. Proc. Appl.*, 123:3466–3496, 2013.

[78] A. J. Bray. Theory of phase-ordering kinetics. *Adv. in Phys.*, 43(3):357–459, 1994.

[79] T. Kibble. Phase-transition dynamics in the lab and the universe. *Phys. Today*, 60:47, 2007.

[80] W. H. Zurek. Cosmological experiments in condensed matter systems. *Phys. Rep.*, 276:177–221, 1996.

[81] D. A. Huse and D. S. Fisher. Residual Energies after Slow Cooling of Disordered System. *Phys. Rev. Lett.*, 57:2203–2206, 1986.

[82] S. J. Cornell, K. Kaski, and R. Stinchcombe. Freezing in a two-dimensional glauber system under continuous cooling. *Phys. Rev. B*, 45:2725–2738, 1992.

[83] K. Vollmayr, W. Kob, and K. Binder. How do the properties of a glass depend on the cooling rate? a computer simulation study of a lennard jones system. *J. Chem. Phys.*, 105(11):4714–4728, 1996.

[84] A. Lipowski and D. Johnston. Cooling-rate effects in a model of glasses. *Phys. Rev. E*, 61:6375–6382, 2000.

[85] G. Biroli, L. F. Cugliandolo, and A. Sicilia. Kibble-Zurek mechanism and infinitely slow annealing through critical points. *Phys. Rev. E*, 81:050101(R), 2010.

[86] S. Suzuki. Cooling dynamics of pure and random Ising chains. *J. Stat. Mech.: Theor. Exp.*, 2009(03):P03032, 2009.

[87] P. L. Krapivsky. Slow cooling of an Ising ferromagnet. *J. Stat. Mech.: Theor. Exp.*, 2010(02):P02014, 2010.

[88] P. Laguna and W. H. Zurek. Density of Kinks after a Quench: When Symmetry Breaks, How Big are the Pieces? *Phys. Rev. Lett*, 78:2519–2522, 1997.

[89] W. H. Zurek, U. Dorner, and P. Zoller. Dynamics of a quantum phase transition. *Phys. Rev. Lett.*, 95:105701, 2005.

[90] V. Mukherjee, U. Divakaran, A. Dutta, and D. Sen. Quenching dynamics of a quantum XY spin $\frac{1}{2}$ chain in a transverse field. *Phy. Rev. B*, 76(8):174403, 2007.

[91] J. Dziarmaga. Dynamics of a quantum phase transition and relaxation to a steady state. *Adv. Phys.*, 59:6:1063–1189, 2010.

[92] A. Chandran, A. Erez, A. Gubser, and A. Sondhi. The Kibble-Zurek problem: Universality and the scaling limit. *Phys. Rev. B*, 86:064304, 2012.

[93] A. del Campo and W. H. Zurek. Universality of phase transition dynamics: Topological defects from symmetry breaking. *Int. J. Mod. Phys. A*, 29(08):1430018, 2014.

[94] A. Jelić and L. F. Cugliandolo. Quench dynamics of the 2d XY model. *J. Stat. Mech.: Theor. Exp.*, 2011(02):P02032, 2011.

[95] S. Deutschländer, G. Dillmann, P.and Maret, and P. Keim. Kibble–Zurek mechanism in colloidal monolayers. *Proc. Natl. Acad. Sci.*, 112:6925–6930, 2015.

[96] D. Karevski and R. J Harris. Defect production in quench from a current-carrying non-equilibrium state. *J. Stat. Mech.: Theor. Exp.*, 2016(3):033204, 2016.

[97] D. Sornette. *Critical Phenomena in Natural Sciences Chaos, Fractals, Selforganization and Disorder: Concepts and Tools*. Springer, New York, 2006.

[98] M. Lässig and H. Kinzelbach. Upper critical dimension of the Kardar-Parisi-Zhang equation. *Phys. Rev. Lett.*, 78:903–906, 1997.

[99] R. P. Boas and C. Stutz. Estimating sums with integrals. *Am. J. Phys.*, 39:745, 1971.

[100] R. M. Corless, G. H. Gonnet, D. E. G. Hare, D. J. Jeffrey, and D. E. Knuth. On the Lambert W function. In *Advances in Computational Mathematics*, pages 329–359, 1996.

[101] M. R. Angel, A. G. Evans and D. Mukamel. Condensation transitions in a one-dimensional zero-range process with a single defect site. *J. Stat. Mech.: Theor. Exp.*, 2004(04):P04001, 2004.

Appendix A

A.1 Partition function in the canonical ensemble

Consider a system of N particles on L sites. If τ is a configuration in this system, let $W(\tau)$ denote the stationary weight of such a configuration. Let $Z_{L,N}$ denote the partition function of the EP in this system. That is to say,

$$Z_{L,N} = \sum_{\tau} W(\tau).$$

We will first give two different recurrence relations for $Z_{L,N}$.

Note that any configuration can be written in the form $0^{k_0}\tau 10^{k_N}$, where τ is a configuration in the system with $L-k_0-k_N-1$ sites and $N-1$ particles. Since we want this representation to be unique, τ_1 has to be 1. Thus,

$$\begin{aligned} Z_{L,N} &= \sum_{0\le k_0+k_N\le L-N} \sum_{\tau} W(0^{k_0}\tau 10^{k_N}) \\ &= \sum_{0\le k_0+k_N\le L-N} \sum_{\tau} f(k_0+k_N) W(\tau) \\ &= \sum_{k=0}^{L-N} (k+1) f(k) \sum_{\tau} W(\tau)\,, \end{aligned}$$

where we set $k = k_0 + k_N$ in the last line and the factor of $k+1$ counts for the number of ways one can split k in this way. The sum over τ now gives the partition function for a system with $L-k-1$ sites and $N-1$ particles where the first site is occupied. Since the system is

translation-invariant, this gives the formula,

$$Z_{L,N} = \sum_{k=0}^{L-N} f(k)(k+1)\frac{N-1}{L-k-1} Z_{L-k-1,N-1}. \tag{A.1}$$

Another recurrence relation for the mass model with short-jump partition function $\tilde{Z}_{\mathscr{L},\mathscr{N}}$ with $\mathscr{L}$ sites and $\mathscr{N}$ particles has been obtained in the reference [45] and is given by

$$\tilde{Z}_{\mathscr{L},\mathscr{N}} = \sum_{k=0}^{n} f(k)\tilde{Z}_{\mathscr{L}-1,\mathscr{N}-k}\,, \tag{A.2}$$

with $\tilde{Z}_{0,\mathscr{N}} = \delta_{\mathscr{N},0}$ since $\tilde{Z}_{1,n} = f(n)$. Since a ZRP can be mapped to EP by regarding the N particles in an EP as $\mathscr{L}$ sites in ZRP and $L-N$ holes in EP as $\mathscr{N}$ particles in ZRP, the two partition functions can be related as

$$Z_{L,N} = \frac{L}{N}\,\tilde{Z}_{N,L-N}\,. \tag{A.3}$$

The prefactor on the right hand site (RHS) of the above equation arises due to the fact that the mapping described above between ZRP and EP assumes that an EP configuration begins with an occupied site. The EP configurations that begin with an empty site are taken care of by the factor L/N using the argument described above.

Therefore, on using the last two equations, we get

$$Z_{L,N} = \frac{L}{N}\sum_{k=0}^{L-N} f(k)\frac{N-1}{L-k-1} Z_{L-k-1,N-1}. \tag{A.4}$$

We have thus shown that both recurrence relations (A.1) and (A.4) with the initial conditions $Z_{L,0} = Z_{L,L} = 1$ give rise to the same formula.

A.2 Exact Formula for the partition function of hole-dependent hop rate

It turns out that one can express $Z_{L,N}$ exactly using integer partitions [2]. To state the result, we need some definitions. An integer partition of a positive integer n is a representation of n in terms of other positive integers which sum up to n. For convenience, the parts are written in weakly decreasing order. For example $(5,3,3,2,1)$ is a partition of 14. If λ is a partition of n, we denote this as $\lambda \vdash n$. Another way of expressing a partition is in the so-called frequency representation, $1^{a_1}2^{a_2}\cdots$, where a_i represents the multiplicity of i in the partition. This information can be encoded as a vector $\bar{a} = (a_1, a_2, \ldots)$. For example, the same partition of 14 above can be written as $1^1 2^1 3^2 4^0 5^1 \equiv (1,1,2,0,1)$ followed by an infinite string of zeros, which we omit. We will write $\bar{a} \vdash n$ to mean a partition of n in this notation.

The number of parts of a partition, denoted by $|\bar{a}|$, is given by $\sum_i a_i$. Given a function f defined on the positive integers, we will denote

$$f(\bar{a}) = f(1)^{a_1} f(2)^{a_2} \cdots .$$

In the same vein, let $\bar{a}! = \prod_i a_i!$. Finally, recall that the Pochhammer symbol or rising factorial $(m)_n$ for nonnegative integer n, is given by the product $m(m+1)\cdots(m+n-1)$ if n is positive and by m if $n = 0$.

The partition function of the EP can be written as

$$Z_{N+M,N} = (N+M) \sum_{\bar{a} \vdash M} \frac{(N - |\bar{a}| + 1)_{|\bar{a}|-1}}{\bar{a}!} f(\bar{a}), \tag{A.5}$$

where the length of the system is $L = N + M$ and $(m)_n$ is the Pochhammer symbol defined after (2.14). We will prove this by equating both representations (A.1) and (A.4). Doing so

for $Z_{N+M,N}$ shows

$$\sum_{k=0}^{M} \frac{(N-1)f(k)}{N+M-k-1} Z_{N+M-k-1,N-1}\left(\frac{M-Nk}{N}\right) = 0.$$

Isolating the $k=0$ term and replacing $N-1$ by N gives a recurrence

$$\frac{M}{N+M} Z_{N+M,N} = \sum_{k=1}^{M} \frac{(N+1)k-M}{N+M-k} f(k)\, Z_{N+M-k,N}.$$

Define $\hat{Z}_{N+M,N} = \frac{Z_{N+M,N}}{N+M}$ to get a recurrence for $\hat{Z}$'s,

$$\hat{Z}_{N+M,N} = \sum_{k=1}^{M} \frac{(N+1)k-M}{M} f(k)\, \hat{Z}_{N+M-k,N}. \tag{A.6}$$

We will now prove the formula for $\hat{Z}_{N+M,N}$ equivalent to (A.5) by induction on M. When $M=1$, there is a single term in the sum corresponding to $\bar{a}=(1,0,\ldots)$. Thus $\hat{Z}_{N+1,N} = f(1)$. This is correct since there is a single vacancy and a factor of $f(1)$ for the particle preceding it.

Now, we assume that (A.5) is true for the number of vacancies being any of $1,\ldots,M-1$. Using (A.6) and the induction assumption, we can write

$$\hat{Z}_{M+N,N} = \sum_{k=1}^{M} \frac{(N+1)k-M}{N+M-k} f(k) \sum_{\bar{a}\vdash M-k} \frac{(N-|\bar{a}|+1)_{|\bar{a}|-1}}{\bar{a}!} f(\bar{a}). \tag{A.7}$$

Notice that each term in the above equation contains the factor $f(k)f(\bar{a})$ where $a \vdash M-k$. We can thus replace $\bar{a}$ in the sum by $\overline{a'}$, where $\overline{a'} = \bar{a} \oplus (k)$. Then $f(k)f(\bar{a})$ can be replaced by $f(\overline{a'})$. Therefore, the sum above can be reinterpreted as a sum over partitions of M. We have to compute the coefficient of $f(\overline{a'})$ in such a term.

Suppose $\overline{a'}$ can be written as $(i_1^{a'_1},\ldots,i_j^{a'_j})$ where each $a'_k \neq 0$. Since there are j distinct parts in $\overline{a'}$, we can express $\overline{a'} = (i_k) \oplus \overline{a'}_k$, where $\overline{a'}_k = (i_1^{a'_1},\cdots,i_k^{a'_k-1},\cdots i_j^{a'_j})$ for $k=1,\ldots,j$. There are thus, exactly j terms that contribute to the partition $\overline{a'}$. Note that

$$|\overline{a'}_k| = |\overline{a'}| - 1, \quad f(\overline{a'}) = f(\overline{a'}_k) f(i_k) \quad \text{and} \quad \overline{a'}! = \overline{a'}_k!\, a'_{i_k}.$$

The terms contributing to $\overline{a'}$ are

$$
\begin{aligned}
&\sum_{k=1}^{j} \frac{(N+1)i_k - M}{M} f(i_k) \frac{(N-|\overline{a'}_k|+1)_{|\overline{a'}_k|-1}}{\overline{a'}_k!} f(\overline{a'}_k) \\
&= \sum_{k=1}^{j} \frac{(N+1)i_k - M}{M} \frac{(N-|\overline{a'}|+2)_{|\overline{a'}|-2}}{\overline{a'}!}\, a'_{i_k}\, f(\overline{a'}) \\
&= \frac{(N-|\overline{a'}|+2)_{|\overline{a'}|-2}}{\overline{a'}!}\, f(\overline{a'}) \sum_{k=1}^{j} \frac{(N+1)i_k a'_{i_k} - M a'_{i_k}}{M} \\
&= \frac{(N-|\overline{a'}|+2)_{|\overline{a'}|-2}}{\overline{a'}!}\, f(\overline{a'})(N+1-|\overline{a'}|) \\
&= \frac{(N-|\overline{a'}|+1)_{|\overline{a'}|-1}}{\overline{a'}!}\, f(\overline{a'}).
\end{aligned}
$$

Appendix B

B.1 Simple exclusion process

For $u(n) = 1\ ,\ n > 0$, as all configurations are equally likely [40], the steady state partition function is given by $Z_{L,N} = \binom{L}{N}$. The two-point correlation function $S(r) = \binom{L-2}{N-2}/\binom{L}{N} = N(N-1)/(L(L-1))\ ,\ r > 0$ vanishes in the limit $L \to \infty$. It can be easily checked that (3.3) also gives this result. For large systems, the free energy defined in (3.4) works out to be

$$\tilde{F}(\varrho) = (1+\varrho)\ln(1+\varrho) - \varrho \ln \varrho\ , \tag{B.1}$$

which is an increasing function of the density ϱ. Furthermore, since $f(m) = 1$, we have $g(\omega) = 1/(1-\omega)$ and therefore

$$G(y) = \rho \frac{1-(1-\rho)y}{1-y} - \frac{\rho^2}{1-y}\ , \tag{B.2}$$

which immediately yields $S(r) = 0\ ,\ r > 0$, as expected in the thermodynamic limit.

B.2 Free particle case

The case of free particles is considered here for which $u(n) = n$ [60] where each particle is endowed with an exponential clock that ticks at rate one, but since the particles are free and act independently, the total hop out rate is equal to the number of particles at the site.

Therefore from (2.3), the ZRP partition function is easily seen to be

$$\tilde{Z}_{\mathscr{L},\mathscr{N}} = \frac{\mathscr{L}^{\mathscr{N}}}{\mathscr{N}!}.$$

Using this in (3.3), we obtain the exact expression for the two-point correlation function as

$$\langle \eta_i \eta_{i+r} \rangle = \frac{\rho}{N^{L-N}} \sum_{k=k_{min}}^{k_{max}} \frac{(r-k)^k}{k!} (N-r+k)^{L-N-k} \frac{(L-N)!}{(L-N-k)!}. \tag{B.3}$$

In the thermodynamic limit, the above expression gives

$$\langle \eta_i \eta_{i+r} \rangle = \rho \sum_{k=0}^{r-1} \frac{(r-k)^k}{k!} \varrho^k e^{-(r-k)\varrho}. \tag{B.4}$$

For this case, we have $g(\omega) = e^{\omega}$ and $\omega = \varrho$. As a result, (3.14) gives

$$G(y) = \frac{\rho}{1 - y e^{\omega(y-1)}} - \frac{\rho^2}{1-y}. \tag{B.5}$$

It can be checked that the correlation function in (B.4) matches that obtained from the series expansion of (B.5).

To obtain an explicit expression for the correlation function $S(r)$, we use the Euler-Maclaurin formula given by [99]

$$\begin{aligned}
\sum_{k=0}^{r} f(k) &\approx \int_0^r dx\, f(x) + \frac{1}{2}(f(0)+f(r)) - \int_0^r dx\, f'(x) \sum_{j=1}^{\infty} \frac{\sin(2j\pi x)}{\pi j} && \text{(B.6)} \\
&= \int_0^r dx\, f(x) + \frac{f(0)}{2} + 2\sum_{j=1}^{\infty} \int_0^r dx\, \cos(2j\pi x) f(x) && \text{(B.7)} \\
&= \int_0^r dx\, f(x) + \frac{f(0)}{2} + 2\sum_{j=1}^{\infty} \mathrm{Re}\left[\int_0^r dx\, e^{i2j\pi x} f(x) \right], && \text{(B.8)}
\end{aligned}$$

where $f(k)$ is the summand in (B.4). Our main task is to calculate the integral on the RHS of the last equation which can be carried out using the saddle point method for large r. We find that

$$\int_0^r dx\, e^{i2j\pi x} f(x) \approx \frac{e^{r(x_0-\varrho)}}{1+x_0}, \tag{B.9}$$

where x_0 is the solution of the saddle point equation

$$\varrho - x_0 + \ln(\varrho/x_0) + i2\pi j = 0. \tag{B.10}$$

Writing $x_0 = \varrho\alpha e^{i\theta}$, we find that α and θ obey the following equations:

$$\varrho = \frac{2\pi j - \theta}{\tan\theta} + \ln\left(\frac{2\pi j - \theta}{\varrho \sin\theta}\right) \tag{B.11a}$$

$$\alpha = \frac{2\pi j - \theta}{\varrho \sin\theta}. \tag{B.11b}$$

For $j = 0$, the saddle point $x_0 = \varrho$ which immediately gives

$$S(r) = 2\rho \sum_{j=1}^{\infty} \int_0^r dx\, \cos(2j\pi x) f(x)\,, \tag{B.12}$$

where the summand is given by

$$e^{r(\frac{2\pi j-\theta}{\tan\theta}-\varrho)}\, \frac{\cos(r(2\pi j-\theta))(1+\frac{2\pi j-\theta}{\tan\theta}) + \sin(r(2\pi j-\theta))(2\pi j-\theta)}{(1+\frac{2\pi j-\theta}{\tan\theta})^2 + (2\pi j-\theta)^2}. \tag{B.13}$$

Since the contribution of the successive terms in the sum decreases with increasing j, we estimate only the $j = 1$ term here. Also, numerical analysis of (B.11a) shows that θ increases with j and therefore we work within small-θ approximation. These considerations finally yield

$$\theta = \frac{2\pi}{W(\varrho e^{1+\varrho})}\,, \tag{B.14}$$

where W is the Lambert function that satisfies $W(\omega)e^{W(\omega)} = \omega$ [100], and

$$S(r) = 2\rho e^{-r(\frac{1}{\rho}-\frac{2\pi}{\theta})}\, \frac{\cos(r\theta)(\frac{2\pi}{\theta}) - \sin(r\theta)(2\pi-\theta)}{(\frac{2\pi}{\theta})^2 + (2\pi-\theta)^2} \tag{B.15}$$

$$\approx \rho e^{-r(\frac{1}{\rho}-\frac{2\pi}{\theta})}\, \frac{\theta\cos(r\theta)}{\pi}\,, \tag{B.16}$$

which is an oscillatory function with decaying amplitude.

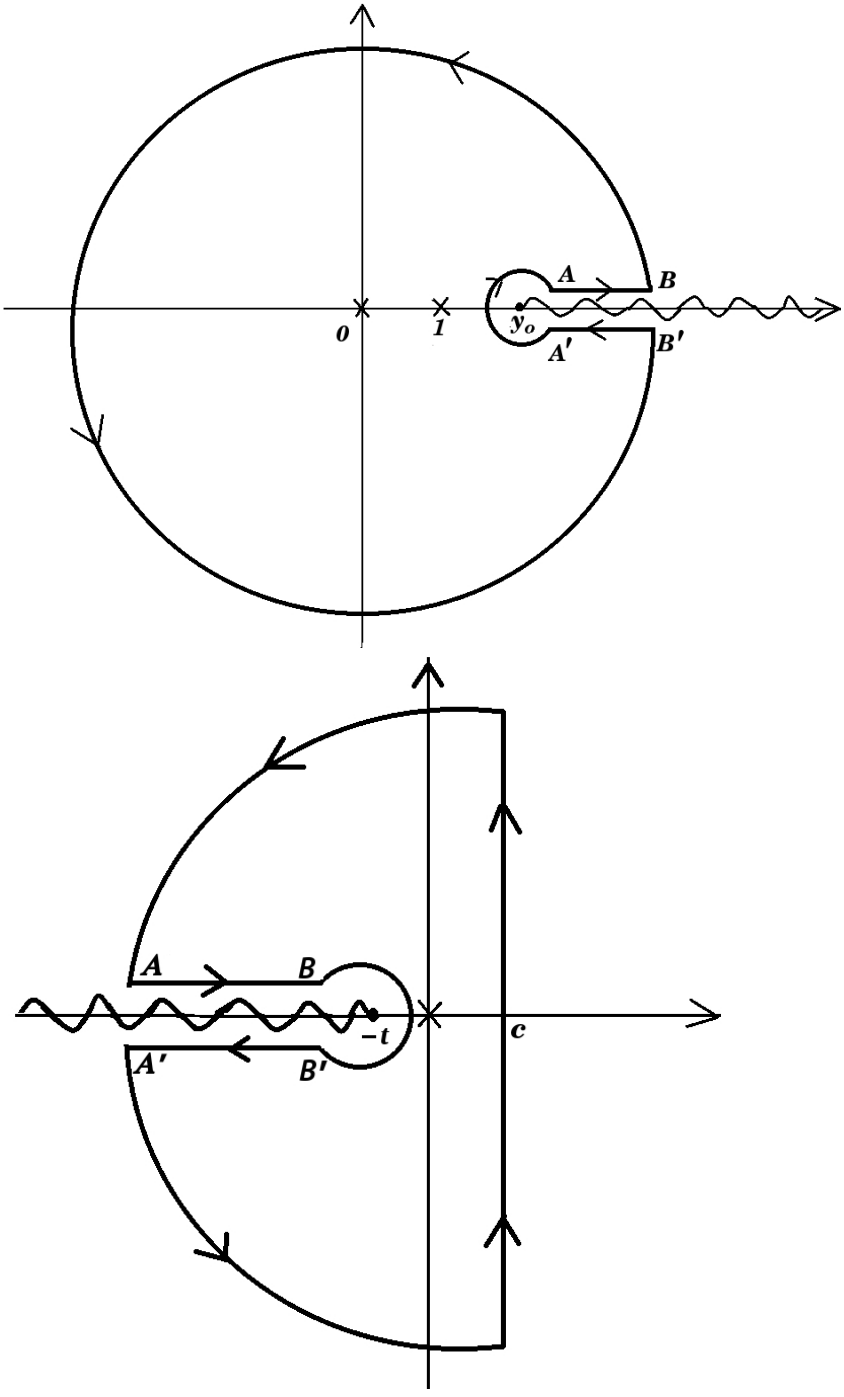

Fig. B.1 Figure to show the closed contour C' appearing in the integral given by (top) equation (3.22) and (bottom) equation (B.17).

B.3 Evaluation of the integral (3.43)

Consider the following integral:

$$I_2 = \frac{1}{2\pi i} \oint_{C'} ds\, e^{sr}\, \frac{(s+t)^{b-1} - t^{b-1}}{s^2}\,,\ t \geq 0\,, \tag{B.17}$$

where the contour C' around the branch cut at $-t$ includes the Bromwich contour along the line $s = c$, c being real and nonnegative given in Fig. B.1b. The residue from the second order pole at $s = 0$ gives $I_2 = (b-1)\,t^{b-2}$. The integral along the large semicircle with radius R decays exponentially fast with increasing R, and the one along the small semicircle with radius ϵ is proportional to ϵ^{b-2} and therefore vanishes as $\epsilon \to 0$. Thus we get

$$I_2 = \frac{1}{2\pi i} \left(\int_{c-i\infty}^{c+i\infty} + \int_{AB} + \int_{B'A'} ds\, e^{sr}\, \frac{(s+t)^{b-1} - t^{b-1}}{s^2} \right). \tag{B.18}$$

Since $s = -t + xe^{\pm i\pi}$ along the upper (lower) branch $AB(B'A')$, we get

$$\int_{c-i\infty}^{c+i\infty} \frac{ds}{2\pi i}\, e^{sr}\, \frac{(s+t)^{b-1} - t^{b-1}}{s^2} \tag{B.19}$$

$$= \frac{\sin(b\pi)}{\pi}\, e^{-tr} \int_0^\infty dx\, e^{-xr}\, \frac{x^{b-1}}{(x+t)^2} + (b-1)\,t^{b-2} \tag{B.20}$$

$$= \frac{\sin(b\pi)}{\pi}\, \Gamma(b-1) e^{-tr}\, \frac{(rt+b-1)E_{b-1}(tr)e^{tr} - 1}{r^{b-2}} + (b-1)\,t^{b-2}. \tag{B.21}$$

For $t = c = 0$, using that $e^x E_{b-1}(x) \overset{x\to 0}{\sim} (b-2)^{-1} + \mathcal{O}(x^{b-2})$ [49], the above integral reduces to

$$\int_{-i\infty}^{i\infty} \frac{ds}{2\pi i}\, e^{sr}\, s^{b-3} = \frac{\sin(b\pi)}{\pi}\, \frac{\Gamma(b-2)}{r^{b-2}}. \tag{B.22}$$

B.4 Single defect particle

We consider a lattice gas model having L sites and N hard core particles. In this model, all the particles are identical except one known as the defect particle which hops with the slower rate than the rest of the paricles. The hop rates corresponding to the defect particle

and a particle μ from the set of identical particles can be defined as

$$u_1(n) = c, \tag{B.23}$$

$$u_\mu(n) = 1 \quad \text{for } \mu > 1. \tag{B.24}$$

Here, particle with sub index 1 is the defect particle, and $c < 1$ indicates that the defect particle hops to the empty nearest neighbor with a slower rate compared to the other particles. This hopping condition leads to a phase separation phenomenon between the fluid phase and jammed phase (see Chapter 2 for details). In the jammed phase, $\rho < \rho_c$, the mean hop rate becomes c while in fluid phase, $\rho > \rho_c$, the mean hop rate is a function of density as explained in Sec. 2.2.3. The canonical partition function of this model can be computed exactly by mapping it to the mass model as shown in Fig. 2.1; it can be expressed as

$$\tilde{Z}_{N,L-N} = \sum_{x=0}^{L-N} \binom{L-x-2}{N-2} c^{-x}. \tag{B.25}$$

Using Stirling approximation, followed by saddle point calculation, the partition function simplifies to

$$\tilde{Z}_{N,L-N} = \frac{1}{2} c^{-(L-N)} (1-c)^{-(N-1)} \left(\operatorname{erf}\left[\sqrt{\frac{(1-c)\,N}{2c}} \right] - \operatorname{erf}\left[\sqrt{\frac{N\,(1-c)^2}{2c}} \left(\frac{c}{(1-c)} - \frac{L-N}{N} \right) \right] \right). \tag{B.26}$$

Two-point correlation function

Two-point correlation function is defined as the probability that the sites i and $i+r$ are occupied. As explained in Sec. 3.2, the two-point correlation function is a product of the partition of two sub-configurations and is given by the equation (3.3). However, in a single defect system the hopping rate of one particle is different from the rest of the particles, so it imposes a condition to consider the correlation function as the sum of the following two configurations.

(i) In the first case, when one sub-configuration of length r from the start contains the defect particle, the partition function of the sub-configuration is given by (B.25). On the other hand, the rest of the subsystem of length $L-r$ sites is the same as a simple exclusion process, and thus, the partition function calculated as sub-configuration is equally likely and is given by a binomial distribution. Therefore, the correlation function of the system in which first r site contain defect particle $S_1(r)$ is given as

$$S_1(r) = \sum_{j=min}^{max} \left(\frac{r-j}{L}\right) \frac{\tilde{Z}_{r,r-j}}{\tilde{Z}_{L,N}} \left(\frac{N-r+j}{L-r}\right) \binom{L-r}{N-r+j}. \tag{B.27}$$

Using (B.26) and the Stirling approximation, the correlation function transforms to

$$S_1(r) = \frac{2}{\pi}(1-c)^2 \left(\frac{r}{L}\right)^{3/2} \frac{(2-c)\sqrt{1-c}}{c}. \tag{B.28}$$

(ii) In the second case, a sub-configuration of length r has normal particles with hop rate one, while the rest of the system of length $L-r$ sites has one defect particle. The partition function of first configuration of site r is given by binomial distribution and rest by (B.25). Hence, the correlation function $S_2(r)$ can be given by

$$S_2(r) = \sum_{j=min}^{max} \left(\frac{r-j}{r}\right) \binom{r}{r-j} \left(\frac{N-r+j}{L}\right) \frac{\tilde{Z}_{L-r,N-r+j}}{\tilde{Z}_{L,N}}. \tag{B.29}$$

By simplifying above equation, we get

$$S_2(r) = (1-c)^2[1+D(c,\rho)], \tag{B.30}$$

where $D(c,\rho)$ is a series in c and ρ. Now, the total correlation function is the sum of the above two correlation functions,

$$\begin{aligned} S(r) &= S_1(r) + S_2(r) && \text{(B.31)} \\ &= \frac{2}{\pi}(1-c)^2 \left(\frac{r}{L}\right)^{3/2} \frac{(2-c)\sqrt{1-c}}{c} + (1-c)^2[1+D(c,\rho)]. && \text{(B.32)} \end{aligned}$$

The total correlation function calculated above shows good agreement with the numerical simulation for any finite system.

Thermodynamic limit

In the grand canonical ensemble, the partition function of ZRP with single defect site is given by (see Sec.2.2)

$$\tilde{\mathcal{Z}}_N(\omega) = \prod_{c=1}^{N}\left[\sum_{n_c=0}^{\infty}\omega^{n_c} f_c(n_c)\right] \tag{B.33}$$

$$= \left[\sum_{n=0}^{\infty}\omega^n c^{-n}\right]\left[\sum_{n=0}^{\infty}\omega^n\right]^{N-1} \tag{B.34}$$

$$= \frac{1}{1-\frac{\omega}{c}}\left(\frac{1}{1-\omega}\right)^{N-1}, \quad N \geq 1. \tag{B.35}$$

From Ref. (3.63), we can write the generating function $G(y)$ of the correlation function in thermodynamic limit as

$$G(y) = \rho\sum_{n=0}^{\infty}(ye^{-P})^n\tilde{\mathcal{Z}}_n(\omega y) \tag{B.36}$$

$$= \rho + \rho\frac{1-y\omega}{1-\frac{\omega y}{c}}\sum_{n=1}^{\infty}\left(\frac{ye^{-P}}{1-\omega y}\right)^n \tag{B.37}$$

$$= \rho + \rho\frac{1-y\omega}{1-\frac{\omega y}{c}}\left(\frac{ye^{-P}}{ye^{-P}-(1-\omega y)}\right), \tag{B.38}$$

where P is the pressure. It can be calculated as

$$PN = \ln\tilde{\mathcal{Z}}_N(\omega) \tag{B.39}$$

$$= -\ln(1-\omega/c) - (N-1)\ln(1-\omega). \tag{B.40}$$

Now at the critical point, $\omega = c$, and the series expansion of generating function (B.38) around $y = 1$, as shown in Sec. 3.2.2, gives

$$G(y) = \rho(1+\rho+\frac{c(1-c)}{N}\,y + ...). \tag{B.41}$$

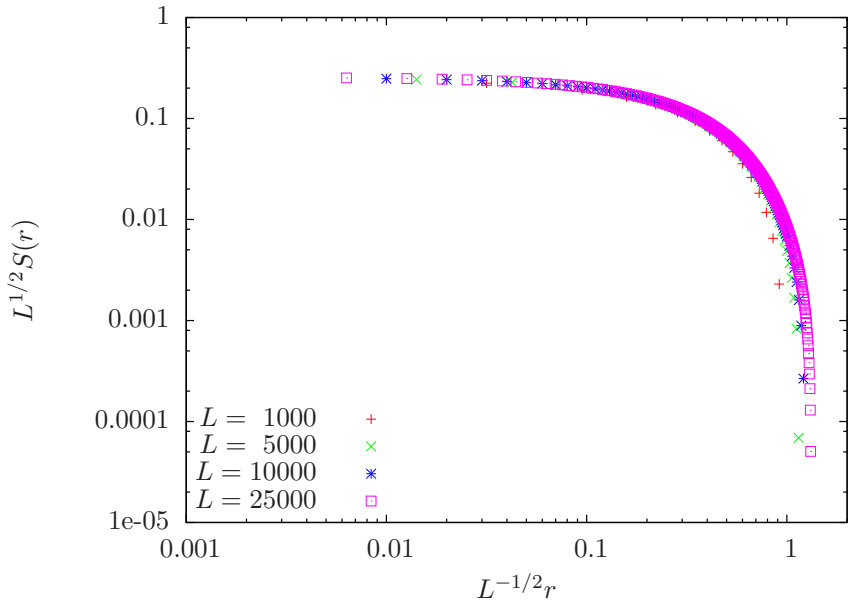

Fig. B.2 Scaled two-point correlation function for the single defect particle model with different system sizes is shown in the figure. The slowest particle has hop rate, $c = 0.25$.

Further, the correlation function is given by (3.16) which shows that the correlation function depends on the system size — as the system size increases the correlation function decreases. It has also been confirmed numerically, see Fig. B.2. Thus, in the thermodynamic limit $L \to \infty$, i.e., the single defect approaches the estimates of simple exclusion. It is because the effect of a single particle is negligible, the particles average hopping rate become 1.

B.5 Single defect particle with hole dependence

In this case, the single defect particle hop rate depends on the number of holes in front of it, and the hop rule of the system is given as

$$u_1(n) = c\left(1+\frac{b}{n}\right), \text{ for } n>0, \tag{B.42}$$

$$u_\mu(n) = 1, \text{ for } \mu>1, \tag{B.43}$$

provided $c < 1$. The canonical partition function for the above choice of hop rate as given in ref. [1] is

$$\tilde{Z}_{N,L-N} = \sum_{x=0}^{n} \frac{x!}{(1+b)_x} \binom{L-x-2}{N-2} c^{-x}. \tag{B.44}$$

The critical point for this model is dependent on the system size and is given as [1]

$$\varrho_c = \frac{c}{1-c} + \frac{2}{1-c}\left(\frac{bc}{N}\right)^{1/2}. \tag{B.45}$$

From the above expression, at the critical point the dependence on b goes away for an infinitely large system and the expression of the critical density for a single defect is recovered. Furthermore, it is useful to simplify the partition function so that we can solve the correlation function exactly as done in the single defect case. The simplified partition function is given by

$$\begin{aligned} \tilde{Z}_{N,L-N} &= \sqrt{\frac{\pi b}{2}} \frac{b}{x}^{b} e^{-b} c^{-(L-N)} (1-c)^{-(N-1)} \\ &\left(\operatorname{erf}\left[\sqrt{\frac{(1-c)\,N}{2c}} \right] - \operatorname{erf}\left[\sqrt{\frac{N\,(1-c)^2}{2c}} \left(\frac{c}{(1-c)} - \frac{L-N}{N} \right) \right] \right). \end{aligned} \tag{B.46}$$

The correlation function for this case is again same as (B.32). By normalising, the dependence on b cancels out and the correlation function for this case becomes the same as that of a single defect particle case.

In thermodynamic limit

For the choice of hop rate $u_p(n)$ (B.43), the steady state weight factor (2.14) can be obtained [101]. It is given as

$$f_1(n) = \frac{1}{c^n} \frac{n!}{(1+b)_n}, \tag{B.47}$$

$$f_p(n) = 1 \quad \text{for} \quad p > 1, \tag{B.48}$$

and from (2.8), we get

$$g_1(\omega) = \sum_{n=0}^{\infty} \left(\frac{\omega}{c}\right)^n \frac{n1}{(1+b)_n} \tag{B.49}$$

$$= {}_2F_1(1,1;1+b;\omega/c)\,, \tag{B.50}$$

$$g_p(\omega) = \frac{1}{1-\omega} \quad \text{for } p>1. \tag{B.51}$$

Now using (B.51), we can write the grand canonical function similar to (B.35). It is given by

$$\tilde{\mathcal{Z}}_N(\omega) = \frac{1-\omega}{g_1(\omega)} \left(\frac{1}{1-\omega}\right)^{N-1}. \tag{B.52}$$

We calculate the generating function in a similar way as we did for the single defect particle case and obtain

$$G(y) = \rho + \rho \frac{(1-\omega y)}{g_1(y\omega)} \sum_{n=1}^{\infty} \left(\frac{ye^{-P}}{1-\omega y}\right)^n, \tag{B.53}$$

where P is the pressure,

$$P = \ln[g_1(\omega) - (N-1)\ln(1-\omega)]. \tag{B.54}$$

In thermodynamic limit, this system has $\rho_c = 1-c$, and the fugacity, $\omega = c$. Using these values for ρ_c and ω, and expanding the generating function $G(y)$ around $y=1$, we get

$$G(y) = \rho(1 + ye^{-p} + ...) \tag{B.55}$$

$$= \rho\left[1 + y\left(1 - \frac{{}_2F_1(1,1;1+b;1)}{N}\right)(1-c)\left(1+\frac{c}{N}\right) + ..(N^{-(L-N)})\right]. \tag{B.56}$$

Here, same as the single defect problem, the correlation function decreases with an increasing system size. Thus, the effect of a defect particle vanishes in the thermodynamics limit and the correlation function becomes the same as that of the simple exclusion process.

Appendix C

C.1 Hydrodynamic equation for the height profile

For the lattice-gas models considered here, the average particle density $\rho_i(t) = \langle \eta_i(t) \rangle$ at site i obeys a continuity equation, $\dot{\rho}_i(t) = j_i(t) - j_{i-1}(t)$ where $j_i(t)$ is the average current in the bond connecting the sites i and $i+1$. On a coarse-grained level, the local density (now defined in continuous space) obeys the following equation

$$\frac{\partial \rho(r,t)}{\partial t} + \frac{\partial J(\rho(r,t))}{\partial r} = 0 \,, \tag{C.1}$$

where, assuming that local stationarity holds, the current depends on the space variable through the density and given by the expression in the stationary state [46, 65]. Writing $\rho(r,t) = \rho + \delta\rho(r,t)$ and expanding the current to quadratic order in the deviation $\delta\rho(r,t)$ about the mean density, we obtain $J(\rho(r,t)) = J(\rho) + v\delta\rho(r,t) + (\lambda/2)(\delta\rho(r,t))^2$ where

$$v = \frac{\partial J}{\partial \rho} \,, \tag{C.2}$$

$$\lambda = \frac{\partial^2 J}{\partial \rho^2} \,. \tag{C.3}$$

Since the lowest order term in $\delta\rho$ obeys the following first order wave equation

$$\frac{\partial \delta\rho(r,t)}{\partial t} + v\frac{\partial \delta\rho(r,t)}{\partial r} = 0 \,, \tag{C.4}$$

the density fluctuations move with a speed v. Using the mapping (4.2) and retaining the quadratic term that carries information about the decay of the density fluctuations, we obtain the KPZ equation for the height profile in one (space) dimension [46, 65]:

$$\frac{\partial h}{\partial t} = -v\left(\frac{\partial h}{\partial r}\right) + \frac{\lambda}{2}\left(\frac{\partial h}{\partial r}\right)^2 + \nu\frac{\partial^2 h}{\partial r^2} + \zeta(r,t)\,, \tag{C.5}$$

where the noise is assumed to be white in both space and time with $\langle\zeta(r,t)\zeta(r',t')\rangle = D\delta(r-r')\delta(t-t')$ and $C(r,0) = (D/\nu)|r|$.

For the exclusion process described in Sec. 2.2, we now consider the above equation for $\rho \geq \rho_c$. As explained in Sec. 4.5, the speed v given by (4.21) is related to the variance of the mass. The coefficient λ above is however related to the third cumulant of mass, κ_3:

$$\lambda = \frac{\omega}{(\rho\sigma^2)^3}\left(\sigma^2 + 2\rho\sigma^4 - \kappa_3\right) - \frac{2\omega}{\rho^2\sigma^2}\,. \tag{C.6}$$

For $\rho > \rho_c$, since the mass distribution is an exponential, all the mass cumulants exist and therefore, using the KPZ exponents, it follows that the autocorrelation function decays as $t^{-2/3}$ in the fluid phase.

We now ask if the KPZ equation describes the dynamics at the critical point as well. As for the speed, we approach the critical point from the high density side to find the coefficient λ. In the vicinity of the critical point, for non-integer b, the generating function $g(\omega)$ for the weight factor $f(m)$ in (2.13) is given by [2]

$$g(\omega) = g(1) - sg'(1) + \frac{s^2}{2!}g''(1) + \ldots + \frac{(-s)^n}{n!}g^{(n)}(1) + \alpha s^{b-1} + \mathcal{O}(s^b)\,, \tag{C.7}$$

where $s = 1-\omega$, n is the integer part of $b-1$ and $\alpha = b\pi\csc(b\pi)$. Using this in the density conservation equation (2.9), we have [2]

$$\frac{1}{\rho} = \begin{cases} \frac{1}{\rho_c} - \frac{\alpha(b-1)g'(1)}{g^2(1)}\,s^{b-2} + \mathcal{O}(s) & ,\ 2<b<3\,, \\ \frac{1}{\rho_c} + \frac{g'(1)}{g(1)}\left(\frac{g'(1)}{g(1)} - \frac{g''(1)}{g'(1)} - 1\right)s - \frac{(b-1)\alpha}{g(1)}s^{b-2} & ,\ 3<b<4\,, \\ \frac{1}{\rho_c} + \frac{g'(1)}{g(1)}\left(\frac{g'(1)}{g(1)} - \frac{g''(1)}{g'(1)} - 1\right)s + \mathcal{O}(s^2) & ,\ b>4\,. \end{cases} \tag{C.8}$$

On inverting this equation for the fugacity to lowest order in the deviation $\epsilon = \rho - \rho_c$, and using it in (4.19) for the current, we get

$$J(\rho) = \begin{cases} \rho_c + v\epsilon + \mathcal{O}(\epsilon^{\frac{1}{b-2}}) & , 2 < b < 3 , \\ \rho_c + v\epsilon + \mathcal{O}(\epsilon^{b-2}) & , 3 < b < 4 , \\ \rho_c + v\epsilon + \mathcal{O}(\epsilon^2) & , b > 4 , \end{cases} \tag{C.9}$$

where v is given by (4.21). The above equation shows that the coefficient λ is finite for $b > 4$ but diverges otherwise at the critical point.

Appendix D

D.1 Calculation of the exponent ν for fixed density

D.1.1 For $b > 3$

From (2.15) the density is related to the generating function as

$$\varrho = \omega \frac{g'(\omega)}{g(\omega)} = B(\omega, b). \tag{D.1}$$

We perform Taylor series expansion of ϱ around $\omega = 1$ and $b = b_c$ which gives us

$$B(\omega, b) = B(1, b_c) + (\omega - 1)\partial_\omega B(\omega, b)|_{1,b_c} + (b - b_c)\partial_b B(\omega, b)|_{1,b_c} . \tag{D.2}$$

Further, (D.2) is written as series expansion in following way

$$\varrho = \frac{g'(1)}{g(1)} + (\omega - 1)\left[\frac{g'(1)}{g(1)} - \left(\frac{g'(1)}{g(1)}\right)^2 + \frac{g''(\omega)}{g(\omega)}\right] + (b - b_c)\left[\frac{\ddot{g}(1)}{g(1)} - g'(1)\frac{\dot{g}}{g^2}\right] , \tag{D.3}$$

which further simplies to

$$\varrho = \varrho_c + (\omega - 1)\left[\varrho_c - \varrho_c^2 + \frac{g''(\omega)}{g(\omega)}\right] + (b - b_c)\left[\frac{\ddot{g}(1)}{g(1)} - g'(1)\frac{\dot{g}}{g^2}\right] , \tag{D.4}$$

where

$$\partial_b g(\omega, b)|_{1,b_c} = \dot{g}(1, b_c). \tag{D.5}$$

For fixed density, $\varrho = \varrho_c$, we obtain the following relation

$$(1-\omega)\left[\varrho_c - \varrho_c^2 + \frac{g''(\omega)}{g(\omega)}\right] = (b-b_c)\left[\frac{\ddot{g}(1)}{g(1)} - g'(1)\frac{\dot{g}}{g^2}\right]. \tag{D.6}$$

The correlation length is defined as $\xi \sim (1-\omega)^{-1} \sim (b-b_c)^{-1}$. Therefore, $\nu = 1$.

D.1.2 For $2 < b < 3$

Here, we use the Laplace transform representation of the single site steady state weight factor $f(m)$. The density is related as

$$\varrho = \frac{\int_0^\infty m f(m) e^{-sm} dm}{\int_0^\infty f(m) e^{-sm} dm}, \tag{D.7}$$

with

$$\int_0^\infty f(m) dm = 1. \tag{D.8}$$

We define the moments of $f(m)$ as

$$\mu_k = \int_0^\infty m^k f(m) dm. \tag{D.9}$$

Now to calculate the exponent ν, we have to expand the Laplace transform $g(s,b)$ of $f(m)$, when s approaches to 0 and b approaches b_c and by defining $b \longrightarrow b_c - \epsilon$. For $f(m) \sim Am^{-b}$, we have

$$g(s, b_c - \epsilon) = \int_0^\infty A m^{-(b_c-\epsilon)} e^{-sm} dm, \tag{D.10}$$

which on expansion gives

$$\begin{aligned} g(s, b+\epsilon) &= \int_0^\infty f(m)(1+\epsilon \ln m) e^{-sm} dm & \text{(D.11)} \\ &= \int_0^\infty f(m) e^{-sm} dm + \epsilon \int_0^\infty f(m) \ln m e^{-sm} dm & \text{(D.12)} \\ &= \int_0^\infty f(m) e^{-sm} dm + \epsilon \int_0^\infty f(m) \ln m (1-sm) dm. & \text{(D.13)} \end{aligned}$$

The above integral can be evaluted using small s expansion

$$g(s,b+\epsilon)=\sum_{k=0}^{n-1}\frac{(-1)^k\mu_k s^k}{k!}+Qs^{b_c-1}+\ldots+\epsilon\left(\frac{1}{(b_c-1)^2}-\frac{s}{(b_c-2)^2}\right), \tag{D.14}$$

and the derivative of $g(s,b+\epsilon)$ is therefore,

$$g^{'}(s,b+\epsilon)=\sum_{k=1}^{n-1}\frac{(-1)^k\mu_k s^{k-1}}{(k-1)!}+Q(b_c-1)s^{b_c-2}+\ldots-\epsilon\left(\frac{1}{(b_c-2)^2}\right), \tag{D.15}$$

where $Q=A\Gamma(1-b)$. Using (D.14) and (D.15), the density in (D.1) can be expanded as

$$\varrho = \frac{\mu_1 s-Q(b_c-1)s^{b_c-2}+\epsilon\left(\frac{1}{(b_c-2)^2}\right)}{\mu_0-\mu_1 s+\epsilon\left(\frac{1}{(b_c-1)^2}\right)}. \tag{D.16}$$

Since s and ϵ are small quantities, we get

$$\varrho = \left[\mu_1-Q(b_c-1)s^{b_c-2}+\epsilon\left(\frac{1}{(b_c-2)^2}\right)\right]\left[\mu_0+\mu_1 s-\epsilon\left(\frac{1}{(b_c-1)^2}\right)\right] \tag{D.17}$$

$$= \mu_1-Q(b_c-1)s^{b_c-2}+\epsilon\frac{1}{(b_c-2)^2}-\epsilon\frac{\mu_1}{(b_c-1)^2}. \tag{D.18}$$

The first moment, μ_1 defined as the critical density ϱ_c, we have

$$\varrho_c = \varrho_c-Q(b_c-1)s^{b_c-2}+\epsilon\frac{1}{(b_c-2)^2}-\epsilon\frac{\varrho_c}{(b_c-1)^2}, \tag{D.19}$$

$$Q(b_c-1)s^{b_c-2} = \epsilon\left[\frac{1}{(b_c-2)^2}-\frac{\mu_1}{(b_c-1)^2}\right]. \tag{D.20}$$

At fixed density, $\varrho=\varrho_c$,

$$s=\left[\left(\frac{1}{(b_c-2)^2}-\frac{\varrho_c}{(b_c-1)^2}\right)\frac{\epsilon}{Q(b_c-1)}\right]^{\frac{1}{b_c-2}}, \tag{D.21}$$

where $\epsilon=b_c-b$ and $s=-\ln\omega$. We get the relation of hop parameter and fugacity as

$$\ln\omega=-\left[\left(\frac{1}{(b_c-2)^2}-\frac{\varrho_c}{(b_c-1)^2}\right)\frac{\epsilon}{Q(b_c-1)}\right]^{\frac{1}{b_c-2}}, \tag{D.22}$$

$$\omega = \exp\left[-\left[\left(\frac{1}{(b_c-2)^2}-\frac{\varrho_c}{(b_c-1)^2}\right)\frac{\epsilon}{Q(b_c-1)}\right]^{\frac{1}{b_c-2}}\right], \tag{D.23}$$

$$= 1-\left[\left(\frac{1}{(b_c-2)^2}-\frac{\varrho_c}{(b_c-1)^2}\right)\frac{\epsilon}{Q(b_c-1)}\right]^{\frac{1}{b_c-2}}, \tag{D.24}$$

$$1-\omega = \left[\left(\frac{1}{(b_c-2)^2}-\frac{\varrho_c}{(b_c-1)^2}\right)\frac{\epsilon}{Q(b_c-1)}\right]^{\frac{1}{b_c-2}}. \tag{D.25}$$

As the function $f(m)$ is normalised,

$$\int_0^\infty f(m)dm = 1,$$

and the normalisation constant $A = b-1$. As $Q = A\Gamma(1-b)$, the relation (D.25) becomes

$$1-\omega = \left[\left(\frac{1}{(b_c-2)^2}-\frac{\varrho_c}{(b_c-1)^2}\right)\frac{\epsilon}{(b_c-1)^2\Gamma(1-b)}\right]^{\frac{1}{b_c-2}}. \tag{D.26}$$

Since, the correlation length is defined as $\xi \sim (1-\omega)^{-1} \sim (b_c-b)^{-1/(b_c-2)}$. Therefore, $\nu = 1/(b_c-2)$.